SUPRAMOLECULAR NANOPARTICLE INTERACTIONS AND BIOMOLECULE DETECTION

Maria Oikonomou

Thesis committee

Promotor

Prof. Dr A.H. Velders

Professor of BioNanoTechnology

Wageningen University

Other members

Dr J.H.B. Sprakel, Wageningen University

Prof. Dr J.P.M. van Duynhoven, Wageningen University

Prof. Dr B.J. Ravoo, University of Münster, Germany

Dr F.W.B. van Leeuwen, Leiden University Medical Center (LUMC)

This research was conducted under the auspices of the Graduate School VLAG (Advanced studies in Food Technology, Agrobiotechnology, Nutrition and Health Sciences).

SUPRAMOLECULAR NANOPARTICLE INTERACTIONS AND BIOMOLECULE DETECTION

Maria Oikonomou

Thesis

submitted in fulfillment for the degree of doctor

at Wageningen University

by the authority of Rector Magnificus

Prof. Dr A.P.J. Mol,

in the presence of the

Thesis Committee appointed by the Academic Board

to be defended in public

on Monday 4 April 2016

at 4 p.m. in the Aula.

Maria Oikonomou

Supramolecular Nanoparticle Interactions and Biomolecule Detection

174 pages.

PhD thesis, Wageningen University, Wageningen, NL (2016)

With references, with summary in English

ISBN :978-94-6257-660-5

«Κατά βάθος ο υλικός κόσμος είναι απλώς ένας σωρός από υλικά, θα εξαρτηθεί από το αν είμαστε καλοί ή κακοί αρχιτέκτονες το τελικό αποτέλεσμα. Ο Παράδεισος ή η Κόλαση που θα χτίσουμε».

"The material world is really only an accumulation of materials. It is for us to show ourselves to be good or bad architects, to build Paradise or Hell".

Οδυσσέας Ελύτης, Απόσπασμα από την ομιλία του στην απονομή του Βραβείου Νόμπελ Λογοτεχνίας, 1979

Odysseas Elytis, Part of his award ceremony speech for Nobel Prize in Literature, 1979

Contents

Chapter 1 General introduction

Abstract

General aspects, current developments and future challenges in the field of Nanotechnology are introduced. The motivation, in this thesis, was to progressively discover and understand molecular interactions that govern natural systems and beyond, and the goal was to acquire the ability to design, direct and control complex matter. Special focus was put on implementing and controlling supramolecular ligand interactions on nanoparticle surfaces with an emphasis on biomolecule sensing. NMR spectroscopy was identified as a main tool to study dynamics of complex matter and supramolecular strategies are developed for recognizing peptides, sugars and proteins called lectins.

1.1 Introduction

Manipulating and understanding matter at the nanoscale describes best the interdisciplinary field of nanotechnology [1]. Nanotechnology is a new branch of science (physics, chemistry, biology and engineering) that deals with molecules and structures at the nanometer scale; typically 1-100 nm (Figure 1-1). To put it in perspective; A nanometer is one billionth of a meter as the size of a tennis ball is one billionth of the size of the earth. The title of the most famous lecture of Richard Feynman [2]; "There's Plenty of Room at the Bottom" summarizes the main reason for the emergence of Nanotechnology. The reduction of size and quantities, that the field of Nanotechnology uses, enabled us to first understand, then combine, and manipulate the smallest units of matter, the atoms.

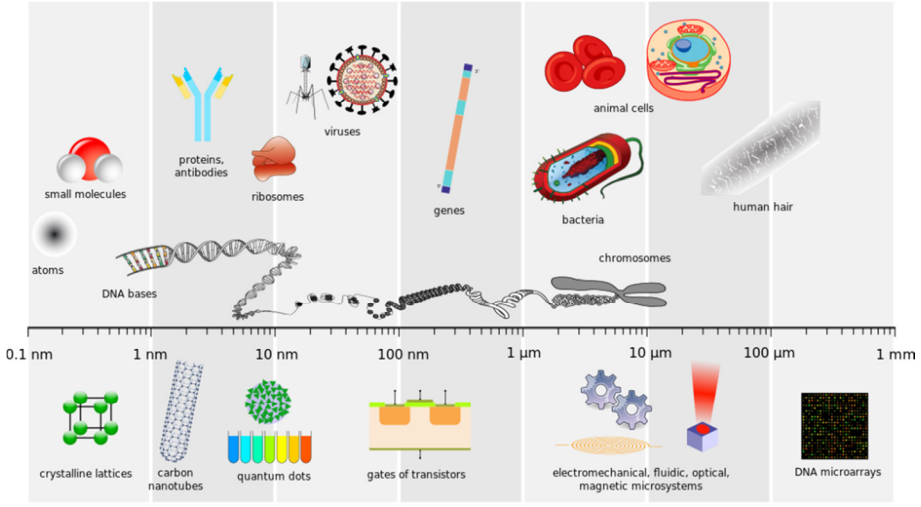

Figure 1-1: Size comparison of nanomaterials with known biological and artificial structures, adapted from https://en.wikipedia.org/wiki/Nanoscopic_scale, Paumier at al.

Nanofabrication, the synthesis of nanomaterials and nanostructures, is performed by two main approaches; top-down and bottom-up [3, 4]. The top-down approach refers to the sizing down (gradual slicing and curving) a bulk material into well-defined nanostructures. Well-known techniques for this approach are photolithography, electron beam lithography, anodization, and ion- and plasma etching [4]. The bottom-up approach is the exact opposite strategy, where simple building blocks such as atoms and molecules are guided by self-assembly [5-7] to form higher-order nanostructures. Physical or chemical triggers (pH, concentration, solvent, application of an electric field etc.) typically induce self-assembly. Self-assembled nanostructures are always a result of thermodynamics and supramolecular forces such as hydrophobicity, hydrogen bonding, electrostatic and van der Waals interactions [8, 9]. The bottom-up approach is inspired by

Nature's strategy [8, 10] for building up functional nano, meso- and macrostructures, from DNA and viruses to plants and animals. Programmable, self-assembled nanostructures have given and will give rise to the most exciting functional materials and systems with almost limitless applications [11-20].

Nanotechnology advanced rapidly in the last century due to the parallel development of highly accurate machines and techniques. Examples of these are advanced microscopic and spectroscopic techniques such as nuclear magnetic resonance [21, 22], electron paramagnetic resonance [23], atomic force microscopy [24], confocal fluorescence microscopy [24], scanning electron microscopy [25], transmission electron microscopy [26], scanning tunneling microscopy [27], X-ray microscopy [28] and optical tweezers [29]. These techniques enabled us to understand and control nanoscale structures, systems and processes.

Currently, nanotechnology is entering a new era, which is described by Jean-Marie Lehn as the era of "complex matter" [30]. Complex matter is the combination of nanomaterials to give rise to superstructures, "structures beyond nanostructures". Some of the latest and most exciting advancements in nanotechnology employ superstructures for the design and development of smart and functional structures, devices and materials and give a small taste of the bright future of nanotechnology.

1.2 Nanostructures as building blocks for superstructures

A nanostructure is a wide term that houses many different types of nanomaterials. Nanostructures can vary in dimension (Figure 1-2), composition and size. They can be zero dimensional such as clusters of Au or Ag atoms, one dimensional like nanotubes, fibers and rods, two dimensional like flat sheets and films and three dimensional such as polycrystals [31]. In the case of the zero dimensional clusters, due to the quantum confinement extending in all three dimensions, nanomaterial properties remain the same regardless of directions.

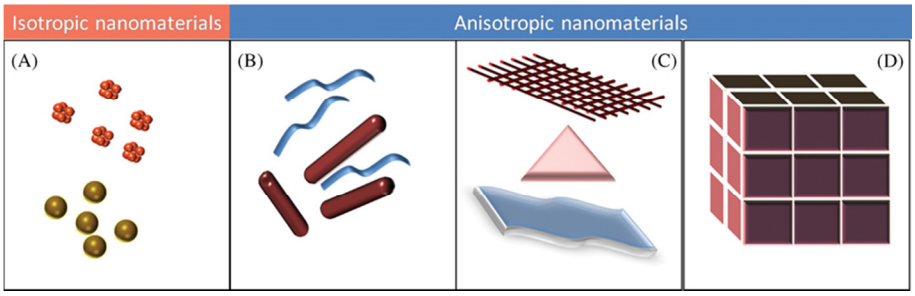

Figure 1-2: Types of nanocrystalline materials by size of their structural elements: 0D (zero-dimensional) clusters (A); 1D (one-dimensional) nanotubes, fibers and rods (B); 2D (two-dimensional) films and coats (C); 3D (three-dimensional) polycrystals (D) [31]

Another way of classifying nanomaterials is by their core composition, which is either hard, composed of inorganic materials [32-34] (CdTe, Au, Ag, iron oxide etc.), or soft [35], composed of organic macromolecules (dendrimers, polymers, liposomes, artificial proteins).

Many of these nanomaterials have size- dependent properties like surface plasmon resonance [36], scattering intensity [37] and fluorescence emission [38]. For example quantum dots [38], which are semiconductor nanocrystals, have small enough size that they exhibit quantum mechanical properties. The band-gap in a quantum dot determines the frequency range of emitted light and is inversely proportional to its size and shape-dependent [33, 34, 39]. Consequently, the color of emitted light shifts from blue to red with increasing quantum dot size (Figure 1-3).

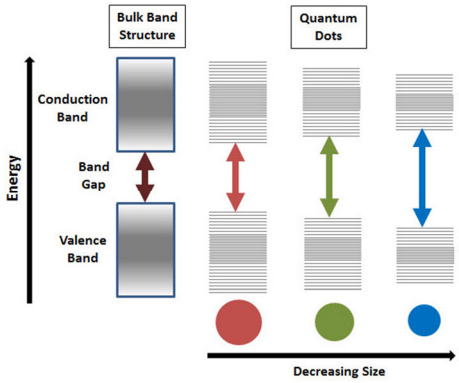

Figure 1-3: Splitting of energy levels in quantum dots due to the quantum confinement effect, semiconductor band gap increases with decrease in size of the nanocrystal

The first applications of nanotechnology mainly exploited the physicochemical properties of just one nanomaterial. For example gold nanoparticles exhibit a red shift in the surface plasmon resonance band upon assembly and also scatter strongly [40]. These are very useful properties of gold nanoparticles, which are still heavily explored for

biomedical imaging, chemical and biological sensing [41], catalysis applications [37, 40, 42].

As nanotechnology progressed, increasingly complex hybrid nanomaterials were made, which consisted of different combinations of nanostructures and/or molecules and are therefore called superstructures. Apart from the individual nanomaterial properties, superstructures exhibit most times new collective properties [43, 44]. Examples are FRET systems of quantum dot combined with gold nanoparticles [45, 46], controlled nanoparticle clusters, sheets and assemblies [43, 47-49], complex supramolecular helical nanoparticle assemblies [50-52], biomolecule-nanoparticle hybrids [53] and more.

1.3 Dynamic ligand interactions at nanoscale interfaces

Engineering complex functional matter in an equivalent manner as Nature does, remains still a big challenge for researchers. Natural meso- and macro-structures are built from nanosized molecules which are engaged in superstructures by supramolecular interactions [6, 8, 54]. Supramolecular interactions found in living systems are highly selective, like a key in a lock, and also abundant and yet quite diverse resulting in unique architectures [54]. Often the selectivity of such systems is reached through multivalency and cooperativity, concepts that go hand in hand with molecular recognition [54-57]. Multivalency is the "operation of multiple molecular recognition events of the same kind occurring simultaneously between two entities" [57]. For example, lectins are multivalent proteins, which are encountered in plants, animals and microbes and bind selectively different types of saccharides [58]. Despite the relatively low binding strength between each binding site and a specific saccharide, lectins exhibit increased overall binding strength by engaging more than one sugar binding sites at the same time. Through their multivalency potency, lectins can act as mediators for cell recognition and adhesion [59]. Cooperativity in multivalent systems happens when, following a first binding event, the second binding event is more (positive) or less favored (negative).

Artificial supramolecular nanosystems are also based on supramolecular interactions incorporating multivalency and often cooperativity. Nanoparticles, for example, can be functionalized with one or more types of ligands, that can even be spatially located e.g. mixed ligand [60], striped [61], Janus [62], patchy [63] nanoparticles. A variety of highly selective ligands bearing interaction motifs and receptors has been synthesized. Cyclodextrins [64], crown ethers [65], calixarenes [66], coordination complexes like bipyridyl [67], cucurbit(n)urils [68] and other biomolecule mimetic macrocycles [69, 70] have been the building blocks for instructing assembly processes [71, 72] for creating superstructures useful in material and sensing applications(Figure 1-4).

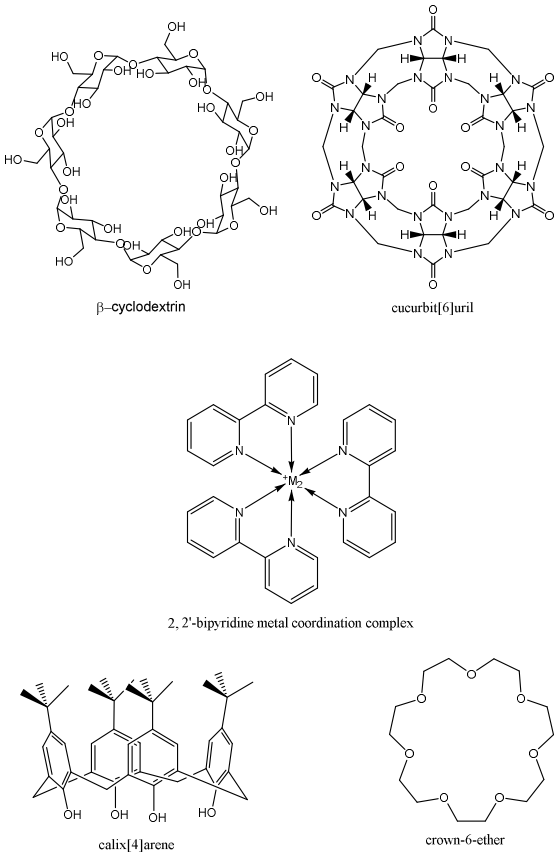

Figure 1-4: Molecular structures of building blocks often used for molecular recognition

The most important aspects in self-assembly are the dynamic and reversible nature of covalent or supramolecular interactions between complimentary interacting pairs of molecules or moieties featured on nanostructures. In supramolecular chemistry, the most well-known interactions are based on cyclodextrin host-guest systems [73]. Cyclodextrins are natural, cheap and non-toxic cyclic oligosaccharides with a cup-like structure. The external structure of cyclodextrins are hydrophilic and their cavity hydrophobic, allowing them to encapsulate hydrophobic guests [73]. Cyclodextrin-adamantane, cyclodextrin-ferrocene and cyclodextrin azobenzene constitute the most well-known complimentary interactions on nanosurfaces. Adamantane is known to bind very strong with β-cyclodextrin, ferrocene binding can be reversed by oxidation and azobenzene binding is UV-light driven [73]. The ability to tune on demand many of the cyclodextrin interactions either by physicochemical triggers or by multivalent or stronger binding monovalent competitors has turned cyclodextrins into one of the most popular nanomaterials [74, 75].

Despite the great advancements of Nanotechnology, one main challenge has to be met. All living systems operate mostly out-of-equilibrium, while most artificial nanostructures and superstructures are designed in equilibrium. For this purpose, a new branch of chemistry, called supramolecular systems chemistry, is being developed. Supramolecular Systems Chemistry [76] is dealing with out-of-equilibrium and far-from equilibrium systems with some exciting [77-79], yet limited applications, like writing self-erasing images using metastable nanoparticle "inks" [77], adamantane molecules that hop, skip and jump on cyclodextrin surfaces [64] and spatially selective nanoparticle functionalization driven by a DNA template [80]. Out-of-equilibrium assemblies are kinetically trapped assemblies, thus trapped in a local minimum of the energy landscape. It would take time, or activation energy, for them to be converted to more stable structures. Far-from-equilibrium assemblies are dissipative systems, therefore requiring a continuous supply of energy to be maintained.

1.4 1D, 2D and Diffusion NMR

Nuclear NMR spectroscopy [81] probes the environment of individual atomic nuclei, thus giving information on molecular structure. By 1H NMR spectroscopy [81] molecular structure can be derived by analyzing the chemical shifts, signal strength (intensity) and spin-spin coupling. Two-dimensional nuclear magnetic resonance spectroscopy (2D NMR) [81] is a set of nuclear magnetic resonance spectroscopy (NMR) techniques which plot data in a space defined by two frequency axes instead of only one. COrrelation SpectroscopY (COSY), J-spectroscopy, EXchange SpectroscopY (EXSY), and Nuclear Overhauser Effect SpectroscopY (NOESY) and Rotating frame Overhauser Effect SpectroscopY (ROESY) are some of two-dimensional NMR techniques. Two-dimensional NMR spectra resolve molecular information in two frequency axes rather than one and are especially useful in determining the structure of a molecule when resolution between frequencies along the chemical shift axis is too complicated. Combination of state-of-the-art 1D and 2D NMR methodologies make possible to measure physicochemical properties not only of a molecule but also "beyond the molecule", thus emerging properties of dynamic systems and supramolecular interactions between molecules [82]. For example, simple 1H titrations of two interacting species are used for stoichiometry and binding constant estimation [83]. Integration of peaks rising or disappearing over time can give insight into molecular reactions and interactions [84]. For nanoparticles, the broadening of the capping ligand peaks gives a first confirmation for the success of the functionalization or modification reaction [85]. Interpretation of two dimensional techniques such NOESY and ROESY detect pairs of nuclei that are close in space directed by non-covalent interactions, revealing the conformation and orientation of supramolecular complexes.

An indispensable NMR technique for studying systems at the nanoscale is Diffusion Ordered SpectroscopY (DOSY NMR) [86, 87]. This spectroscopic technique measures the translational diffusion of different species in solution, which under given conditions (viscosity, temperature) is dependent on the species shape [88] and size [89]. Other complimentary techniques that are used for the size and shape determination are Dynamic Light Scattering (DLS) [90, 91] and Transmission Electron Microscopy (TEM) [92, 93]. DLS is a very fast technique, giving accurate values for a wide range of sizes, from few nanometers to a few micrometers. Main drawbacks of DLS are sensitivity to contamination and also aggregation processes that take place. TEM provides information on element and compound structure giving high quality and very detailed images. Main disadvantages of TEM are the low contrast of organic molecules and potential artifacts from sample preparation. DOSY NMR is quite advantageous and many times superior technique in comparison to DLS and TEM, because it gives very detailed molecular information in combination with size and shape measurements. It required no tedious sample preparation and relatively low-volume, dilute samples. The main limitation of DOSY is its size range capability; it can measure from sub nanometer to only a few nanometers range.

DOSY NMR is a “virtual chromatography” [94], there is no need for physical separation of species in a mixture and therefore allows us to study complex and diverse systems such as natural and artificial self-assembled structures and their interactions in equilibrium [95]. Supramolecular interactions can be measured by observing the “apparent” diffusion of interacting species [94, 95]. For example, in nanoparticle-ligand interactions [96] the diffusion coefficient of an interacting ligand, a relatively small molecule, will appear to be lower because it interacts with a relatively bigger molecule, which diffuses slower, in this case the protein. The “apparent” value of the diffusion coefficient can help in the evaluation of binding strength of an interaction. Moreover, quantitative information can be extracted for possible multivalency and cooperativity effects. The usefulness of DOSY NMR is therefore evident because it has and can be used not only for characterizing the shape and size of novel types of nanostructures but also to evaluate selectivity, functionality and biological activity of natural and artificial nanostructures and superstructures.

DOSY NMR gives insight into equilibrium structures, but could also be used for the study of dynamic and kinetic processes and out of equilibrium systems with a concentration gradient [76]. Such systems and processes gather high scientific interest, because, as mentioned in the previous section, Nature operates mostly under out-of-equilibrium conditions and also because recently novel artificial out-of-equilibrium systems have been developed. Measuring accurately diffusion over time becomes an issue only when the concentration changes exhibit from several minutes to several hours. Rapid processes as well as very slow processes that extend for days don’t exhibit the problem of

diffusion inaccuracy over time. Efforts to overcome the problem of diffusion inaccuracy over time in systems under concentration gradients have led to the development of advanced processing software [97, 98], but still the study of such systems is in its infancy.

1.5 Nanomaterial based biomolecule sensors

Nanotechnology opened up new opportunities in the field of biomolecule sensing. Nanomaterial-based biosensors have significant advantages over conventional diagnostic systems in terms of simplicity, cost efficiency, sensitivity, specificity, and portability. Main parameters [99] to be considered when designing nanomaterial-based biosensors are a) the physicochemical properties of the nanomaterial core e.g. for quantum dots [38] their fluorescence excitation and emission wavelength and quantum yield, b) their surface chemistry [38] and functionalization e.g. for quantum dots can be thiol, triphenylphosphine oxide based ligands and others c) the selectivity and binding strength towards the target biomolecule. The majority of nanomaterial biosensors are designed to imitate natural biomolecule receptors and for that fact, they are based on supramolecular interactions and self-assembly [100] between the target biomolecule and the nanomaterial. A plethora of nanosensors has been developed for sensing all types of biomolecules; sugars [101], lipids [102], proteins [103], enzymes [104], antigens [105] and nucleic acids [60, 106]. The latest advancements in the field of bionanotechnology are engineered nanoparticles for theranostic applications [107]. One wonders what the future in nanosensing is since already so many applications both in vitro [108] and in vivo [109-111] have been developed. It is striking that despite the vast numbers of developed nanosensors published, still only a few [99] have been marketed. Toxicity of many core materials, reproducibility of the nanoparticle synthesis, nanoparticle or ligand instability are major bottlenecks [112, 113] to overcome for the commercialization of nanosensors.

1.6 Motivation, aim and outline of this research

In this thesis, the motivation was to progressively discover and understand molecular interactions that govern natural systems and beyond, and the goal was to acquire the ability to design, direct and control complex matter. Special focus was put on implementing and controlling supramolecular ligand interactions on nanoparticle surfaces with an emphasis on biomolecule sensing. Special focus was put on implementing and controlling supramolecular ligand interactions on nanoparticle surfaces with an emphasis on biomolecule sensing. NMR spectroscopy was identified as a main tool to study dynamics of complex matter and supramolecular strategies are implemented for designing nanoparticle based peptide receptors based on mixed ligand monolayers and ternary supramolecular quantum dot selective lectin sensors by varying the multivalency potency

of adamantane based sugar linkers. In detail, the following aspects are addressed in separate Chapters of this thesis:

In Chapter 2 a difficulty in the DOSY experiments performed in concentration evolving systems was brought to light. On such a system, the evolution of the concentration of species interferes with the measurement process, and creates a bias on the diffusion coefficient determination that may lead to erroneous interpretations. In this chapter, performing random permutation of the series of gradient strengths used during the DOSY experiment, which allows averaging out this bias, is proposed as solution. This approach, named as p-DOSY does not require changes in the pulse sequences nor in the processing software, and restores completely the full accuracy of the measure. This technique is demonstrated on the monitoring of the anomerization reaction of α- to β-glucose and can be extended to monitor the rate of reaction kinetics, to characterize in-operando transient species and measure their diffusion coefficients, or to observe molecular organization phenomena and dynamics effects. Specifically, in Nanotechnology, p-DOSY is an excellent tool for monitoring reactions on nanoparticle surfaces, such as end-group modification and ligand exchange reactions. Moreover, by p-DOSY, assembly kinetics or aggregation of nanoparticles could be studied by observing the shift of the diffusion coefficient to lower values.

Chapter 3 deals with the concept of multivalency and cooperativity in mixed monolayer protected gold nanoparticles featuring functional groups on their surfaces that can engage in interactions with peptides. Introduction of the functional groups required for peptide recognition was achieved by decoration of AuNPs with α,ω-functionalized thiols containing as recognition moieties a terminal trimethylalkyl ammonium group, an 18-crown-6 moiety, and a phenyl group, respectively. Main goal is to recognize selectively and bind stronger dipeptides that contain aromatic groups as a side chain, which should exhibit trivalent interactions with the AuNPs featuring all three functional groups. The sensitivity of DOSY NMR to the inherent size differences between ligands and receptors, often encountered in nanoparticle molecular recognition systems, turns DOSY NMR into the best choice for the elucidation of such interactions. Turning to DOSY NMR for quantifying the binding efficiency and selectivity of the devised nanoparticles was considered the most appropriate solution.

Chapter 4 explores the possibility to employ asymmetric sugar-adamantane linkers, exhibiting different supramolecular interactions, for crosslinking cyclodextrin nanoparticles with multivalent proteins called lectins into ternary, supramolecular NanoParticle Networks (NPN). The three building blocks are β-cyclodextrin-capped CdTe quantum dots, tetraethylene glycol-tethered mannose-adamantane cross-linkers (ADTEGMan) and the tetravalent lectin Concanavalin A. Only when lectin is present, sequential binding events take place; from quantum dot to linker and from linker to lectin,

leading to self-organization in-situ of the sensor through the formation of ternary supramolecular networks. The main goal of this Chapter is to selectively detect a tetravalent lectin called Concanavalin A by monitoring the loss of fluorescence signal of quantum dots in solution over time, caused by controlled network formation and consecutive flocculation and sedimentation.

Chapter 5 continues and extends the study of selective lectin sensing through controlled formation, flocculation and precipitation of ternary supramolecular quantum dot networks. In this chapter, asymmetric tetraethylene glycol-based mannose-tri-adamantane linkers (TriADTEGMan) are employed which, due to their multivalency potency, are bound in a non-dynamic fashion on the nanoparticle surface in aqueous solutions. The goal is to compare flocculation kinetics, tunability and specificity of lectin sensors that employ either trivalent or monovalent adamantane mannose linkers and to prove that these systems combine advantages from covalent e.g. stability, and from supramolecular systems e.g. tunability, reversibility. Ultimately, these systems are tested for detecting other mannose-binding lectins (Galanthus Nivalis and Lens Culinaris) as well.

Chapter 6 summarizes the most important findings of every chapter. By linking all the findings of this thesis, the questions answered are evaluated and a general conclusion is reached. With an eye on the future, some observations to extend the discussion further and beyond this thesis are added and new questions arisen are identified. Finally, a conclusion is reached by providing insight, guidelines and suggestions on designing and controlling multivalent, supramolecular interactions on the nanoparticle bionanointerface, between nanomaterials, ligands and biomolecules.

1.7 References

1. Whitesides, G.M., Nanoscience, nanotechnology, and chemistry. Small, 2005. 1(2): p. 172-179.
2. Feynman, R.P., There's plenty of room at the bottom. Engineering and science, 1960. 23(5): p. 22-36.
3. Biswas, A., et al., Advances in top–down and bottom–up surface nanofabrication: Techniques, applications & future prospects. Advances in Colloid and Interface Science, 2012. 170(1–2): p. 2-27.
4. Xia, Y., et al., Unconventional methods for fabricating and patterning nanostructures. Chemical reviews, 1999. 99(7): p. 1823-1848.
5. Wang, L., et al., Dynamic Nanoparticle Assemblies. Accounts of Chemical Research, 2012. 45(11): p. 1916-1926.
6. Whitesides, G.M. and B. Grzybowski, Self-assembly at all scales. Science, 2002. 295(5564): p. 2418-2421.

7. Whitesides, G.M., J.P. Mathias, and C.T. Seto, Molecular self-assembly and nanochemistry: a chemical strategy for the synthesis of nanostructures. 1991, DTIC Document.
8. Philp, D. and J.F. Stoddart, Self-assembly in natural and unnatural systems. Angewandte Chemie International Edition in English, 1996. 35(11): p. 1154-1196.
9. Cademartiri, L., et al., Using shape for self-assembly. Philosophical Transactions of the Royal Society of London A: Mathematical, Physical and Engineering Sciences, 2012. 370(1969): p. 2824-2847.
10. Whitesides, G.M., Bioinspiration: something for everyone. Interface Focus, 2015. 5(4): p. 20150031.
11. Chen, X., et al., Nanomaterials for renewable energy production and storage. Chemical Society Reviews, 2012. 41(23): p. 7909-7937.
12. Franklin, A.D., Nanomaterials in transistors: From high-performance to thin-film applications. Science, 2015. 349(6249): p. aab2750.
13. Gangadoo, S., A. Taylor-Robinson, and J. Chapman, From Replacement to Regeneration: Are Bio-Nanomaterials the Emerging Prospect for Therapy of Defective Joints and Bones. J Biotechnol Biomater, 2015. 5(187): p. 2.
14. Gogotsi, Y., What nano can do for energy storage. ACS nano, 2014. 8(6): p. 5369-5371.
15. Kamyshny, A. and S. Magdassi, Conductive nanomaterials for printed electronics. Small, 2014. 10(17): p. 3515-3535.
16. Korgel, B.A., Nanomaterials Developments for Higher-Performance Lithium Ion Batteries. The Journal of Physical Chemistry Letters, 2014. 5(4): p. 749-750.
17. Leary, S.P., et al., Toward the emergence of nanoneurosurgery: Part I—Progress in nanoscience, nanotechnology, and the comprehension of events in the mesoscale realm. Neurosurgery, 2005. 57(4): p. 606-634.
18. Mitragotri, S., et al., Accelerating the Translation of Nanomaterials in Biomedicine. ACS nano, 2015. 9(7): p. 6644-6654.
19. Oehlke, K., et al., Potential bioavailability enhancement of bioactive compounds using food-grade engineered nanomaterials: a review of the existing evidence. Food & function, 2014. 5(7): p. 1341-1359.
20. Xavier, J.R., et al., Advanced Nanomaterials: Promises for Improved Dental Tissue Regeneration, in Nanotechnology in Endodontics. 2015, Springer. p. 5-22.
21. DeVience, S.J., et al., Nanoscale NMR spectroscopy and imaging of multiple nuclear species. 2015. 10(2): p. 129-134.
22. Baccile, N., Application of Advanced Solid-State NMR Techniques to the Characterization of Nanomaterials: A Focus on Interfaces and Structure, in Ideas in Chemistry and Molecular Sciences. 2010, Wiley-VCH Verlag GmbH & Co. KGaA. p. 139-182.
23. Jeschke, G., Distance measurements in the nanometer range by pulse EPR. ChemPhysChem, 2002. 3(11): p. 927-932.
24. Kassies, R., et al., Combined AFM and confocal fluorescence microscope for applications in bio-nanotechnology. Journal of microscopy, 2005. 217(1): p. 109-116.
25. Müllerová, I., et al., Very low energy scanning electron microscopy in nanotechnology. International Journal of Nanotechnology, 2012. 9(8-9): p. 695-716.
26. Wang, Z.L., New developments in transmission electron microscopy for nanotechnology. Advanced Materials, 2003. 15(18): p. 1497-1514.

27. Horcas, I., et al., WSXM: a software for scanning probe microscopy and a tool for nanotechnology. Review of Scientific Instruments, 2007. 78(1): p. 013705.
28. Sun, Y. and Y. Ren, In situ synchrotron x-ray techniques for real-time probing of colloidal nanoparticle synthesis. Particle and Particle Systems Characterization, 2013. 30(5): p. 399-419.
29. Grigorenko, A., et al., Nanometric optical tweezers based on nanostructured substrates. Nature Photonics, 2008. 2(6): p. 365-370.
30. Jean-Marie, L., Supramolecular chemistry: from molecular information towards self-organization and complex matter. Reports on Progress in Physics, 2004. 67(3): p. 249.
31. Sajanlal, P.R., et al., Anisotropic nanomaterials: structure, growth, assembly, and functions. Nano Reviews, 2011. 2: p. 10.3402/nano.v2i0.5883.
32. Ferrando, R., J. Jellinek, and R.L. Johnston, Nanoalloys: From theory to applications of alloy clusters and nanoparticles. Chemical Reviews, 2008. 108(3): p. 845-910.
33. Leutwyler, W.K., S.L. Bürgi, and H. Burgl, Semiconductor clusters, nanocrystals, and quantum dots. Science, 1996. 271(5251): p. 933-937.
34. Tao, A.R., S. Habas, and P. Yang, Shape control of colloidal metal nanocrystals. Small, 2008. 4(3): p. 310-325.
35. Hamley, I., Nanotechnology with soft materials. Angewandte Chemie International Edition, 2003. 42(15): p. 1692-1712.
36. Guo, X., Surface plasmon resonance based biosensor technique: A review. Journal of Biophotonics, 2012. 5(7): p. 483-501.
37. Huang, X. and M.A. El-Sayed, Gold nanoparticles: Optical properties and implementations in cancer diagnosis and photothermal therapy. Journal of Advanced Research, 2010. 1(1): p. 13-28.
38. Michalet, X., et al., Quantum dots for live cells, in vivo imaging, and diagnostics. science, 2005. 307(5709): p. 538-544.
39. Burda, C., et al., Chemistry and properties of nanocrystals of different shapes. Chemical reviews, 2005. 105(4): p. 1025-1102.
40. Daniel, M.-C. and D. Astruc, Gold nanoparticles: assembly, supramolecular chemistry, quantum-size-related properties, and applications toward biology, catalysis, and nanotechnology. Chemical reviews, 2004. 104(1): p. 293-346.
41. Saha, K., et al., Gold nanoparticles in chemical and biological sensing. Chemical Reviews, 2012. 112(5): p. 2739-2779.
42. Huang, T., F. Meng, and L. Qi, Facile Synthesis and One-Dimensional Assembly of Cyclodextrin-Capped Gold Nanoparticles and Their Applications in Catalysis and Surface-Enhanced Raman Scattering. The Journal of Physical Chemistry C, 2009. 113(31): p. 13636-13642.
43. Chen, W., et al., Nanoparticle Superstructures Made by Polymerase Chain Reaction: Collective Interactions of Nanoparticles and a New Principle for Chiral Materials. Nano Letters, 2009. 9(5): p. 2153-2159.
44. Pileni, M.-P., Self-assembly of inorganic nanocrystals: fabrication and collective intrinsic properties. Accounts of chemical research, 2007. 40(8): p. 685-693.
45. Uddayasankar, U. and U.J. Krull, Energy Transfer Assays Using Quantum Dot–Gold Nanoparticle Complexes: Optimizing Oligonucleotide Assay Configuration Using Monovalently Conjugated Quantum Dots. Langmuir, 2015. 31(29): p. 8194-8204.

46. Shi, J., et al., A fluorescence resonance energy transfer (FRET) biosensor based on graphene quantum dots (GQDs) and gold nanoparticles (AuNPs) for the detection of mecA gene sequence of Staphylococcus aureus. Biosensors and Bioelectronics, 2015. 67: p. 595-600.
47. Chou, L.Y.T., K. Zagorovsky, and W.C.W. Chan, DNA assembly of nanoparticle superstructures for controlled biological delivery and elimination. 2014. 9(2): p. 148-155.
48. Duan, J., et al., Azobenzene mesogen-passivated gold nanoparticles: Controlled preparation, self-organized superstructures, thermal behavior and photoisomerization. Materials Chemistry and Physics, 2014. 148(3): p. 1013-1021.
49. Li, L.-L. and Y. Lu, Regiospecific Hetero-Assembly of DNA-Functionalized Plasmonic Upconversion Superstructures. Journal of the American Chemical Society, 2015. 137(16): p. 5272-5275.
50. Chen, C.-L., P. Zhang, and N.L. Rosi, A new peptide-based method for the design and synthesis of nanoparticle superstructures: construction of highly ordered gold nanoparticle double helices. Journal of the American Chemical Society, 2008. 130(41): p. 13555-13557.
51. Singh, G., et al., Self-assembly of magnetite nanocubes into helical superstructures. Science, 2014. 345(6201): p. 1149-1153.
52. Song, C., et al., Tailorable Plasmonic Circular Dichroism Properties of Helical Nanoparticle Superstructures. Nano Letters, 2013. 13(7): p. 3256-3261.
53. Katz, E. and I. Willner, Integrated Nanoparticle–Biomolecule Hybrid Systems: Synthesis, Properties, and Applications. Angewandte Chemie International Edition, 2004. 43(45): p. 6042-6108.
54. Mammen, M., S.-K. Choi, and G.M. Whitesides, Polyvalent interactions in biological systems: implications for design and use of multivalent ligands and inhibitors. Angewandte Chemie International Edition, 1998. 37(20): p. 2754-2794.
55. Badjić, J.D., et al., Multivalency and cooperativity in supramolecular chemistry. Accounts of Chemical Research, 2005. 38(9): p. 723-732.
56. Mulder, A., J. Huskens, and D.N. Reinhoudt, Multivalency in supramolecular chemistry and nanofabrication. Organic and Biomolecular Chemistry, 2004. 2(23): p. 3409-3424.
57. Krishnamurthy, V.M., L.A. Estroff, and G.M. Whitesides, Multivalency in ligand design. Fragment-based approaches in drug discovery, 2006. 34: p. 11-53.
58. Wittmann, V. and R.J. Pieters, Bridging lectin binding sites by multivalent carbohydrates. Chemical Society Reviews, 2013. 42(10): p. 4492-4503.
59. Lindhorst, T.K. and S. Kubik, Supramolecular Approaches to the Study of Glycobiology, in Supramolecular Chemistry. 2012, John Wiley & Sons, Ltd.
60. Pan, W., et al., Multiplexed Detection and Imaging of Intracellular mRNAs Using a Four-Color Nanoprobe. Analytical Chemistry, 2013. 85(21): p. 10581-10588.
61. Cho, E.S., et al., Ultrasensitive detection of toxic cations through changes in the tunnelling current across films of striped nanoparticles. 2012. 11(11): p. 978-985.
62. Lattuada, M. and T.A. Hatton, Synthesis, properties and applications of Janus nanoparticles. Nano Today, 2011. 6(3): p. 286-308.
63. Walker, D.A., et al., Geometric curvature controls the chemical patchiness and self-assembly of nanoparticles. 2013. 8(9): p. 676-681.
64. Turnbull, W.B., Multivalent interactions: A hop, skip and jump. 2011. 3(4): p. 267-268.

65. Zhang, M., et al., Self-Healing Supramolecular Gels Formed by Crown Ether Based Host–Guest Interactions. Angewandte Chemie, 2012. 124(28): p. 7117-7121.
66. Wei, A., Calixarene-encapsulated nanoparticles: self-assembly into functional nanomaterials. Chemical communications (Cambridge, England), 2006(15): p. 1581-1591.
67. Chichak, K.S., et al., Molecular Borromean Rings. Science, 2004. 304(5675): p. 1308-1312.
68. Taylor, R.W., et al., Precise subnanometer plasmonic junctions for SERS within gold nanoparticle assemblies using cucurbit [n] uril "glue". ACS nano, 2011. 5(5): p. 3878-3887.
69. Kubik, S., Carbohydrate recognition: A minimalistic approach to binding. Nature chemistry, 2012. 4(9): p. 697-698.
70. Lippe, J. and M. Mazik, Carbohydrate Receptors Combining Both a Macrocyclic Building Block and Flexible Side Arms as Recognition Units: Design, Syntheses, and Binding Studies. The Journal of organic chemistry, 2015. 80(3): p. 1427-1439.
71. Hu, X.-Y., et al., Dynamic Supramolecular Complexes Constructed by Orthogonal Self-Assembly. Accounts of Chemical Research, 2014. 47(7): p. 2041-2051.
72. Saha, M.L., et al., Orthogonality in discrete self-assembly - survey of current concepts. Chemical Society Reviews, 2013. 42(16): p. 6860-6909.
73. Liu, B.-w., et al., Macromolecules based on recognition between cyclodextrin and guest molecules: Synthesis, properties and functions. European Polymer Journal, 2015. 65: p. 63-81.
74. Harada, A. and Y. Takashima, Macromolecular Recognition and Macroscopic Interactions by Cyclodextrins. The Chemical Record, 2013. 13(5): p. 420-431.
75. Hashidzume, A., H. Yamaguchi, and A. Harada, Cyclodextrin-Based Molecular Machines, in Molecular Machines and Motors. 2014, Springer. p. 71-110.
76. Mattia, E. and S. Otto, Supramolecular systems chemistry. 2015. 10(2): p. 111-119.
77. Klajn, R., et al., Writing Self-Erasing Images using Metastable Nanoparticle "Inks". Angewandte Chemie International Edition, 2009. 48(38): p. 7035-7039.
78. Nguyen, R., et al., Dynamic Combinatorial Evolution within Self-Replicating Supramolecular Assemblies. Angewandte Chemie International Edition, 2009. 48(6): p. 1093-1096.
79. Ragazzon, G., et al., Light-powered autonomous and directional molecular motion of a dissipative self-assembling system. 2015. 10(1): p. 70-75.
80. Nowak, P., et al., Localized Template-Driven Functionalization of Nanoparticles by Dynamic Combinatorial Chemistry. Angewandte Chemie International Edition, 2015. 54(14): p. 4192-4197.
81. Friebolin, H. and J.K. Becconsall, Basic one-and two-dimensional NMR spectroscopy. 1993: VCH Weinheim.
82. García, J., L.G. Martins, and M. Pons, NMR Spectroscopy in Solution, in Supramolecular Chemistry. 2012, John Wiley & Sons, Ltd.
83. Funasaki, N., et al., NMR Chemical Shift References for Binding Constant Determination in Aqueous Solutions. The Journal of Physical Chemistry B, 2001. 105(30): p. 7361-7365.

84. Pastor, A. and E. Martínez-Viviente, NMR spectroscopy in coordination supramolecular chemistry: A unique and powerful methodology. Coordination Chemistry Reviews, 2008. 252(21–22): p. 2314-2345.
85. Liu, X., et al., Determination of monolayer-protected gold nanoparticle ligand–shell morphology using NMR. 2012. 3: p. 1182.
86. Stejskal, E.O., Use of spin echoes in a pulsed magnetic-field gradient to study anisotropie, restricted diffusion and flow. The Journal of Chemical Physics, 1965. 43(10): p. 3597-3603.
87. Stejskal, E.O. and J.E. Tanner, Spin diffusion measurements: Spin echoes in the presence of a time-dependent field gradient. The Journal of Chemical Physics, 1965. 42(1): p. 288-292.
88. Allouche, L., A. Marquis, and J.M. Lehn, Discrimination of Metallosupramolecular Architectures in Solution by Using Diffusion Ordered Spectroscopy (DOSY) Experiments: Double-Stranded Helicates of Different Lengths. Chemistry-A European Journal, 2006. 12(28): p. 7520-7525.
89. Mirtschin, S., et al., A coordination cage with an adaptable cavity size. Journal of the American Chemical Society, 2010. 132(40): p. 14004-14005.
90. Jans, H., et al., Dynamic Light Scattering as a Powerful Tool for Gold Nanoparticle Bioconjugation and Biomolecular Binding Studies. Analytical Chemistry, 2009. 81(22): p. 9425-9432.
91. Khlebtsov, B.N. and N.G. Khlebtsov, On the measurement of gold nanoparticle sizes by the dynamic light scattering method. Colloid Journal, 2011. 73(1): p. 118-127.
92. Wang, Z.L., Transmission Electron Microscopy of Shape-Controlled Nanocrystals and Their Assemblies. The Journal of Physical Chemistry B, 2000. 104(6): p. 1153-1175.
93. Pyrz, W.D. and D.J. Buttrey, Particle Size Determination Using TEM: A Discussion of Image Acquisition and Analysis for the Novice Microscopist. Langmuir, 2008. 24(20): p. 11350-11360.
94. Gounarides, J.S., A. Chen, and M.J. Shapiro, Nuclear magnetic resonance chromatography: Applications of pulse field gradient diffusion NMR to mixture analysis and ligand-receptor interactions. Journal of Chromatography B: Biomedical Sciences and Applications, 1999. 725(1): p. 79-90.
95. Cohen, Y., L. Avram, and L. Frish, Diffusion NMR spectroscopy in supramolecular and combinatorial chemistry: An old parameter - New insights. Angewandte Chemie - International Edition, 2005. 44(4): p. 520-554.
96. Valentini, M., et al., Diffusion NMR Spectroscopy for the Characterization of the Size and Interactions of Colloidal Matter: The Case of Vesicles and Nanoparticles. Journal of the American Chemical Society, 2004. 126(7): p. 2142-2147.
97. Khajeh, M., et al., Reaction kinetics studied using diffusion-ordered spectroscopy and multiway chemometrics. Analytical chemistry, 2010. 82(5): p. 2102-2108.
98. Nilsson, M., et al., Diffusion NMR and trilinear analysis in the study of reaction kinetics. Chem. Commun., 2009(10): p. 1252-1254.
99. Howes, P.D., R. Chandrawati, and M.M. Stevens, Bionanotechnology. Colloidal nanoparticles as advanced biological sensors. Science (New York, N.Y.), 2014. 346(6205): p. 1247390.

100. Petryayeva, E., W.R. Algar, and I.L. Medintz, Quantum dots in bioanalysis: A review of applications across various platforms for fluorescence spectroscopy and imaging. Applied Spectroscopy, 2013. 67(3): p. 215-252.
101. Alivisatos, P., The use of nanocrystals in biological detection. Nature Biotechnology, 2004. 22(1): p. 47-52.
102. Katz, E. and I. Willner, Integrated nanoparticle-biomolecule hybrid systems: Synthesis, properties, and applications. Angewandte Chemie - International Edition, 2004. 43(45): p. 6042-6108.
103. Busseron, E., et al., Supramolecular self-assemblies as functional nanomaterials. Nanoscale, 2013. 5(16): p. 7098-7140.
104. Aslan, K., et al., Saccharide sensing using gold and silver nanoparticles - A review. Journal of Fluorescence, 2004. 14(4): p. 391-400.
105. Raj, V., et al., Detection of cholesterol by digitonin conjugated gold nanoparticles. Biosensors and Bioelectronics, 2011. 27(1): p. 197-200.
106. Samanta, A. and B.J. Ravoo, Magnetic Separation of Proteins by a Self-Assembled Supramolecular Ternary Complex. Angewandte Chemie International Edition, 2014. 53(47): p. 12946-12950.
107. De La Rica, R., D. Aili, and M.M. Stevens, Enzyme-responsive nanoparticles for drug release and diagnostics. Advanced drug delivery reviews, 2012. 64(11): p. 967-978.
108. de la Rica, R. and M.M. Stevens, Plasmonic ELISA for the ultrasensitive detection of disease biomarkers with the naked eye. 2012. 7(12): p. 821-824.
109. Zhang, J., et al., Sequence-specific detection of femtomolar DNA via a chronocoulometric DNA sensor (CDS): Effects of nanoparticle-mediated amplification and nanoscale control of DNA assembly at electrodes. Journal of the American Chemical Society, 2006. 128(26): p. 8575-8580.
110. Xie, J., S. Lee, and X. Chen, Nanoparticle-based theranostic agents. Advanced Drug Delivery Reviews, 2010. 62(11): p. 1064-1079.
111. De La Rica, R. and M.M. Stevens, Plasmonic ELISA for the ultrasensitive detection of disease biomarkers with the naked eye. Nature nanotechnology, 2012. 7(12): p. 821-824.
112. Åkerman, M.E., et al., Nanocrystal targeting in vivo. Proceedings of the National Academy of Sciences of the United States of America, 2002. 99(20): p. 12617-12621.
113. Lewin, M., et al., Tat peptide-derivatized magnetic nanoparticles allow in vivo tracking and recovery of progenitor cells. Nature Biotechnology, 2000. 18(4): p. 410-414.
114. Qian, X., et al., In vivo tumor targeting and spectroscopic detection with surface-enhanced Raman nanoparticle tags. Nature Biotechnology, 2008. 26(1): p. 83-90.
115. Desai, N., Challenges in Development of Nanoparticle-Based Therapeutics. The AAPS Journal, 2012. 14(2): p. 282-295.
116. Khanna, P., et al., Nanotoxicity: An interplay of oxidative stress, inflammation and cell death. Nanomaterials, 2015. 5(3): p. 1163-1180.

Chapter 2 Accurate DOSY measure for concentration evolving systems using permutated DOSY (p-DOSY)

Abstract

NMR spectroscopy is an excellent tool for monitoring in-situ chemical reactions. In particular, DOSY is well suited to characterize transient species by the determination of their sizes. However, here a difficulty in the DOSY experiments performed in concentration evolving systems was brought to light. On such a system, the evolution of the concentration of species interferes with the measurement process, and creates a bias on the diffusion coefficient determination that may lead to erroneous interpretations. In this chapter, a random permutation of the series of gradient strengths used during the DOSY experiment is showed to average out this bias. This approach, named as p-DOSY does not require changes in the pulse sequences nor in the processing software, and restores completely the full accuracy of the measure. This technique is demonstrated on the monitoring of the anomerization reaction of α- to β-glucose and can be extended to the analysis of chemical reactions and kinetic processes away from equilibrium and can be used to monitor the rate of reaction kinetics, to characterize in-operando transient species and measure their diffusion coefficients, or to observe molecular organization phenomena and dynamics effects. Specifically, in Nanotechnology, p-DOSY is an excellent tool for monitoring reactions on nanoparticle surfaces, such as end-group modification and ligand exchange reactions. Moreover, by p-DOSY, assembly kinetics or aggregation of nanoparticles could be studied by observing the shift of the diffusion coefficient to lower values.

Part of this Chapter has been published as: M. Oikonomou, J. Asencio-Hernández, A.H. Velders, M.-A. Delsuc, Accurate DOSY measure for out-of-equilibrium systems using permutated DOSY (p-DOSY), Journal of Magnetic Resonance, 258 (2015) 12-16

2.1 Introduction

Diffusion Ordered SpectroscopY (DOSY) is an NMR technique separating components in a mixture spectroscopically according to their translational diffusion [1, 2]. Considered as an NMR chromatographic technique, DOSY NMR has been widely used in life sciences and chemistry for the analysis of complex mixtures, such as biological extracts [3], environmental fluids [4], supramolecular chemistry [5, 6], nanoparticles [7, 8], or pharmaceutical formulations [9]. For spherical shaped components the diffusion coefficient D is inversely proportional to the hydrodynamic radius, r_H as described by the Stokes–Einstein Equation 2-1:

$$D = \frac{k_B T}{6 \pi \eta r}$$

Equation 2-1

,where D is the diffusion coefficient, k_B is Boltzmann's constant, T is the absolute temperature, η is viscosity, r is the hydrodynamic radius. Other shapes can be handled either with extended analytical models [10] or by a statistical description [11, 12].

A DOSY experiment typically consists in a series of spin echo or stimulated echo spectra recorded with increasing gradient field strength. When measured with the Stimulated Echo pulse sequence (STE), diffusion coefficients can be determined by analyzing the signal amplitude as a function of the square of the gradient pulse area using the Stejskal–Tanner equation, [13] given here for squared pulses in Equation 2-2:

$$I = I_0 e^{-D \gamma^2 g^2 \delta^2 (\Delta - \frac{\delta}{3})}$$

Equation 2-2

where I and I_0 are the signal intensities obtained with gradients strengths of g and 0, respectively, D is the diffusion coefficient, δ is the gradient pulse duration, Δ is the effective diffusion delay defined as the time between the bipolar gradients, and γ is the gyromagnetic ratio of the spin under study; see [14-18]for details.

The analysis of the diffusion coefficients is a powerful tool to gain insight on molecular sizes and shapes [7, 19, 20], and can also be used to investigate molecular interactions [21-23], polymer polydispersity [18, 24], or to characterize reactive intermediates [15-18].

However, when measuring DOSY experiment on a concentration evolving system, a difficulty arises. According to the classical Stejskal–Tanner equation, the intensity, at each gradient strength, depends on the intensity I_0 with no gradient applied.

Usually, I_0 is measured at the beginning of the DOSY experiment and considered constant throughout the measurement. However, in concentration evolving systems, I_0 is not constant anymore but varies continuously, due to evolution of the concentrations. Consequently, throughout the DOSY measurement, the signal intensity measured for a given species will depend on the concentration evolution as well as the increasing gradient strength, and will appear to decay either too rapidly or too slowly, depending on the evolution of the concentration, decreasing or increasing over the time of the measurement, creating a bias in the analysis.

The kinetic rates of a concentration evolving system have to be taken into account and be compared to the timeframe of the DOSY measurement. Rapid DOSY measurements, of a few minutes or less, monitoring systems with slow kinetic rates, where equilibrium is reached in hours, are not affected to a significant degree, because only minor concentration changes occur over the experimental time. On the other extreme, long DOSY measurements, lasting a couple hours, monitoring systems with fast kinetic rates, where equilibrium is reached in a few minutes or less, are not affected either, but fail to record dynamic information of the system such as reactive intermediates. The effect is most obvious for systems with intermediate kinetic rates (e.g. for first-order kinetics, rate constants between 10^{-3} to 10^{-5} sec^{-1}) monitored by DOSY measurements performed in an experimental time similar to the rate constant of the chemical systems, so from few minutes to a few hours. In this case, the DOSY spectra display a shift of the peaks along the diffusion coefficient axis leading to wrong results.

Nilsson et al. [25] proposed the use of trilinear multivariate analysis in order to characterize both the reaction kinetics and the diffusion coefficient, in the analysis of a set of diffusion experiments measured during the chemical reaction. In this case the concentration variation is used as a third dimension in the multiway analysis. However, in this approach, the DOSY measurements are supposed to be rapid compared to the kinetic rates, and there is no compensation for the unavoidable bias in the diffusion coefficient measure. After a literature study, the DOSY studies performed so far on concentration evolving systems [15-17, 25, 26] seem not to have taken into account the analytical bias caused by concentration variations.

Within a single DOSY measurement, a series of stimulated echo spectra with pulse gradient strengths sampled in a permutated manner is proposed to be measured, as it was already proposed in order to reduce F_1 artifacts in 2D NMR spectroscopy [27].

A permutation of the list of gradient strengths allows the separation of the experimental time, during which the system evolves, from the gradient strength sampling, thus removing the experimental bias. Knowing the actual evolution of the concentration, an optimal permutation could eventually be designed. However, this knowledge is usually

not available and such an optimal permutation not accessible, so random permutations of the gradient list is performed. This permutation distributes randomly the concentration variation over the whole range of gradients, actually transforming an experimental bias into an additional random noise. The analysis of the permutated experiment leads to a less precise measure (larger error-bars) but eventually more accurate (less systematic error). Each realization of the random permutation may remove only partially the systematic error, and the accuracy is improved with a larger number of gradient levels.

2.2 Experimental

DOSY NMR measurements were carried out both on a Bruker and on a Varian instrument (for Varian experiments see SI, S3-S6). The Bruker instrument was a 500 Advance I NMR spectrometer, operating at 500.137 MHz for 1H, equipped with a 5 mm TXI probe. The pulse sequence used was a longitudinal eddy current delay bipolar gradient pulse (ledbpgp2s). An exponential gradient list of 32 values was created by using the standard AU program dosy. Experiments were acquired with 8 scans, $\delta/2$ of 3.0 ms and Δ of 150 ms, for an overall time of 23:09 min. A series of 15 DOSY measurements was acquired at a temperature of 300 K for a total duration of 6.0 h. Before and after every DOSY measurement, an 8 scans proton spectrum was recorded. The experiment was duplicated, once with regularly increasing series of gradients, and once with a permutated series.

The permutated series are computed by randomizing the sequential list of pulse field gradient strengths, and the DOSY is measured with a new list of gradient strengths in permutated order. This protocol has been named permutated-DOSY (p-DOSY). To permutate the list of pulse field gradient strengths an ad-hoc python script (see SI, S7) is employed, and the permutated list was used for acquisition and processing. On the Bruker instrument, in order to perform and process a p-DOSY measurement, the files Difframp and difflist created by the standard AU program dosy has to be replaced with the permutated file versions of Difframp and difflist created by the python script. On the Varian instrument, the permutation of the list of pulse field gradients is performed by activating the randomization flag in the acquisition parameters.

The p-DOSY approach and its capacity to restore accuracy in the determination of diffusion coefficients was tested using glucose anomerization as a test case for concentration evolving systems. Thus, the diffusion coefficient of glucose was monitored during the equilibration from pure α-glucose to the anomeric equilibrium of α and β-glucose [28] (Figure 2-1).

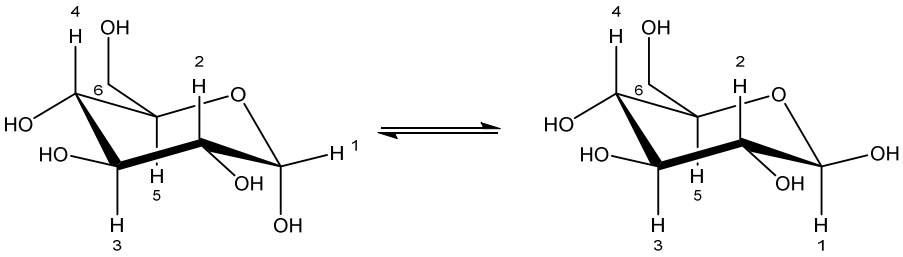

Figure 2-1: Anomerization of α-glucose to β-glucose with proton numbering.

The anomerization of α to β-glucose was followed by acquiring a series of 15 DOSY measurements for approximately 6.0 h, with α-d-glucose varying from 96.6% to 44.6%. A stock solution of 100.0 mM α-d-glucose in DMSO was prepared. 100 µL of the glucose stock solution were added in 900 µL D2O resulting in final concentration of 10.0 mM. Glucose crystalizes in the α form, as a consequence, this form is dominant in the solution just after dissolution.

The DOSY spectra acquired on Bruker were processed with the NMR notebook program (version 2.7, NMRTEC France), using the DOSY MaxEnt implementation [29, 30]. The experiments performed on Varian were analyzed with the vnmrj (version 6.3) software. In both cases, no modification had to be made to the computation protocol despite the permutated entries in the DOSY file.

The final diffusion coefficients were calculated from the average position of the anomeric signal for each species. Error bars were estimated as the standard deviation along the diffusion axis of the different signals. Minor viscosity variations were compensated by normalizing all measurements to the DMSO diffusion coefficient.

2.3 Results and Discussion

The diffusion coefficients in water of both species α and β-glucose are expected to be very similar, as they have very similar shapes. However, they appear with quite different diffusion coefficients when measured with a standard DOSY experiment, acquired in a sequential manner, as can be seen in Figure 2-2 and Figure 2-4b. In particular, the signals from the β-glucose, such as the β-H1 proton at 4.56 ppm, are found initially at a markedly slower diffusion coefficient and recover the normal value over the course of the experiment. This is the result of the progressive increase of concentration of β-glucose over the duration of a single DOSY measurement, which creates a bias in the exponential analysis of the signal. At the end of the 6 h experiment, thus at the 15th DOSY

measurement, the diffusion recovery is not complete although the reaction is almost at equilibrium (Figure 2-4a and Figure 2-4b).

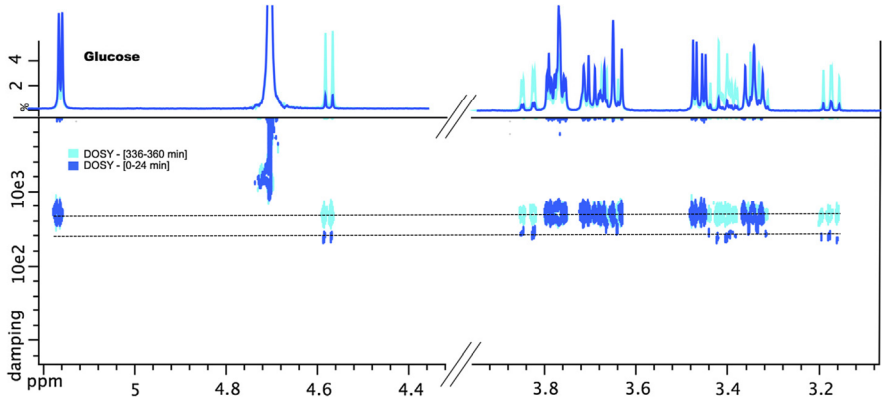

Figure 2-2: Overlay of two standard DOSY experiments with their corresponding 1H spectra, showing diffusion bias for both glucose anomers, acquired at the beginning of glucose anomerization reaction (0–24 min) (blue color) and (b) at the end of the reaction (at equilibrium) (336-360 min) (light blue color).

On the other hand, this bias is completely absent when the anomerization equilibrium is monitored using the p-DOSY measurements, run under the same conditions (Figure 2-3).

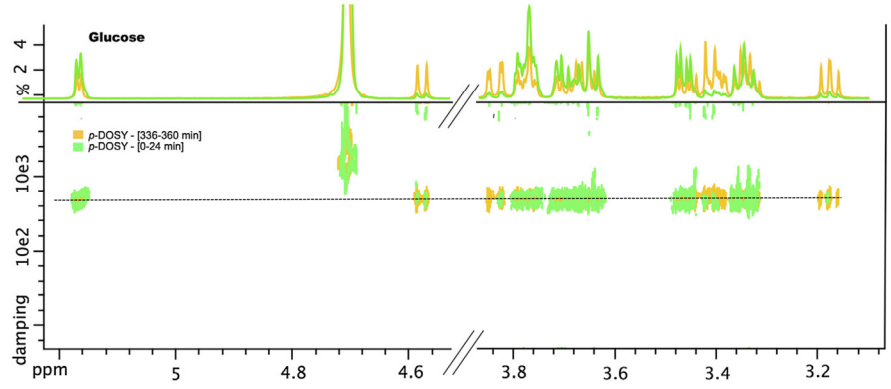

Figure 2-3: Overlay of two p-DOSY experiments with their corresponding 1H spectra, showing the restoration of diffusion accuracy of both glucose anomers, acquired at the beginning of glucose anomerization reaction (0–24 min) (green color) and (b) at the end of the reaction (at equilibrium) (336-360 min) (yellow color).

In both experiments, the diffusion coefficients of water and DMSO display the standard values for all experiments run during the kinetics, indicating that the error on β-glucose is not due to an experimental bias but solely due to the variation of the concentration. Figure 2-4 presents the evolution of the DOSY signal intensities and of the apparent diffusion coefficients over the course of the experiment. It shows that the initial

β-glucose concentration is very low, and that the two populations equilibrate slowly, so that 6 h are not sufficient to reach the complete equilibrium. When measured with the standard DOSY experiment, the apparent β-glucose diffusion coefficient varies in an anomalous manner before converging toward the correct value, while the p-DOSY measure presents stable measurements for both species.

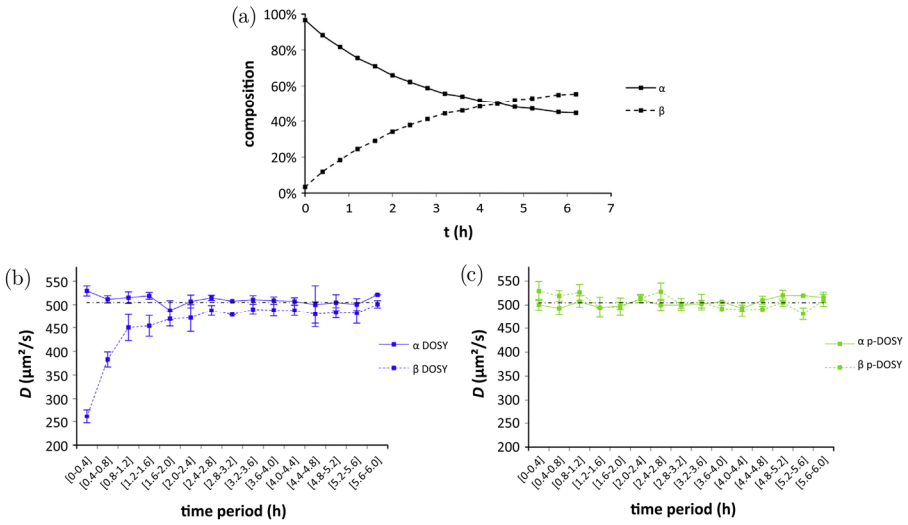

Figure 2-4: (a) Concentration evolution of α, β-glucose over experimental time, measured as the intensity of the anomeric proton peak based on 1D experiments interleaved during the p-DOSY experiment series; (b) evolution of the apparent diffusion coefficients of α and β-glucose over experimental time based on a series of sequential conventional DOSY measurements; (c) same as b, obtained with the p-DOSY experiment. In (b) and (c) the horizontal dotted line is located at the diffusion coefficient of α-glucose, measured as the mean value of p-DOSY value over the whole period.

The poor accuracy of the diffusion coefficient of β -glucose is attributed to miscalculation of the analysis of the reference intensity, I_0. The diffusion coefficient of β-glucose consequently, appears to have an incorrect low value. This effect is stronger in the first DOSY measurements since there is a higher kinetic rate. Similarly, the α-glucose that evolves in the opposite direction, displays an apparent diffusion coefficient slightly larger than expected in the first DOSY measurements. The effect is less marked because the relative concentration variation of the α-glucose is less important than in the case of β-glucose.

On the other hand, the experiment performed with a series of p-DOSY measurements does not display this systematic error, and accurate values are determined throughout the whole experiment. Because of the dispersion effect of the random permutation operation, the systematic evolution of the concentration is transformed here into random errors on the I_0 value. This added random noise has no effect on the analysis, but disperses in a random manner the concentration variation over the gradient list, thus

providing a way to average out bias. However, because of the added noise, a slightly less precise determination of the diffusion coefficients is expected. This effect, while not very strong, can be observed Figure 2-4c by the evolution of the error bars on the p-DOSY determined diffusion coefficients. The error bars present a somewhat larger spreading in the beginning of the kinetic and converge toward a minimal value.

In a nutshell, one can say that the p-DOSY experiment provides on concentration evolving chemical systems, a slightly less precise, but much more accurate determination of the diffusion coefficient than in the standard DOSY experiment.

2.4 Conclusion

The accurate estimation of diffusion coefficients is challenging in many systems away from equilibrium such as chemical reactions or dissipative, far-from equilibrium systems. An inherent characteristic of these systems is the evolution of the concentration of the different components during a DOSY NMR experiment. Since the basis of a single DOSY measurement is the analysis of the exponential decay of the signal with increasing gradient strength. Concentration evolution, within the characteristic measurement time, creates a bias, which can lead to large errors in the diffusion coefficient estimation. This was observed for the test case of the anomerization of glucose. Randomizing the list of gradient strength arrays within a single DOSY measurement, decouples the gradient evolution from the concentration evolution and removes the bias in the analysis, thus restoring the accuracy of the measure. The concentration evolution is still there though, as a noise source, and may impact the precision of the measure compared to a static sample, although its impact is minimal. Depending on the spectrometer software, this experiment requires little or no modification of the standard procedure, and the produced data-set can easily be analyzed using regular processing programs.

Altogether, the DOSY experiment with a randomized list of gradients (the permutated DOSY or p-DOSY) is an unbiased experiment in the presence of an evolving system, in contrast to conventional DOSY. It is perfectly suited for the analysis of chemical reactions and kinetic processes of systems away from equilibrium. It can be used to monitor the rate of reaction kinetics, to characterize in-operando transient systems or to observe kinetics of assembly phenomena and dynamics effects. To measure kinetic rates, the calculated, by fitting, I_0 intensity values, acquired by a series of DOSY measurements, can be plotted over time. Since intensity at zero gradients, I_0 is proportional to concentration; the kinetic rates are represented by the slope of the curve. Other kinetic processes, such as assembly kinetics, aggregation, formation of reactive intermediates and dynamics effects in slow exchange can also be monitored by observing the appearance or disappearance of components with different diffusion coefficient than the initial

components of the mixture. Specifically, in Nanotechnology, p-DOSY is an excellent tool for monitoring reactions on nanoparticle surfaces, such as end-group modification and ligand exchange reactions. Moreover, by p-DOSY, assembly kinetics or aggregation of nanoparticles could be studied by observing the shift of the diffusion coefficient to lower values.

The robustness of p-DOSY can also be used to protect diffusion results from any experimental artifact, such as temperature shift or spectrometer drift when such artifacts are known and cannot be easily compensated for. As it does not add any burden in the acquisition step nor at the processing step, spectroscopists are recommended to use p-DOSY in these experimental cases.

2.5 References

1. Antalek, B., Using pulsed gradient spin echo NMR for chemical mixture analysis: how to obtain optimum results. Concepts in Magnetic Resonance, 2002. 14(4): p. 225-258.
2. Johnson Jr, C.S., Diffusion ordered nuclear magnetic resonance spectroscopy: principles and applications. Progress in Nuclear Magnetic Resonance Spectroscopy, 1999. 34(3–4): p. 203-256.
3. Barjat, H., et al., High-Resolution Diffusion-Ordered 2D Spectroscopy (HR-DOSY) - A New Tool for the Analysis of Complex Mixtures. Journal of Magnetic Resonance, Series B, 1995. 108(2): p. 170-172.
4. Morris, K.F., et al., Analysis of Diffusion Coefficient Distributions in Humic and Fulvic Acids by Means of Diffusion Ordered NMR Spectroscopy. Analytical Chemistry, 1999. 71(23): p. 5315-5321.
5. Allouche, L., A. Marquis, and J.-M. Lehn, Discrimination of Metallosupramolecular Architectures in Solution by Using Diffusion Ordered Spectroscopy (DOSY) Experiments: Double-Stranded Helicates of Different Lengths. Chemistry – A European Journal, 2006. 12(28): p. 7520-7525.
6. Giuseppone, N., et al., DOSY NMR Experiments as a Tool for the Analysis of Constitutional and Motional Dynamic Processes: Implementation for the Driven Evolution of Dynamic Combinatorial Libraries of Helical Strands. Angewandte Chemie International Edition, 2008. 47(12): p. 2235-2239.
7. Gomez, M.V., et al., NMR Characterization of Fourth-Generation PAMAM Dendrimers in the Presence and Absence of Palladium Dendrimer-Encapsulated Nanoparticles. Journal of the American Chemical Society, 2009. 131(1): p. 341-350.
8. Van Lokeren, L., et al., Characterization of Titanium Dioxide Nanoparticles Dispersed in Organic Ligand Solutions by Using a Diffusion-Ordered Spectroscopy-Based Strategy. Chemistry – A European Journal, 2007. 13(24): p. 6957-6966.
9. Gilard, V., et al., DOSY NMR for drug analysis. NMR Spectroscopy in Pharmaceutical Analysis, 2011. 269.
10. Evans, R., et al., Quantitative Interpretation of Diffusion-Ordered NMR Spectra: Can We Rationalize Small Molecule Diffusion Coefficients? Angewandte Chemie International Edition, 2013. 52(11): p. 3199-3202.

11. Augé, S., et al., NMR measure of translational diffusion and fractal dimension. Application to molecular mass measurement. The Journal of Physical Chemistry B, 2009. 113(7): p. 1914-1918.
12. Santiago, A.A.H., et al., Shape-independent model (SHIM) approach for studying aggregation by NMR diffusometry. The Journal of chemical physics, 2015. 142(10): p. 104202.
13. Stejskal, E.O. and J.E. Tanner, Spin Diffusion Measurements: Spin Echoes in the Presence of a Time-Dependent Field Gradient. The Journal of Chemical Physics, 1965. 42(1): p. 288-292.
14. Sinnaeve, D., The Stejskal–Tanner equation generalized for any gradient shape—an overview of most pulse sequences measuring free diffusion. Concepts in Magnetic Resonance Part A, 2012. 40A(2): p. 39-65.
15. García-Álvarez, P., R.E. Mulvey, and J.A. Parkinson, "LiZn (TMP) 3", a Zincate or a Turbo-Lithium Amide Reagent? DOSY NMR Spectroscopic Evidence. Angewandte Chemie, 2011. 123(41): p. 9842-9845.
16. Li, D., et al., Characterization of Reactive Intermediates by Multinuclear Diffusion-Ordered NMR Spectroscopy (DOSY). Accounts of Chemical Research, 2009. 42(2): p. 270-280.
17. Nguyen, R., et al., Dynamic Combinatorial Evolution within Self-Replicating Supramolecular Assemblies. Angewandte Chemie International Edition, 2009. 48(6): p. 1093-1096.
18. Viéville, J., M. Tanty, and M.-A. Delsuc, Polydispersity index of polymers revealed by DOSY NMR. Journal of Magnetic Resonance, 2011. 212(1): p. 169-173.
19. Floquet, S., et al., Molecular weights of cyclic and hollow clusters measured by DOSY NMR spectroscopy. Journal of the American Chemical Society, 2009. 131(47): p. 17254-17259.
20. Wilkins, D.K., et al., Hydrodynamic radii of native and denatured proteins measured by pulse field gradient NMR techniques. Biochemistry, 1999. 38(50): p. 16424-16431.
21. Cohen, Y., et al., Diffusion NMR in Supramolecular Chemistry and Complexed Systems, in Analytical Methods in Supramolecular Chemistry. 2012, Wiley-VCH Verlag GmbH & Co. KGaA. p. 197-285.
22. Lucas, L.H. and C.K. Larive, Measuring ligand-protein binding using NMR diffusion experiments. Concepts in Magnetic Resonance Part A, 2004. 20(1): p. 24-41.
23. Nonappa, D. Šaman, and E. Kolehmainen, Studies on supramolecular gel formation using DOSY NMR. Magnetic Resonance in Chemistry, 2015. 53(4): p. 256-260.
24. Stchedroff, M.J., et al., 2D and 3D DOSY methods for studying mixtures of oligomeric dimethylsiloxanes. Physical Chemistry Chemical Physics, 2004. 6(13): p. 3221-3227.
25. Nilsson, M., et al., Diffusion NMR and trilinear analysis in the study of reaction kinetics. Chemical Communications, 2009(10): p. 1252-1254.
26. Schlörer, N.E., E.J. Cabrita, and S. Berger, Characterization of Reactive Intermediates by Diffusion-Ordered NMR Spectroscopy: A Snapshot of the Reaction of 13CO2 with [Cp2Zr(Cl)H]. Angewandte Chemie International Edition, 2002. 41(1): p. 107-109.
27. Bowyer, P.J., A.G. Swanson, and G.A. Morris, Randomized Acquisition for the Suppression of Systematic F1 Artifacts in Two-Dimensional NMR Spectroscopy. Journal of Magnetic Resonance, 1999. 140(2): p. 513-515.

28. Gurst, J.E., NMR and the structure of D-glucose. Journal of Chemical Education, 1991. 68(12): p. 1003.
29. Delsuc, M. and T. Malliavin, Maximum entropy processing of DOSY NMR spectra. Analytical Chemistry, 1998. 70(10): p. 2146-2148.
30. Van Lokeren, L., et al., ERETIC implemented in diffusion-ordered NMR as a diffusion reference. Magnetic Resonance in Chemistry, 2008. 46(S1): p. S63-S71.

2.6 Supplementary Information

Details on glucose assignment of the 1H NMR peaks of glucose anomers, Varian experiments and the script used for permutation are given in this section.

General details. Crystalized α-d-glucose (anhydrous, 96% purity) was purchased from Sigma–Aldrich (USA). Deuterated solvents DMSO-d6 (99.96%) and D_2O (99.9%) were purchased from Euriso-Top (France). All samples were measured in 5.0 mm tubes.

Glucose study by NMR. The α,β-D-glucose was studied by NMR and the assignment of the molecule have been done, to be able to characterize the α and β protons for further analysis. This assignment is shown in the 1D spectrum in Figure S 2-1 and it corresponds to the numbering of both anomeric molecules in Figure 2-1.

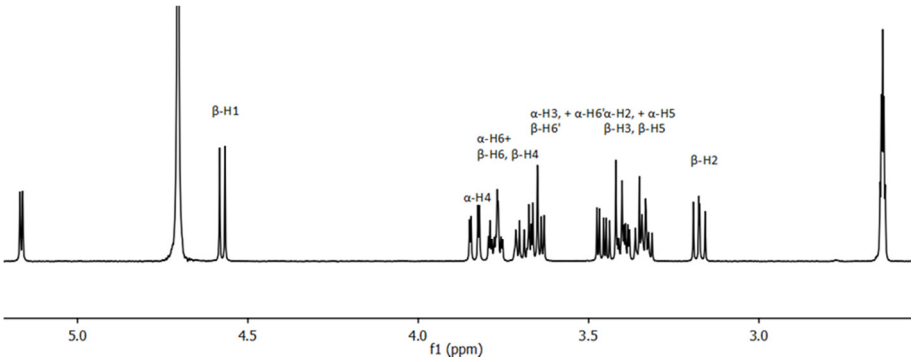

Figure S 2-1: Proton assignment of a mixture of α,β-D-glucose (42.7% α-D glucose and 57.4% of β-D-glucose) at equilibrium

p-DOSY. The DOSY experiment and the p-DOSY experiment, measured on α-glucose sample after solubilization at the beginning of the anomerization kinetics are shown superimposed in Figure S 2-2. The bias on the diffusion coefficient can be seen for the β-H1.

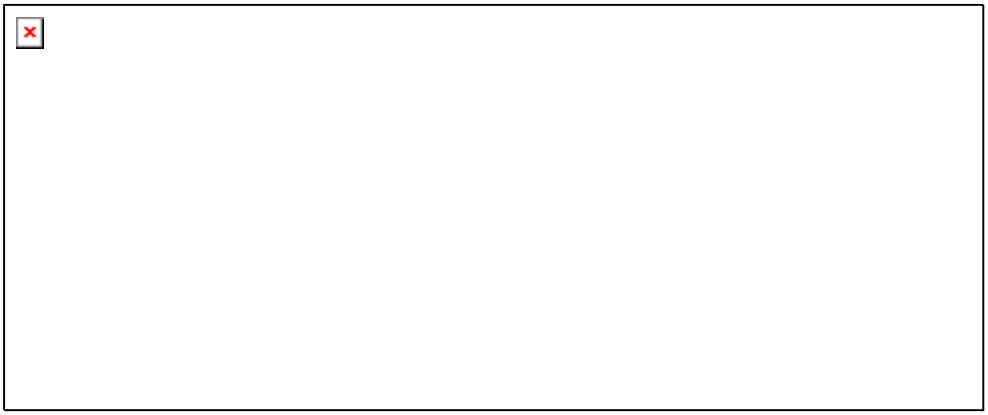

Figure S 2-2: Overlay of two DOSY measurements acquired by the 1st DOSY measurement (0-24 minutes), by p-DOSY arrays (green color) and sequential (blue color) DOSY arrays.

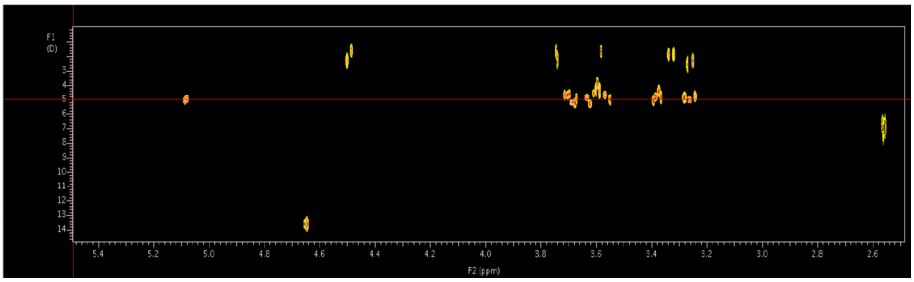

Figure S 2-3: Sequential DOSY measurement acquired between 0-24 minutes in Varian

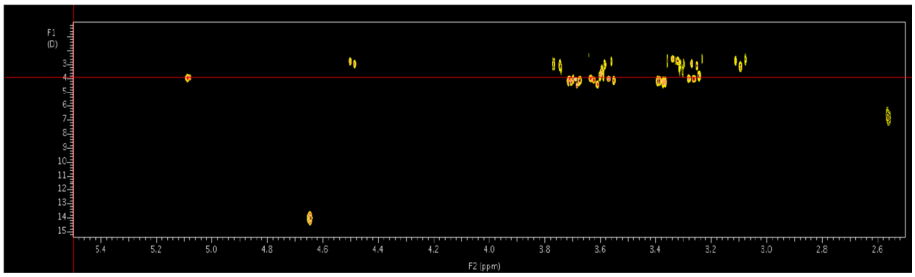

Figure S 2-4: Interleaved DOSY measurement acquired between 0-24 minutes in Varian

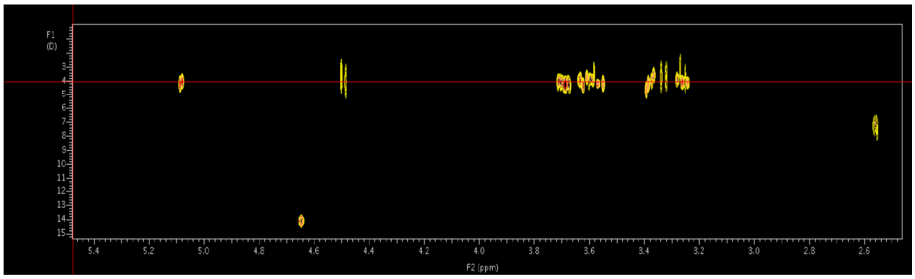

Figure S 2-5: Permutated DOSY measurement acquired between 0-24 minutes in Varian

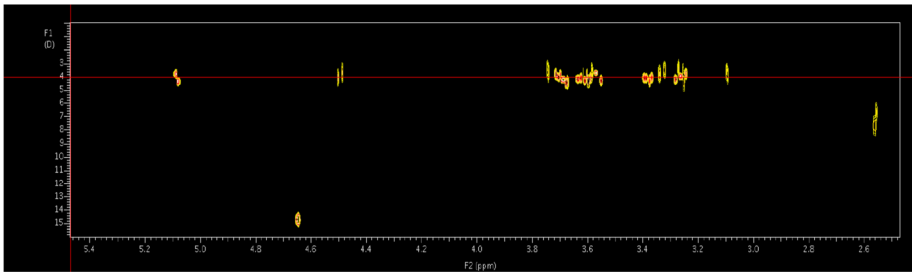

Figure S 2-6: Combination of permutated and interleaved DOSY measurement between 0-24 minutes in Varian

Permutated Difframp and difflist. Here is presented the ¨Permute¨ script to permutate the Difframp and difflist for acquisition and processing the p-DOSY experiments. The original Difframp, created by TopSpin when a DOSY experiment is launched, has to be replaced by the permutated Difframp before running the p-DOSY experiment. The same procedure has to been followed for the difflist before processing the spectrum.

```
"""
Randomizes a Difframp list
Created by DELSUC Marc-Andre and Julia Asencio on 2013-12-18.
"""

import random

N=64 # Adapt to your system

lperm = random.sample(range(N-1), N-1)
perm = [0] + [i+1 for i in lperm]

print N, "points :", perm

filelist = ['difflist', '/opt/topspin/exp/stan/nmr/lists/gp/user/Difframp']

for fname in filelist:
     F = open(fname,'r')
     FF = open(fname+'P','w')
     ll = []
     for l in F:
          if not l.startswith('#'):
               ll.append(l)
          elif l[0:6] != '##END=':
               FF.write(l)
     F.close()
     if len(ll) != N:
          raise Exception( 'This prgm is meant for %d points'%N )
     for i in range(N):
          FF.write(ll[perm[i]])
     FF.write('##END=')
     FF.close()
```

Figure S 2-7: python permute.py script used to compute a random permutation of the standard Difframp and difflist files, for acquisition and processing of the p-DOSY experiment.

Chapter 3 Selective dipeptide binding on mixed ligand gold nanoparticles by DOSY NMR

Abstract

In this Chapter, the goal was to implement orthogonal selective interactions in order to design nanoparticle based dipeptide receptors. For this purpose, mixed monolayer protected gold nanoparticles (AuNPs) were decorated with the α,ω-functionalized thiols containing as recognition elements a terminal trimethylalkyl ammonium group, an 18-crown-6 moiety, and a phenyl group, respectively. To evaluate binding affinities, the suitability of 1H NMR chemical shift titrations method was tested. Although, clearly visible downfield shifts of peptide signals were observed when increasing the AuNP concentration, their extent combined with pronounced overlaps with AuNP signals did not allow using this method for the quantification of binding strength. Turning to DOSY NMR spectroscopy, the evaluation of binding equilibria that are fast on the NMR timescale is based on the reduction of the diffusion coefficient of a small molecule once it binds to a larger receptor. The resulting diffusion coefficient Dobs represents a weighted average of the coefficients of the free and the bound states. The fraction χ of bound substrate on AuNPs was calculated for all combinations of peptides (Gly-Gly and Gly-Phe) with AuNPs. The χ value for Gly-Phe with the AuNPs containing all three functional groups was found to be 78%, twice or more times higher than all other ligand combinations. To evaluate peptide binding quantitatively, DOSY NMR titrations were performed with AuNPs capped either with quaternary ammonium (NPQ) or a combination of the latter with crown ether and aromatic groups (NPQPC). The resulting χ values were plotted against peptide concentration and the obtained curves were fitted to Langmuir isotherms. The adsorption equilibrium constants K thus obtained amount to 4770 ± 1180 M^{-1} for NP_Q and 8260 ± 1480 M^{-1} for NP_{QPC}, clearly confirming the increase of peptide affinity upon combining the three ligands on the nanoparticle surface. In conclusion, this work proves by DOSY NMR that combining different functional groups on the surface of AuNPs affords selective receptors for dipeptides.

Part of this Chapter has been published as: S. Yapar, M. Oikonomou, A.H. Velders, S. Kubik, Dipeptide recognition in water mediated by mixed monolayer protected gold nanoparticles, Chemical Communications, 51 (2015)

3.1 Introduction

Designing a synthetic receptor typically involves arranging suitable binding sites on a molecular scaffold that mediate the interaction with a structurally complementary substrate. While this strategy afforded numerous potent receptors in the past, it is usually associated with a considerable synthetic effort. A conceptually more straightforward approach involves the use of a core structure for receptor development that allows easy decoration with a wide range of different recognition units. In this context, nanoparticles, in particular gold nanoparticles (AuNPs), have recently emerged as a versatile platform for the development of polyfunctional receptors and chemosensors with applications in biology, medicine, or catalysis [1-7].

AuNPs are relatively easy to prepare with controllable size distributions thus allowing regulation of surface curvature and number of functional groups on the gold core. They are stable in solution once they are protected with appropriate ligands such as organic thiols. They can be made soluble in a wide range of solvents, including water, by varying the structures of the surface-bound ligands. The optical properties of AuNPs allow the facile development of sensing systems, [8, 9] and substrate recognition (including the subsequent catalytic transformation of the substrate) can benefit from multivalent effects, or from cooperativity of different functional groups on the surface [10, 11].

The size of AuNPs, which is typically in a similar range as that of small proteins or nucleic acids, renders AuNPs particularly useful for designing receptors that selectively attach to protein surfaces or DNA sequences [12]. However, also AuNP-based receptors for low molecular weight compounds have been described. Examples are Rotello's flavine receptor, [13, 14] Scrimin's AuNPs that catalytically cleave esters or phosphodiesters, [15-19] the receptors for nucleotide triphosphates developed by Prins, [20-24] and Rastrelli's and Mancin's salicylaldehyde receptor [25, 26]. Yet AuNP-based receptors for small peptides such as dipeptides are rare[†] and the hypothesis that they could be accessible by using known strategies for developing covalently constructed peptide receptors [27, 28] was explored. In this context, inspired by a classical receptor described by Hossain and Schneider [29]. This compound contains a crown ether moiety and a quaternary ammonium ion along a rigid scaffold for binding to the N- and the C-terminal ends of an unprotected peptide, respectively. Both binding sites were carefully chosen such that they do not interact with each other so that intramolecular conformational collapse of the receptor or its intermolecular self-aggregation is avoided. An aromatic moiety was introduced as a third binding site to induce selectivity for peptides with aromatic side chains. The corresponding receptor was shown to interact with dipeptides and tripeptides in methanol and water and indeed exhibited improved affinity for peptides with aromatic side chains in some cases.

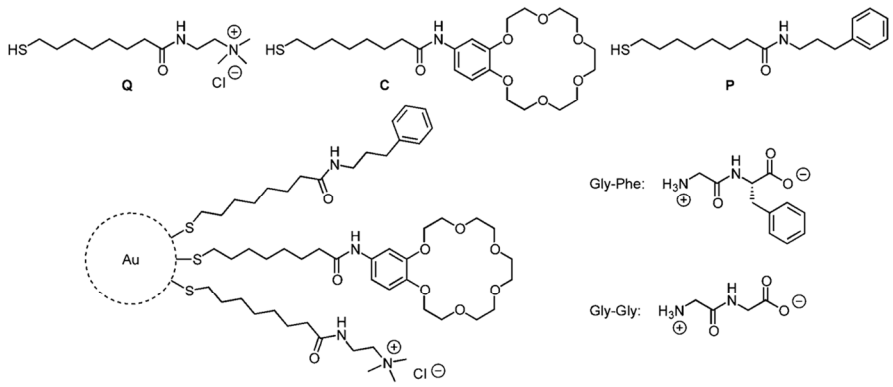

Figure 3-1: Ligands Q, C, P, schematic representation of the AuNPs prepared thereof using NP_{QPC} as an example, and structures of the peptides used as substrates.

Based on this concept analogous mixed monolayer AuNPs were devised and their interaction with dipeptides in water was investigated. Introduction of the functional groups required for peptide recognition was achieved by decoration of AuNPs with the α,ω-functionalized thiols Q, C and P containing as recognition elements a terminal trimethylalkyl ammonium group, an 18-crown-6 moiety, and a phenyl group, respectively (Figure 3-1, for ligand syntheses, see SI, Figure S 3-1-Figure S 3-6).

A quantitative measure for the binding interactions and selectivity between the devised mixed monolayer nanoparticles and different dipeptides is the association constant Ka [30]. Selecting the most appropriate technique to measure association constant is rather puzzling, since many different analytical methods have been presented in literature [31, 32]. To choose the most appropriate technique, the physicochemical aspects of the studied system must be considered. The physical parameter, which changes significantly when a small ligand (e.g. dipeptides) bind on a big receptor (e.g. nanoparticles) is the apparent ligand (dipeptide) hydrodynamic radius [33]. Since diffusion coefficients are inversely proportional to hydrodynamic radii, binding constants can accurately be measured by Diffusion Ordered SpectroscopY titrations [34]. In the case of slow exchange on the NMR time scale, the association constant can be determined by monitoring the diffusion coefficients of the peaks reflecting to the free and bound state of the dipeptide [34]. In the case of fast exchange, the nanoparticles and dipeptides have certain diffusion coefficients in the free state corresponding to their shape and size, but when a binding event takes place, the observed (measured) diffusion coefficient (D_{obs}) is a weighted average of the free and bound diffusion coefficients (D_{free} and D_{bound}, respectively) [34]. For determining the association constant from diffusion NMR measurements, the same graphical and curve-fitting methodologies used to obtain Ka values from changes in chemical shifts in titration experiments can be used [35]. Herein

diffusion NMR measurements were employed in order to evaluate and quantify binding efficiency of the devised mixed monolayer AuNPs.

3.2 Experimental

AuNP synthesis was achieved by first preparing dioctylamine-protected nanoparticles and subsequently replacing the weakly bound amine ligands with the functionalized thiols (see SI, Figure S 3-1-Figure S 3-6 and Table S 3-1). This strategy has the advantage of allowing a more straightforward control over the ratio of different ligands on the AuNPs surface than the alternative strategy starting from thiol protected AuNPs and thiol exchange reactions [36, 37]. After purification of the obtained AuNPs by microfiltration the ^{1}H NMR spectra exhibited broad signals of the ligands indicating successful ligand attachment to the gold surface and the absence of unbound species. Altogether four AuNPs were thus prepared, NP_Q containing only ammonium groups on the surface and AuNPs NP_{QC}, NP_{QP}, and NP_{QPC} containing, respectively, ligands C, P, or a mixture thereof in addition to Q. Nanoparticles without ammonium groups turned out to be insufficiently soluble to allow binding studies in water.

TEM images of the nanoparticles were by using a JEOL JEM1011 microscope with an acceleration voltage of 80 kV. The images were processed with the program ImageJ to determine the average diameters of the nanoparticles.

All DOSY NMR measurements were performed on a 500 MHz Bruker Avance III NMR spectrometer, proton frequency 500.137 MHz, equipped with a 5 mm TXI probehead at 300 K. The pulse sequence was a stimulated echo bipolar gradient pulse (stebpgp1s) with the DOSY spectra acquired for each sample having 32 increments (exponential array), 32 scans, gradient pulse length (δ) 6.0 ms and big delta (Δ) 150.0 ms. Samples were prepared in D2O (99.96%) with the same nanoparticle concentrations (0.048 mM). Diffusion coefficients of AuNPs were used to estimate the hydrodynamic radii of the nanoparticles by using the Stokes-Einstein equation (Equation 3-1) where k is the Boltzmann's constant, T is the temperature (300 K), η is the viscosity of the solvent (D_2O), D is the diffusion coefficient of the AuNPs, and R_h is the hydrodynamic radius.

$$D=\frac{k_B T}{6\,\pi\eta r}$$

Equation 3-1

The diffusion coefficients of the individual species in solution were corrected by considering the diffusion coefficient of water (2.18×10^{-9} m^2 s^{-1}). In the case of overlapping signals of nanoparticle and peptide peaks (for NP_{QP} and NP_{QPC}) D_{obs} values were obtained from resolving the decay of the overlapping peaks by biexponential fitting

and using the independently determined nanoparticle diffusion coefficient as a known value. Diffusion of HOD exhibited excellent reproducibility throughout all measurements.

For the estimation of the fraction χ of bound peptides by DOSY NMR spectroscopy, solutions were prepared by mixing stock solutions of the nanoparticles (0.08 mM, 300 µL) and of the peptides (12 mM, 3 µL) in D_2O in NMR tubes. The total volume of the NMR tubes was adjusted to 500 µL by adding 197 µL of D_2O. After recording the DOSY NMR spectrum of each sample, the diffusion coefficients of the peptides and of the nanoparticles were determined separately. The fraction χ of bound peptides was calculated by using Equation 3-2.

$$\chi = \frac{(D_{free} - D_{obs})}{(D_{free} - D_{bound})}$$

Equation 3-2

For the quantitative estimation of the affinity of Gly-Phe to nanoparticles NP_Q and NP_{QPC} a series of solutions were prepared containing the same nanoparticle concentration (0.048 mM) and increasing concentrations of the peptide. Eight samples were prepared by mixing stock solutions of the nanoparticles (0.08 mM, 300 µL) and peptide (12 mM, 3 to 120 µL) in D_2O in individual NMR tubes and adjusting the overall volume of each sample to 500 µL. The diffusion coefficients of the peptides D_{obs} were determined from the DOSY NMR spectra of these solutions and the corresponding fractions of bound peptides χ were calculated from equation (2) by considering the diffusion coefficient of free peptide D_{free} (5.81×10^{-10} m^2 s^{-1}) and of the respective nanoparticle D_{bound} (8.05×10^{-11} m^2 s^{-1} for NP_Q and 8.00×10^{-11} m^2 s^{-1} for NP_{QPC}). D_{free} and D_{bound} were determined from the DOSY NMR spectra of two additional samples obtained by mixing the nanoparticle stock solution (0.08 mM, 300 µL) with D_2O (200 µL) and the peptide stock solution (12 mM, 200 µL) with D_2O (300 µL). Plotting χ against the peptide concentration afforded curves that were fitted to Langmuir isotherms according to Equation 3-3.

$$\chi = \frac{(C_{max} * K_a)}{(1 + K_a * C_{pep})}$$

Equation 3-3

The corresponding non-linear regression yielded the equilibrium constants K and the maximum fraction of bound peptide c_{max}. Relating this concentration to the one of the nanoparticle provided information about the average number of peptides bound to the AuNPs.

3.3 Results and Discussion

The prepared AuNPs were characterized by UV/vis spectroscopy, transmission electron microscopy (TEM), and DOSY NMR spectroscopy. In the UV/vis spectra of NP_Q solutions in water a very weak absorption band at ca. 515 nm was observed (see SI, Figure S 3-8), indicating that the average diameter of these AuNPs is around 2 nm [38]. The TEM images of the four AuNPs revealed mostly small particles with a relatively narrow size distribution and only few larger particles (Figure 3-2-Figure 3-5).

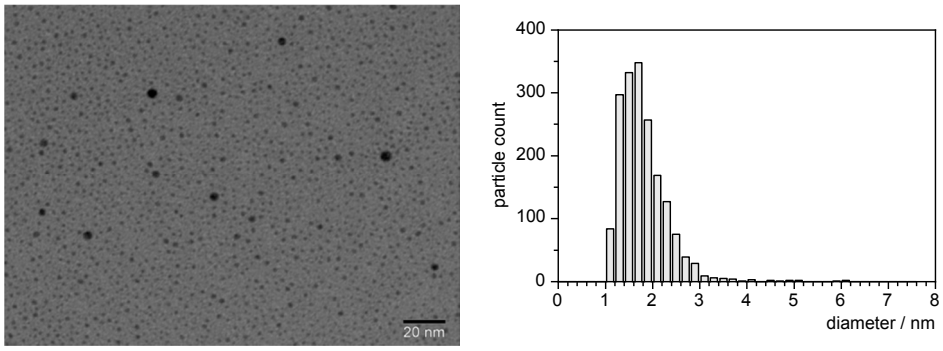

Figure 3-2: TEM image of NP_Q.

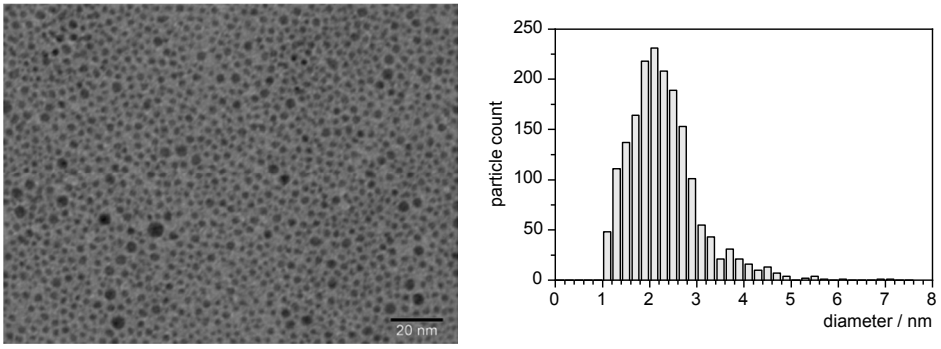

Figure 3-3: TEM image of NP_{QC}.

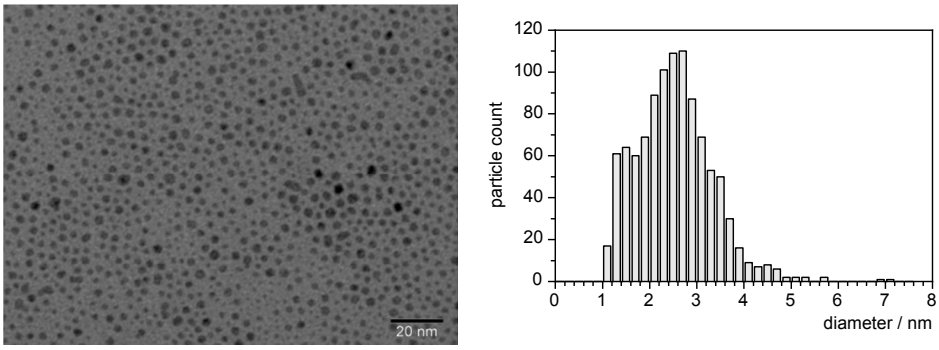

Figure 3-4: TEM image of NP_{QP}.

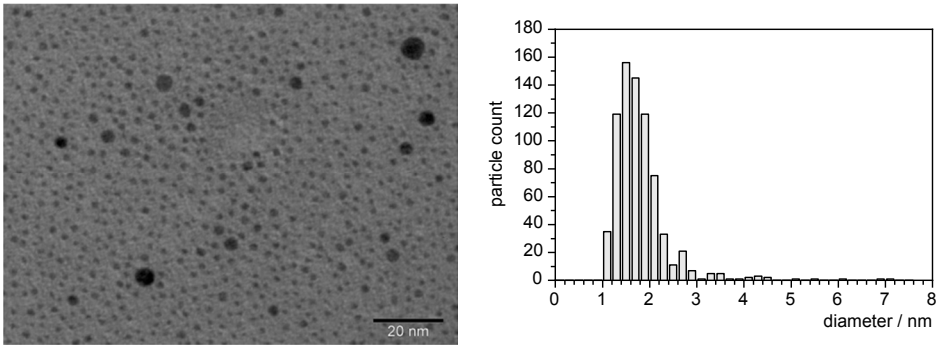

Figure 3-5: TEM image of NP_{QPC}.

The hydrodynamic diameters of the prepared AuNPs were calculated by using the Stokes-Einstein Equation 3-1 from the diffusion coefficients measured by DOSY NMR [34]. An example of a DOSY spectrum of the nanoparticles is given in Figure 3-6.

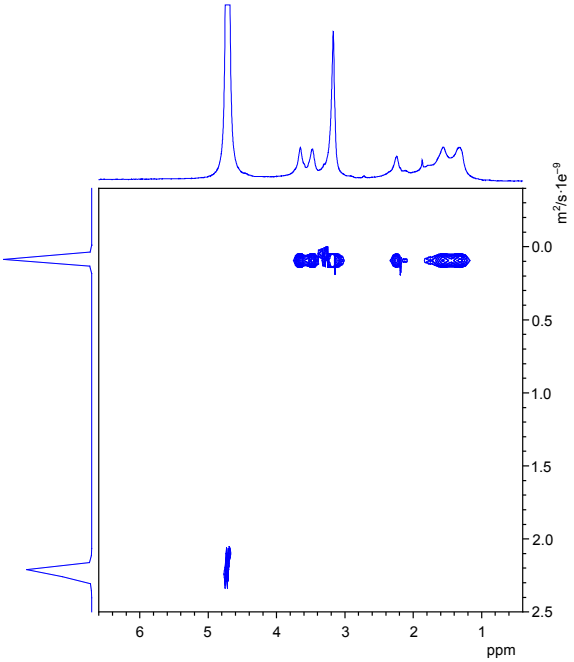

Figure 3-6: DOSY NMR spectrum of NP_Q in D_2O.

The average diameters dTEM of the gold cores estimated from the TEM images are summarized in Table 3-1. This table also contains the hydrodynamic diameters of the prepared AuNPs obtained by DOSY NMR [34]. Comparison of dDOSY with the corresponding dTEM values indicates that the surface layers of the AuNPs have thicknesses of ca. 1.6 nm.

Table 3-1: Averaged diameters of mixed monolayer AuNPs NP_Q, NP_{QC}, NP_{QP}, and NP_{QPC}.

AuNP	d_{TEM}[a] / nm	D[b] / m^2s^{-1}	d_{DOSY}[c] / nm
NP_Q	1.9	8.1×10^{-11}	5.0
NP_{QC}	2.5	7.3×10^{-11}	5.6
NP_{QP}	2.6	7.1×10^{-11}	5.7
NP_{QPC}	1.9	8.0×10^{-11}	5.0

[a] Average diameters determined by transmission electron microscopy; [b] diffusion coefficients determined by DOSY NMR spectroscopy in D_2O (99.96%) at 300 K; [c] hydrodynamic diameters calculated from D by using the Stokes-Einstein equation.

For understanding the contribution in binding of the three different thiol ligands on these AuNPs, the ratio of the ligands could not be estimated directly from the ^1H NMR spectra because of pronounced signal broadening (Figure 3-7).

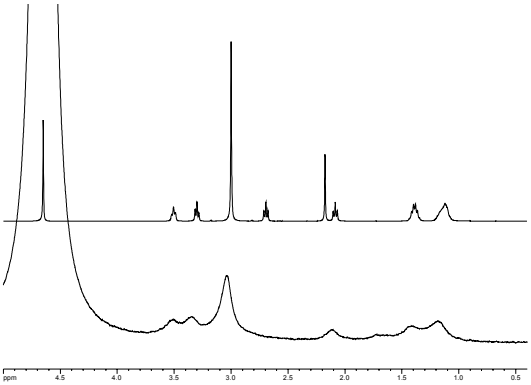

Figure 3-7: ^{1}H NMR spectrum of NP_Q in D_2O (bottom) in comparison with the spectrum of the protected ligand Q (top) in the same solvent.

Therefore, the nanoparticles were decomposed and the ligands released by addition of iodine to a nanoparticle solution in methanol-d_4 [39]. The ^{1}H NMR spectra of the respective solutions exhibited sharp signals, which allowed calculation of the relative amount of each ligand in the mixture by integration of characteristic ligand signals. By performing these measurements in the presence of an internal standard with known concentration also allowed assessing the total amount of ligands on each nanoparticles as well as average nanoparticle composition (Table 3-2, for details see SI, Figure S 3-7). The molecular weight of the nanoparticles was calculated by assuming the composition $Au_{144}(SR)_{60}$ and considering the NMR spectroscopically determined ratio of the ligands Q, C, P on their surfaces. Thus, it was ensured that every solution contained an almost equal amount of AuNPs. The obtained compositions are in good agreement with compositions calculated for such AuNPs by using the theoretical model proposed by Leff et al [40], indicating that the chosen synthetic strategy allows a reliable control over surface composition.

Table 3-2: Relative amounts of ligands Q, C, and P on the surfaces of AuNPs NP_Q, NP_{QC}, NP_{QP}, and NP_{QPC}.[a]

AuNP	Q / %	C / %	P / %	Amount of ligands per nanoparticle /mol mg^{-1}	Ligand molecules/ #Au atoms	Experimental #of ligands	Theoretical #of ligands calculated by Leff et al [39]	Average Composition
NP_Q	100			8.76 x 10^{-7}	4.29	49	53	$Au_{211}Q_{49}$
NP_{QC}	53	47		7.47 x 10^{-7}	4.84	99	92	$Au_{481}Q_{52.5}C_{46.5}$
NP_{QP}	47		53	8.21 x 10^{-7}	4.69	115	99	$Au_{541}Q_{54.0}P_{61.0}$
NP_{QPC}	48	25	27	8.57 x 10^{-7}	4.17	51	53	$Au_{211}Q_{24.5}C_{12.8}P_{13.7}$

[a] Determined ^{1}H NMR spectroscopically after iodine decomposition of the respective nanoparticle, with an estimated error of ± 5 %.

Table 3-2 shows that all AuNPs contain at least ca. 50% of ligand Q to ensure water solubility. The other half is made up of either the same type of ligand in the case of NP_Q, another ligand type in the case of NP_{QC} and NP_{QP}, or an approximate 1:1 mixture of ligands C and P in the case of NP_{QPC}. In light of their overall average compositions, these nanoparticles likely feature surface arrangements with functional groups of different ligands located in close proximity, allowing cooperative action in substrate binding.

To evaluate whether ^{1}H NMR spectroscopy is a suitable method to quantify binding of peptides to the prepared AuNPs, increasing amounts of NP_Q were added to a solution of the dipeptide Gly-Gly in D_2O. Small but clearly visible downfield shifts of peptide signals were observed when increasing the AuNP concentration, indicating an interaction between the dipeptide and the nanoparticles. The extent of these shifts combined with pronounced overlaps with AuNP signals did not allow using this method for the quantification of binding strength, however. In the case of Gly-Phe, the position and multiplicity of some peptide signals further complicated ^{1}H NMR spectroscopic binding studies. Turning to DOSY NMR spectroscopy to gain insight into the correlation of surface composition and peptide affinity was considered as an appropriate solution. The results of these binding studies, which involved the use of dipeptides Gly-Gly and Gly-Phe as substrates and D_2O as solvent, are summarized in Table 3-3.

Table 3-3: Fractions χ of bound dipeptides to the functionalized nanoparticles.[a]

AuNP	χ (Gly-Phe) / %	χ (Gly-Gly) / %
NP_Q	38	32
NP_{QC}	31	23
NP_{QP}	21	19
NP_{QPC}	78	48

[a] Determined by DOSY NMR spectroscopy in D_2O (99.96%) at 300 K and total ligand concentrations of 1.9 ± 0.1 mM and peptide concentrations of 0.072 mM.

Table 3-3 shows that the DOSY NMR measurements provide clear evidence for the interaction between the peptides and the AuNPs. Moreover, the determined fractions of bound peptides χ depend on the functional groups present on the particles. AuNP NP_Q, containing only quaternary ammonium ions binds to Gly-Gly and Gly-Phe with similar affinity, presumably by electrostatic interactions between the ammonium groups on the AuNP surfaces and the peptide carboxylate groups. The additional presence of the crown ether in NP_{QC} or the aromatic groups in NP_{QP} has a small and not necessarily beneficial effect on the overall affinity although it must be considered that these AuNPs only contain half the number of the quaternary ammonium groups in comparison to NP_Q. Thus, in contrast to Schneider's low molecular weight receptor a pronounced cooperativity of the ammonium and the crown ether groups in binding to the terminal ends of short peptides could not be observed for NP_{QC} [27, 28]. Nanoparticle NP_{QPC}, however, exhibits a higher

affinity than the other AuNPs, maybe because the presence of additional aromatic units is required to induce an arrangement of the quaternary ammonium ions and crown ether moieties on the particle surface that allows their cooperative action in peptide binding. This effect is substantially more pronounced for Gly-Phe binding, indicating that aromatic interactions are likely to contribute to complex stability.

To evaluate peptide binding quantitatively, DOSY NMR titrations were performed with NP_Q and NP_{QPC} during which the Gly-Phe concentrations were progressively increased while keeping those of the nanoparticles constant. The resulting χ values were plotted against peptide concentration and the obtained curves were fitted to Langmuir isotherms (Figure 3-8, for details, see SI, Table S 3-3 and Figure S 3-9 and Figure S 3-10) [41, 42]. Titrations using other batches of independently prepared nanoparticles were performed analogously (see SI, Table S 3-5). The equilibrium constant obtained for binding of Gly-Phe to NP_Q is the same as the one obtained in Table S 3-5 within the error limits (3880 ± 860 M^{-1}). The one for NP_{QPC} is slightly different (6090 ± 1380 M^{-1}), clearly confirming the increase of peptide affinity upon combining the three ligands on the nanoparticle surface. The Langmuir treatment also yielded the maximum concentration of bound peptides as a second fitted parameter, which showed that NP_Q and NP_{QPC} bind, respectively, 2.6 and 3.6 peptide molecules on average (see SI, Table S 3-5).

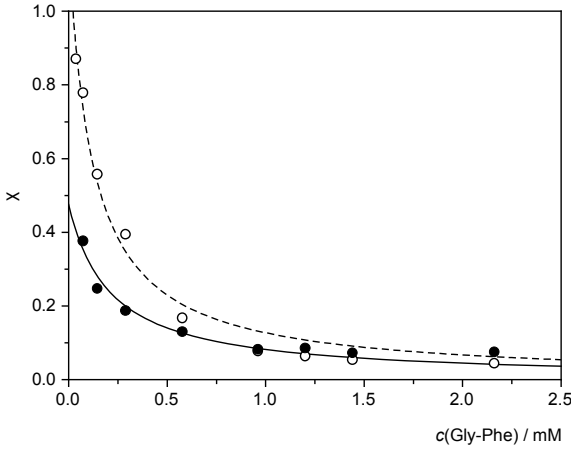

Figure 3-8: Dependence fraction of bound Gly-Phe to NPQ (filled circles) and NPQPC (open circles) determined spectroscopically by DOSY NMR on peptide concentration and fitting of the data to Langmuir isotherms. The points represent the experimental data and the lines the fitted curves.

In conclusion, this work shows that combining different functional groups on the surface of AuNPs affords receptors for low molecular weight compounds, in this case for peptides. The individual functional groups on these AuNPs contribute to substrate recognition by presenting specific binding sites and/or surface arrangements suitable for substrate binding. The attractiveness of the presented approach lies in the ease with

which the receptors can be prepared once a library of functional thiols is available and its enormous flexibility.

3.4 Conclusion

In conclusion, this work shows that combining different functional groups on the surface of AuNPs affords receptors for low molecular weight compounds, in this case for dipeptides. The individual functional groups on these AuNPs contribute to substrate recognition by presenting specific binding sites and/or surface arrangements suitable for substrate binding. The attractiveness of the presented approach lies in the ease with which the receptors can be prepared once a library of functional thiols is available and its enormous flexibility. The sensitivity of DOSY NMR to the inherent size differences between ligands and receptors, often encountered in nanoparticle molecular recognition systems, turns DOSY NMR into an excellent candidate for the elucidation of supramolecular interactions on nanoparticle interfaces.

3.5 References

1. Corma, A. and H. Garcia, Supported gold nanoparticles as catalysts for organic reactions. Chemical Society Reviews, 2008. 37(9): p. 2096-2126.
2. Dykman, L. and N. Khlebtsov, Gold nanoparticles in biomedical applications: recent advances and perspectives. Chemical Society Reviews, 2012. 41(6): p. 2256-2282.
3. Giljohann, D.A., et al., Gold Nanoparticles for Biology and Medicine. Angewandte Chemie International Edition, 2010. 49(19): p. 3280-3294.
4. Shenhar, R. and V.M. Rotello, Nanoparticles: Scaffolds and Building Blocks. Accounts of Chemical Research, 2003. 36(7): p. 549-561.
5. Sperling, R.A., et al., Biological applications of gold nanoparticles. Chemical Society Reviews, 2008. 37(9): p. 1896-1908.
6. Wilson, R., The use of gold nanoparticles in diagnostics and detection. Chemical Society Reviews, 2008. 37(9): p. 2028-2045.
7. Yeh, Y.-C., B. Creran, and V.M. Rotello, Gold nanoparticles: preparation, properties, and applications in bionanotechnology. Nanoscale, 2012. 4(6): p. 1871-1880.
8. Rosi, N.L. and C.A. Mirkin, Nanostructures in Biodiagnostics. Chemical Reviews, 2005. 105(4): p. 1547-1562.
9. Saha, K., et al., Gold Nanoparticles in Chemical and Biological Sensing. Chemical Reviews, 2012. 112(5): p. 2739-2779.
10. Fasting, C., et al., Multivalency as a Chemical Organization and Action Principle. Angewandte Chemie International Edition, 2012. 51(42): p. 10472-10498.
11. Pieters, G. and L.J. Prins, Catalytic self-assembled monolayers on gold nanoparticles. New Journal of Chemistry, 2012. 36(10): p. 1931-1939.
12. Verma, A. and V.M. Rotello, Surface recognition of biomacromolecules using nanoparticle receptors. Chemical Communications, 2005(3): p. 303-312.

13. Bayir, A., et al., Model systems for flavoenzyme activity: Recognition and redox modulation of flavin mononucleotide in water using nanoparticles. Chemical Communications, 2006(38): p. 4033-4035.
14. Boal, A.K. and V.M. Rotello, Fabrication and Self-Optimization of Multivalent Receptors on Nanoparticle Scaffolds. Journal of the American Chemical Society, 2000. 122(4): p. 734-735.
15. Bonomi, R., et al., Phosphate Diester and DNA Hydrolysis by a Multivalent, Nanoparticle-Based Catalyst. Journal of the American Chemical Society, 2008. 130(47): p. 15744-15745.
16. Diez-Castellnou, M., F. Mancin, and P. Scrimin, Efficient Phosphodiester Cleaving Nanozymes Resulting from Multivalency and Local Medium Polarity Control. Journal of the American Chemical Society, 2014. 136(4): p. 1158-1161.
17. Manea, F., et al., Nanozymes: Gold-Nanoparticle-Based Transphosphorylation Catalysts. Angewandte Chemie International Edition, 2004. 43(45): p. 6165-6169.
18. Zaramella, D., P. Scrimin, and L.J. Prins, Self-Assembly of a Catalytic Multivalent Peptide–Nanoparticle Complex. Journal of the American Chemical Society, 2012. 134(20): p. 8396-8399.
19. Zaupa, G., et al., Catalytic Self-Assembled Monolayers on Au Nanoparticles: The Source of Catalysis of a Transphosphorylation Reaction. Chemistry – A European Journal, 2011. 17(17): p. 4879-4889.
20. Maiti, S., et al., Multivalent Interactions Regulate Signal Transduction in a Self-Assembled Hg2+ Sensor. Journal of the American Chemical Society, 2014. 136(32): p. 11288-11291.
21. Pezzato, C., et al., Pattern-based sensing of nucleotides with functionalized gold nanoparticles. Chemical Communications, 2013. 49(5): p. 469-471.
22. Pezzato, C., et al., Label-free fluorescence detection of kinase activity using a gold nanoparticle based indicator displacement assay. Organic & Biomolecular Chemistry, 2015. 13(4): p. 1198-1203.
23. Pieters, G., et al., Self-assembly and selective exchange of oligoanions on the surface of monolayer protected Au nanoparticles in water. Chemical Communications, 2012. 48(13): p. 1916-1918.
24. Pieters, G., C. Pezzato, and L.J. Prins, Controlling Supramolecular Complex Formation on the Surface of a Monolayer-Protected Gold Nanoparticle in Water. Langmuir, 2013. 29(24): p. 7180-7185.
25. Perrone, B., et al., "NMR Chemosensing" Using Monolayer-Protected Nanoparticles as Receptors. Journal of the American Chemical Society, 2013. 135(32): p. 11768-11771.
26. Salvia, M.-V., et al., Nanoparticle-Assisted NMR Detection of Organic Anions: From Chemosensing to Chromatography. Journal of the American Chemical Society, 2015. 137(2): p. 886-892.
27. Peczuh, M.W. and A.D. Hamilton, Peptide and Protein Recognition by Designed Molecules. Chemical Reviews, 2000. 100(7): p. 2479-2494.
28. Schneider, H.-J., Models for Peptide Receptors. Angewandte Chemie International Edition in English, 1993. 32(6): p. 848-850.
29. Hossain, M.A. and H.-J. Schneider, Sequence-Selective Evaluation of Peptide Side-Chain Interaction. New Artificial Receptors for Selective Recognition in Water. Journal of the American Chemical Society, 1998. 120(43): p. 11208-11209.

30. Connors, K.A., Binding constants: the measurement of molecular complex stability. 1987: Wiley-Interscience.
31. Simova, S. and S. Berger, Diffusion Measurements vs. Chemical Shift Titration for Determination of Association Constants on the Example of Camphor–Cyclodextrin Complexes. Journal of inclusion phenomena and macrocyclic chemistry, 2005. 53(3-4): p. 163-170.
32. Thordarson, P., Determining association constants from titration experiments in supramolecular chemistry. Chemical Society Reviews, 2011. 40(3): p. 1305-1323.
33. Cameron, K.S. and L. Fielding, NMR diffusion spectroscopy as a measure of host-guest complex association constants and as a probe of complex size. The Journal of organic chemistry, 2001. 66(21): p. 6891-6895.
34. Cohen, Y., L. Avram, and L. Frish, Diffusion NMR Spectroscopy in Supramolecular and Combinatorial Chemistry: An Old Parameter—New Insights. Angewandte Chemie International Edition, 2005. 44(4): p. 520-554.
35. Foo, K. and B. Hameed, Insights into the modeling of adsorption isotherm systems. Chemical Engineering Journal, 2010. 156(1): p. 2-10.
36. Jana, N.R. and X. Peng, Single-Phase and Gram-Scale Routes toward Nearly Monodisperse Au and Other Noble Metal Nanocrystals. Journal of the American Chemical Society, 2003. 125(47): p. 14280-14281.
37. Manea, F., et al., Expeditious Synthesis of Water-Soluble, Monolayer-Protected Gold Nanoparticles of Controlled Size and Monolayer Composition. Langmuir, 2008. 24(8): p. 4120-4124.
38. Rance, G.A., D.H. Marsh, and A.N. Khlobystov, Extinction coefficient analysis of small alkanethiolate-stabilised gold nanoparticles. Chemical Physics Letters, 2008. 460(1–3): p. 230-236.
39. Leff, D.V., et al., Thermodynamic Control of Gold Nanocrystal Size: Experiment and Theory. The Journal of Physical Chemistry, 1995. 99(18): p. 7036-7041.
40. Lennon, A.J., et al., Hemoglobin affinity for 2,3-bisphosphoglycerate in solutions and intact erythrocytes: studies using pulsed-field gradient nuclear magnetic resonance and Monte Carlo simulations. Biophysical Journal, 1994. 67(5): p. 2096-2109.
41. Brewer, S.H., et al., Probing BSA Binding to Citrate-Coated Gold Nanoparticles and Surfaces. Langmuir, 2005. 21(20): p. 9303-9307.
42. Ross, R.D. and R.K. Roeder, Binding affinity of surface functionalized gold nanoparticles to hydroxyapatite. Journal of Biomedical Materials Research Part A, 2011. 99A(1): p. 58-66.

3.6 Supplementary Information

Details on the ligand syntheses, nanoparticle synthesis, functionalization and characterization, and binding studies by DOSY NMR are given in this section.

Ligand Syntheses.

General details. Analyses were carried out as follows: melting points, Müller SPM-X 300; NMR, Bruker DPX 400; MALDI-TOF-MS, Bruker Ultraflex TOF/TOF; elemental analysis, Elementar vario Micro cube; IR, FT-IR System Spectrum BX, Perkin-Elmer; Silica gel 60 A (0.06-0.20 mm) Acros Organics, Silica gel 60 (flash) (0.04-0.06 mm) Macherey-Nagel. All starting materials are commercially available and were used without further purification.

Synthesis of 8-(Acetylthio)octanoic Acid. To a solution of 8-bromooctanoic acid (3 g, 13.4 mmol) in methanol (100 mL), potassium thioacetate (3 g, 26 mmol) was added and the mixture was refluxed for 24 h. After cooling, the solvent was evaporated and the crude product was dissolved in dichloromethane (50 mL). The solution was extracted three times with water, the organic layer was dried, and the solvent was evaporated. The obtained material was purified by column chromatography (SiO_2, dichloromethane/hexane, 1:1) to afford the product as beige solid. Yield: 2.5 g, 85%;

^{1}H NMR (400 MHz, 25 °C, $CDCl_3$) δ = 2.86 (t, 2H, ^{3}J = 7.3 Hz, SCH_2), 2.35 (t, 2H, ^{3}J = 7.6 Hz, $COCH_2$), 2.33 (s, 3H, $SCOCH_3$); 1.65-1.55 (m, 4H, 2 × CH_2), 1.38-1.34 (m, 6H, 3 × CH_2) ppm; ^{13}C NMR (100.6 MHz, 25 °C, $CDCl_3$) δ = 196.9, 180.2, 34.6, 31.1, 30.1, 29.8, 29.6, 29.4, 29.3, 25.3 ppm; IR wavenumber/cm^{-1}: 3474 (m), 2931 (m), 2858 (w), 1723 (w), 1660 (s), 1487 (w), 1438 (m), 1408 (m), 1386 (s), 1255 (m), 1090 (s), 1063 (w), 658 (s).

Synthesis of Ligand Q. To a solution of 8-(acetylthio)octanoic acid (600 mg, 2.7 mmol) in Dichloromethane (50 mL) and dimethylformamide (5 mL), N,N'-dicyclohexylcarbodiimide (800 mg, 3.9 mmol) and 4-dimethylaminopyridine (50 mg, 0.4 mmol) were added, followed by 2-amino N,N,N-trimethyl ethanaminium chloride (500 mg, 3.6 mmol). The reaction mixture was refluxed for 16 hours under a nitrogen atmosphere. Afterwards, the solvent was evaporated, cold acetone (2 mL) was added to the residue, and the solution was filtered to remove residual DCU. The filtrate was evaporated and the addition of acetone, filtration, and evaporation was repeated twice more. The crude product was thus obtained as light yellow sticky oil. Further purification was achieved by flash column chromatography (SiO_2, methanol). Fractions containing the product were collected and evaporated to dryness. The residue was dissolved by addition of dichloromethane (2 mL), and the resulting suspension was filtered to remove silica gel.

The filtrate was evaporated to afford the product as colorless sticky oil. Yield: 650 mg, 60%;

^{1}H NMR (400 MHz, 25 °C, $CDCl_3$) δ = 8.69 (s, 1H, NH), 3.74 (m, 4H, 2 × NCH_2), 3.38 (s, 9H, $N(CH_3)_3$), 2.77 (t, 2H, ^{3}J = 7.5 Hz, SCH_2), 2.25 (s, 3H, $SCOCH_3$), 2.22 (t, 2H, ^{3}J = 7.7 Hz, $COCH_2$,), 1.60-1.42 (2 × m, 4H, 4 × CH_2), 1.18-1.29 (m, 6H, 3 × CH_2) ppm; ^{13}C NMR (100.6 MHz, 25 °C, $CDCl_3$) δ = 196.2, 174.8, 65.8, 54.2, 36.2, 34.4, 30.7, 29.4, 29.1, 29.1, 28.8, 28.6, 25.3 ppm; IR wavenumber/cm^{-1}: 3364 (m) 3252 (m), 3026 (w), 2928 (s), 2855 (m), 1687 (s), 1654 (s), 1541, 1480, 1353, 1133, 955; MALDI-TOF MS m/z (%): 303.1 (100) $[M-Cl]^{+}$; elemental analysis calcd (%) for $C_{15}H_{31}ClN_2O_2S{\cdot}0.5H_2O$: C 51.78, H 9.27, N 8.05, S 9.22; found C 51.64, H 9.00, N 7.91, S 9.13.

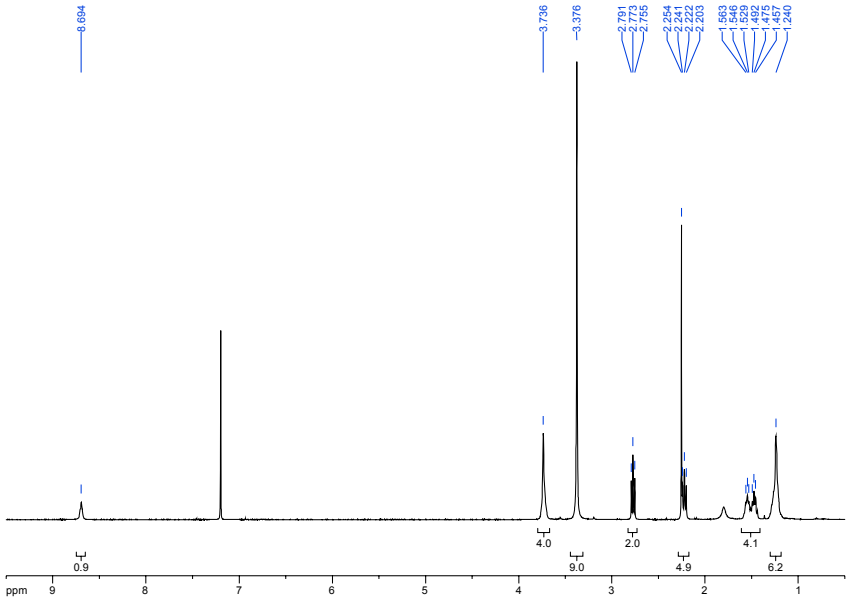

Figure S 3-1: ^{1}H NMR spectrum of ligand Q in $CDCl_3$.

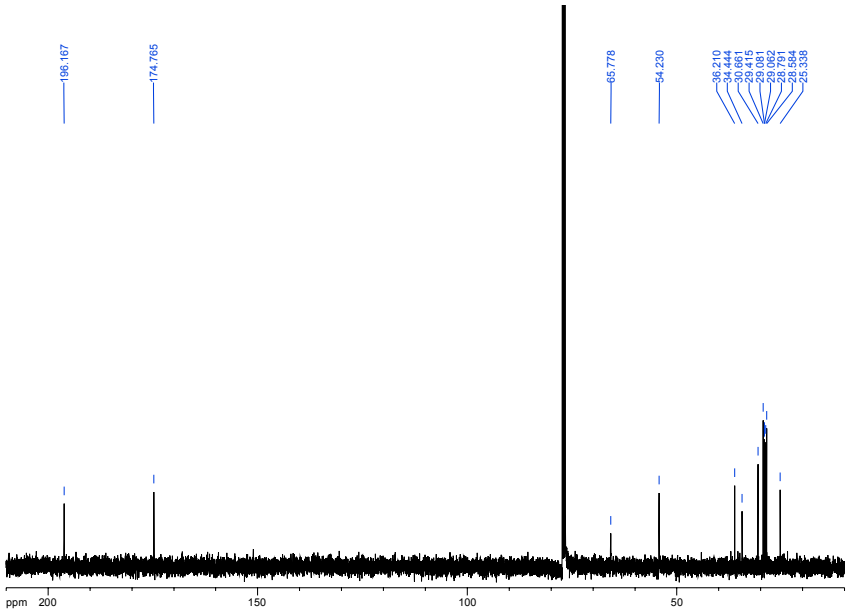

Figure S 3-2: ^{13}C NMR spectrum of ligand Q in $CDCl_3$.

Synthesis of Ligand C. To a solution of 8-(acetylthio)octanoic acid (160 mg, 0.7 mmol) in dichloromethane (30 mL) and dimethylformamide (3 mL), N,N'-dicyclohexylcarbodiimide (185 mg, 0.9 mmol) and 4-dimethylaminopyridine (12 mg, 0.1 mmol) were added, followed by 4'-aminobenzo-18-crown-6 (200 mg, 0.6 mmol). The resulting reaction mixture was refluxed for 16 h under a nitrogen atmosphere. Afterwards, the solvent was evaporated and the product was purified chromatographically (SiO_2, ethyl acetate) to afford a white powder. Yield: 170 mg, 54 %; mp. 113-115 °C;

^{1}H NMR (400 MHz, 25 °C, $CDCl_3$) δ = 7.30 (s, 1H, PhH), 6.98 (s, 1H, NH), 6.76 (s, 2H, PhH); 4.11-4.05 (2 × m, 4H, 2 × OCH_2), 3.83-3.85 (m, 4H, 2 × OCH_2), 3.62-3.70 (m, 12H, 6 × OCH_2), 2.79 (t, 2H, ^{3}J = 7.3 Hz, SCH_2), 2.27-2.23 (m, 5H, $COCH_2$, $SCOCH_3$), 1.70-1.61 (m, 2H, CH_2), 1.55-1.44 (m, 2H, CH_2), 1.29-1.35 (m, 6H, 3 × CH_2) ppm; ^{13}C NMR (100.6 MHz, 25 °C, $CDCl_3$) δ = 196.2, 171.1, 149.2, 145.4, 132.2, 114.8, 112.1, 106.9, 70.8, 70.8, 70.7, 70.6, 69.7, 69.6, 69.5, 68.9, 37.5, 30.7, 29.4, 29.0, 28.7, 28.5, 25.4 ppm; IR wavenumber/cm^{-1}: 3285 (m), 3075 (w), 2929 (m), 2854 (m), 1681 (s), 1650 (s), 1601 (w), 1544 (m), 1513 (m), 1410, 1247, 1126 (s), 1086, 1055, 947, 845, 721; MALDI-TOF MS m/z (%): 527.4 (63) $[M+H]^+$, 550.5 (100) $[M+Na]^+$, 566.5 (68) $[M+K]^+$; elemental analysis calcd (%) for $C_{26}H_{41}NO_8S$: C 59.18, H 7.83, N 2.66, S 6.08; found C 59.16, H 8.06, N 2.62, S 5.67.

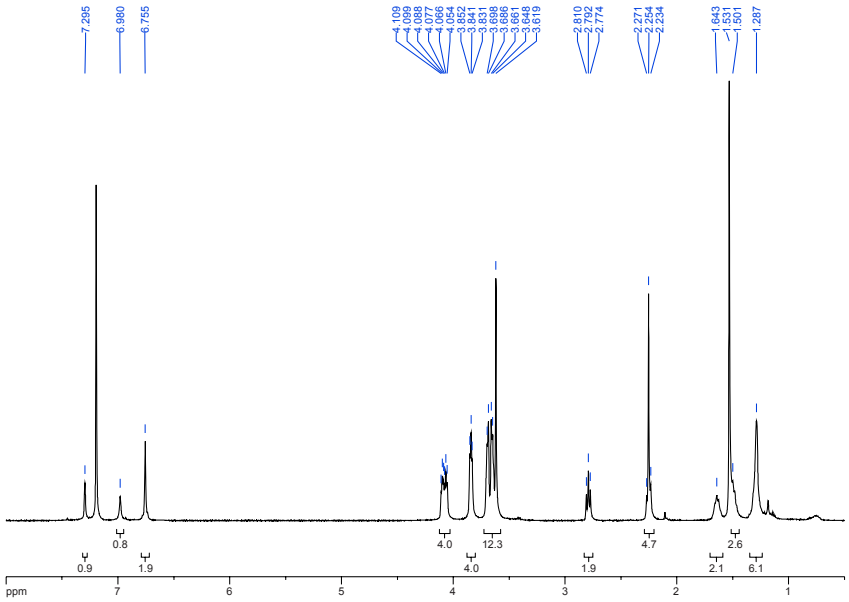

Figure S 3-3: ^{1}H NMR spectrum of ligand C in $CDCl_3$.

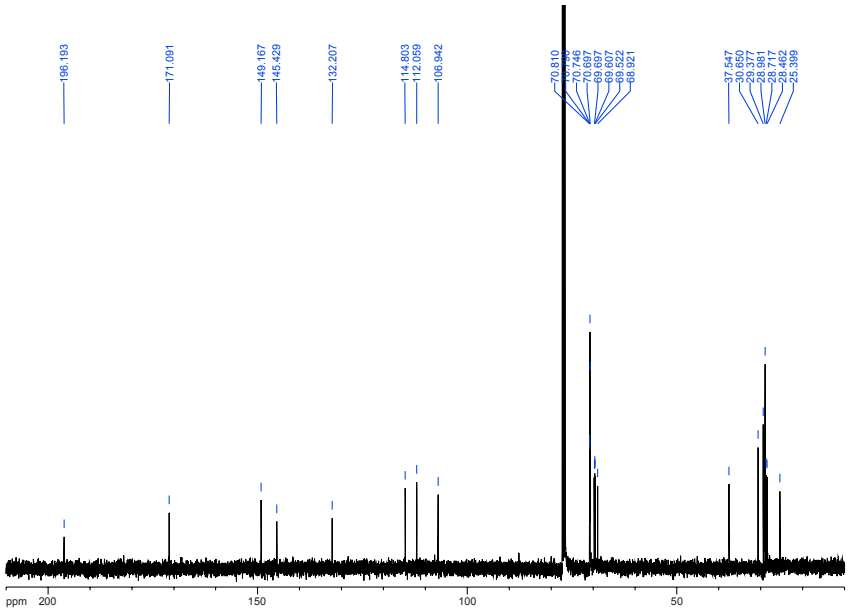

Figure S 3-4: ^{13}C NMR spectrum of ligand C in $CDCl_3$.

Synthesis of Ligand P. To a solution of 8-(acetylthio)octanoic acid (500 mg, 2.3 mmol) in dichloromethane (30 mL), N,N'-dicyclohexylcarbodiimide (700 mg, 3.4 mmol) and 4-dimethylaminopyridine (70 mg, 0.6 mmol) were added, followed by 3-phenylpropanamine (0.27 mL, 1.9 mmol). The resulting reaction mixture was refluxed for 16 h under a nitrogen atmosphere. Afterwards, the solvent was evaporated and product was purified chromatographically (SiO_2, acetone/hexane, 1:1). The yellow solid collected after evaporation of the product fractions was dissolved in dichloromethane and precipitated in cold ether. The beige product was collected by filtration, washed with ether, and dried. Yield: 480 mg, 75 %; mp. 205-207 °C;

^{1}H NMR (400 MHz, 25 °C, $CDCl_3$) δ = 7.33-7.04 (m, 5H, PhH), 5.32 (s, 1H, NH), 3.22 (q^{app}, 2H, ^3J = 6.6 Hz, NCH_2), 2.78 (t, 2H, ^3J = 7.2 Hz, SCH_2), 2.59 (t, 2H, ^3J = 7.6 Hz, $PhCH_2$), 2.25 (s, 3H, $SCOCH_3$), 2.04 (t, 2H, ^3J = 7.5 Hz, $COCH_2$), 1.77 (q, 2H, ^3J = 7.3 Hz, CH_2), 1.43-1.54 (m, 4H, 2 × CH_2), 1.19-1.24 (m, 6H, 3 × CH_2) ppm; ^{13}C NMR (100.6 MHz, 25 °C, $CDCl_3$) δ = 196.1, 173.1, 141.4, 128.4, 128.3, 126.0, 39.2, 36.6, 33.3, 31.2, 30.6, 29.4, 29.0, 28.7, 28.5, 25.6 ppm; IR wavenumber/cm^{-1}: 3325 (m), 3063 (w), 3029 (w), 2926 (m), 2851 (m), 1682 (m), 1640 (s), 1544 (s), 1452 (w), 1244 (m), 1115 (m), 1088 (m), 744, 698, 634; MALDI-TOF MS m/z (%): 336.3 (100) $[M+H]^+$, 358.3 (56) $[M+Na]^+$, 374.3 (10) $[M+K]^+$; elemental analysis calcd (%) for $C_{19}H_{29}NO_2S$: C 68.02, H 8.71, N 4.18, S 9.56; found C 67.44, H 8.88, N 4.07, S 9.29.

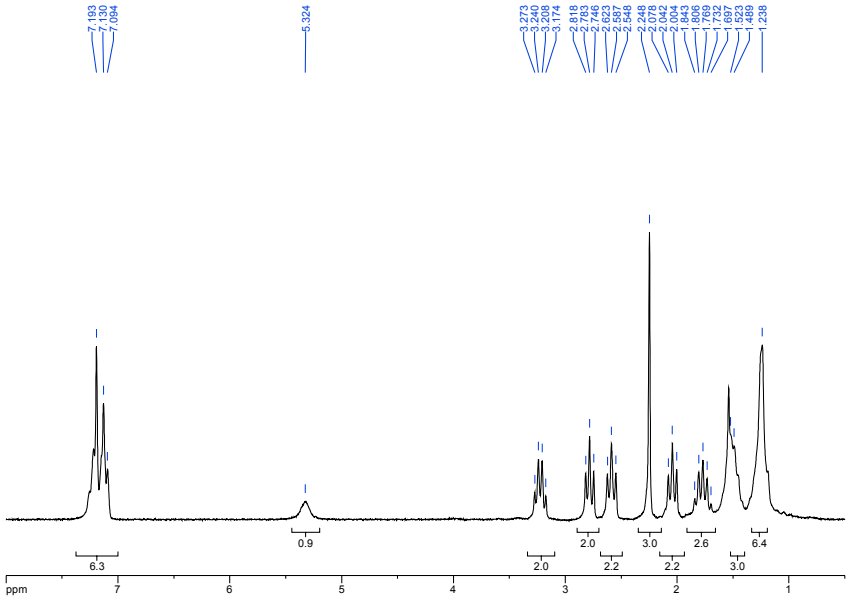

Figure S 3-5: ^{1}H NMR spectrum of ligand P in $CDCl_3$.

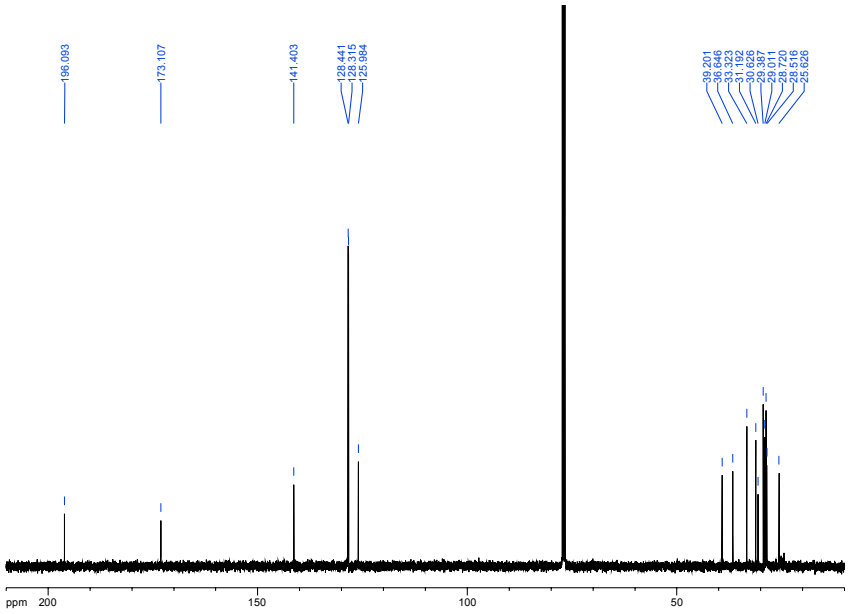

Figure S 3-6: ^{13}C NMR spectrum of ligand P in $CDCl_3$.

General Procedure of the Deprotection of the Ligands. The protected ligands Q, C, P (0.2 mmol) were dissolved in degassed methanol (2 mL) in separate vials and the solutions were purged thoroughly with argon. Afterward, HCl in dry 1,4-dioxan (5 N, 2 mL) was added to each solution and the resulting mixtures were stirred at 25 °C under argon. The reactions were followed by ^1H NMR spectroscopy, which revealed progressive disappearance of the methyl signals of the thioacetate groups. After 4 h, each sample was evaporated under vacuum and the thiols thus obtained were kept under argon to prevent disulfide formation.

Nanoparticle Syntheses and Characterization

Synthesis of Dioctylamine-protected Gold Nanoparticles (NP_A). A solution of $HAuCl_4 \cdot 3\ H_2O$ (40 mg, 0.12 mmol) in water (15 mL) was mixed with a solution of tetraoctylammonium bromide (2.18 g, 4 mmol) in degassed toluene (100 mL). The yellow aqueous solution turned colorless and the organic layer became reddish-orange. Di-n-octylamine (2.78 mL, 9.2 mmol) was added and the mixture was vigorously stirred for 40 min while the color disappeared. Afterwards, a solution of $NaBH_4$ (37 mg, 0.97 mmol) in H_2O (10 mL) was added within 20 s under vigorous stirring. The solution was stirred for another 3 h. Then, the aqueous layer was separated and the remaining resulting nanoparticle solution was kept under a nitrogen atmosphere for 24 h at 10 °C.

Synthesis of Mixed-Monolayer Gold Nanoparticles. Deprotected ligands Q, P, and C were dissolved in degassed methanol (2 mL) separately or as mixtures in the desired ratios and added to the solution of NP_A (40 mL) under an argon atmosphere in a closed vial. This reaction mixture was stirred for 2 h at 25 °C. Afterwards, water (2 ml) was added and the nanoparticles were transferred to the aqueous layer by stirring for 30 min. The aqueous layer was separated, the solvent was removed, and the nanoparticles were purified four times by dissolving them in methanol and removing the solvent by centrifugation through a molecular weight cutoff membrane (Hydrosart membrane, 5K). The nanoparticle layer was collected and dried. Purity was checked by ^{1}H NMR spectroscopy using D_2O as solvent. Typical yields: 15-20 mg.

Table S 3-1: Conditions used for the preparation of nanoparticles NP_Q, NP_{QC}, NP_{QP}, NP_{QPC}.

nanoparticles	NP_A solution / mL	Q / mmol	C / mmol	P / mmol
NP_Q	40	0.04	-	-
NP_{QC}	40	0.02	0.02	-
NP_{QP}	40	0.02	-	0.02
NP_{QPC}	40	0.015	0.015	0.015

Iodine Decomposition. Iodine decomposition of the nanoparticles in the presence of an internal standard (2,4,6-trimethoxy-1,3,5-triazine) followed by ^{1}H NMR spectroscopic investigation of the resulting solution was used to determine the ratio of ligands bound to nanoparticle core. To a sample of a functionalized nanoparticle (3 mg, ~ 0.06 µmole) in an NMR tube, a solution of iodine (25 mg, 0.098 mmole) in methanol-d_4 (0.5 mL) followed by a stock solution of 2,4,6-trimethoxy-1,3,5-triazine (73 mM, 100 µL) in methanol-d_4 were added. The resulting mixture was sonicated for 30 min at 40 °C to complete the decomposition of the nanoparticles. Afterward, a ^{1}H NMR spectrum was recorded and the ratio of the integrals of characteristic signals from the individual ligands were estimated by also considering the respective number of absorbing protons. Specifically, the signal of the N-methyl group of Q at 3.09 ppm, corresponding to 9 protons, the signals of aromatic protons of C at 7.20 and 6.90-6.77 ppm, corresponding to 1 and 2 protons, respectively, and the signal of the aromatic protons of P between 7.16-7.02 ppm, corresponding to 5 protons, were used. Complete decomposition of the nanoparticles was ensured by relating the integral of the signal of the internal standard (3.95 ppm) to the experimental integrals of ligand signals as well as the expected ones calculated on the basis of the amount of nanoparticles used and their composition.

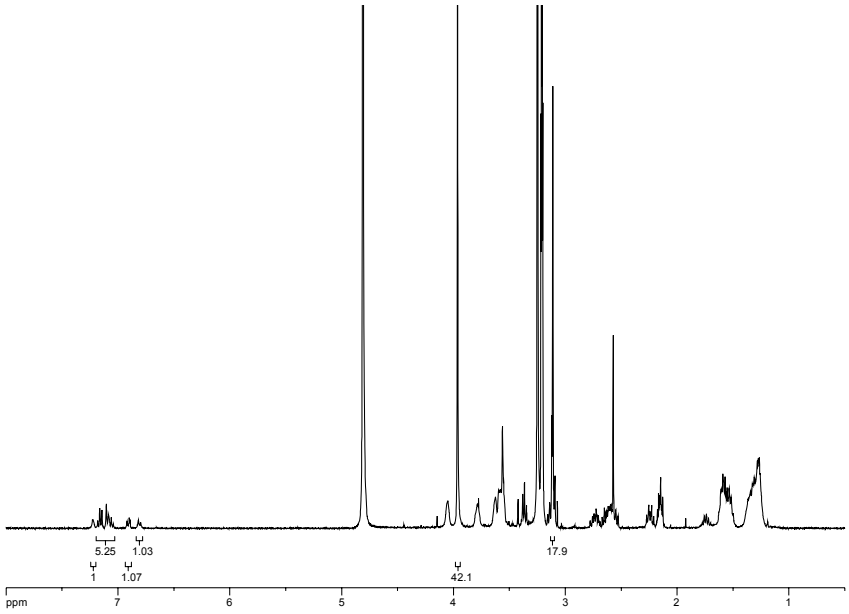

Figure S 3-7: ^{1}H NMR spectrum of NP_{QPC} in methanol-d_4 after I_2 decomposition.

UV/vis Spectroscopy. NP_Q was characterized by UV/vis spectroscopy (Varian Cary 100 Conc UV/vis Spectrophotometer) to estimate the average size of the nanoparticles. To this end, a solution of NP_Q (2 µM) in water was prepared and the UV/vis spectrum recorded in the range 200-800 nm. The spectrum exhibits a very weak absorption band at ca. 515 nm indicating that the average diameter of gold core of NP_Q is below 2 nm.

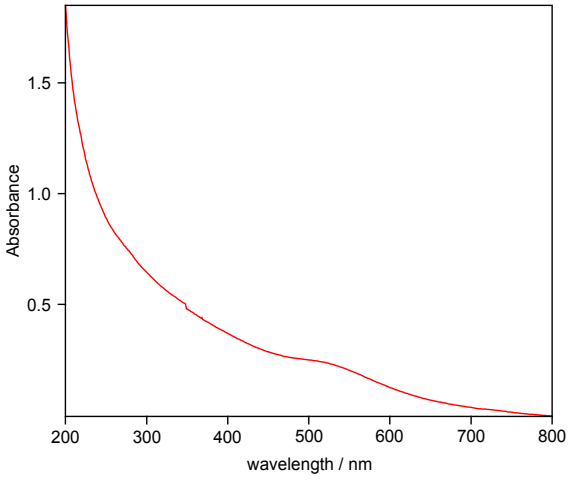

Figure S 3-8: UV/vis spectrum of NP_Q (0.2 µM) in water.

Estimation of the fraction χ of bound peptides by DOSY NMR spectroscopy.

Table S 3-2: Diffusion coefficients Dfree of peptides Gly-Phe and Gly-Gly (4.8 mM) and of the prepared mixed monolayer nanoparticles Dbound (0.048 mM) in water and diffusion coefficients D_{obs} of the peptides (0.072 mM) in the presence of nanoparticles (0.048 mM).

	D_{free} / × 10^{10} m^2 s^{-1}	D_{bound} / × 10^{10} m^2 s^{-1}	D_{obs} / × 10^{10} m^2 s^{-1}	χ / %
NP_Q + Gly-Phe	5.81	0.81	3.93	38
NP_{QC} + Gly-Phe	5.81	0.72	4.74	31
NP_{QP} + Gly-Phe	5.81	0.74	4.24	21
NP_{QPC} + Gly-Phe	5.81	0.80	1.91	78
NP_Q + Gly-Gly	7.49	0.81	5.36	32
NP_{QC} + Gly-Gly	7.49	0.72	5.94	23
NP_{QP} + Gly-Gly	7.49	0.74	6.22	19
NP_{QPC} + Gly-Gly	7.49	0.80	4.25	48

Quantitative evaluation of peptide affinity.

Table S 3-3: Results of the titration of NP_Q with Gly-Phe.

c_{Pep} /mM	D_{obs} /× 10^{10} m^2 s^{-1}	χ
0.072	3.93	0.377
0.144	4.58	0.248
0.288	4.88	0.188
0.567	5.17	0.131
0.096	5.41	0.083
0.120	5.39	0.086
0.144	5.46	0.073
0.216	5.44	0.076

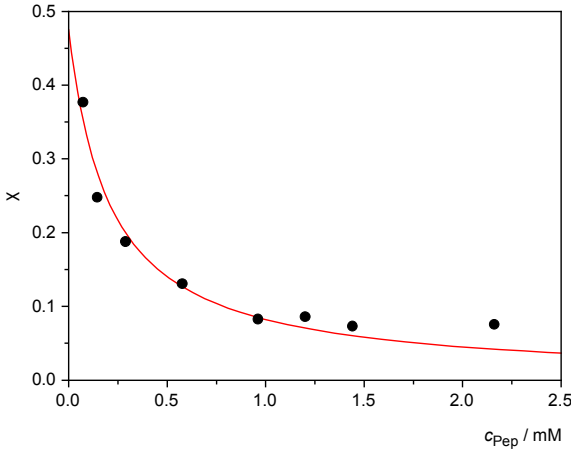

Figure S 3-9: Dependence of the DOSY NMR spectroscopically determined fraction of bound Gly-Phe to NP_Q on peptide concentration.

Table S 3-4: Results of the titration of NP_{QPC} with Gly-Phe.

c_{Pep} /mM	D_{obs} /× 10^{10} m^2 s^{-1}	χ
0.036	1.45	0.871
0.072	1.91	0.779
0.144	3.02	0.558
0.288	3.84	0.395
0.567	4.98	0.168
0.096	5.43	0.786
0.120	5.50	0.646
0.144	5.55	0.547
0.216	5.60	0.447

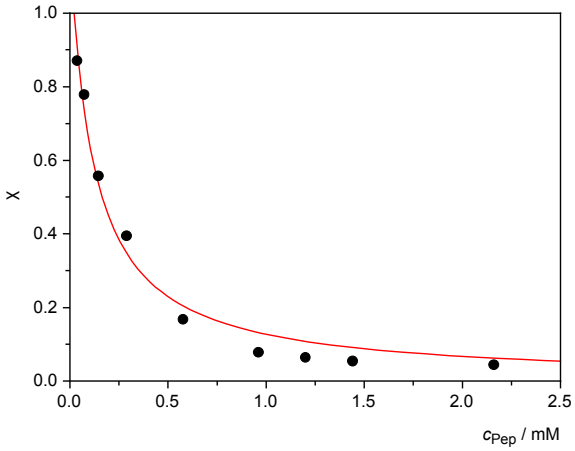

Figure S 3-10: Dependence of the DOSY NMR spectroscopically determined fraction of bound Gly-Phe to NP_{QPC} on peptide concentration.

Table S 3-5: Summary of the results of the titrations

AuNP	K / M^{-1}	c_{max} / mM	c_{max} / c_{NP}
NP_Q	4770 ± 1180[a]	0.100	2.1
NP_{QPC}	8260 ± 1480[a]	0.143	3.0

a The calculated errors describe the goodness of the fit of the regression curve and the experimental results.

Chapter 4 Ternary quantum dot supramolecular networks for selective lectin detection

Abstract

A versatile, tunable and selective nanoparticle-based lectin biosensor is presented, based on flocculation of ternary supramolecular nanoparticle networks (NPN), where NPN form due to sequential binding events of three orthogonal building blocks. The three building blocks are β-cyclodextrin-capped CdTe quantum dots, tetraethylene glycol-tethered mannose-adamantane cross-linkers (ADTEGMan) and the tetravalent lectin Concanavalin A. The working principle of this selective sensor lies in the dual orthogonal molecular interactions of the linker, combining, on one hand, adamantane- β-cyclodextrin interactions and on the other hand, mannose-lectin interactions. Only when lectin is present, sequential binding events take place; from quantum dot to linker and from linker to lectin, leading to self-organization in-situ of the sensor through the formation of ternary supramolecular networks. Monitoring the loss of fluorescence signal of quantum dots in solution over time, caused by controlled network formation and consecutive flocculation and sedimentation, leads to selective, qualitative and quantitative lectin detection. Fluorescent sedimented networks can be observed by naked-eye or under UV illumination up to 10^{-8} M. Quantitative detection is possible at 100 minutes with lower quantitation limit of approximately 4.0×10^{-8} M.

Part of this Chapter is based on: M. Oikonomou, J. Wang, R.R. Carvalho and A. H. Velders, Ternary Supramolecular Quantum Dot Network Flocculation for Selective Lectin Detection, Accepted in Nano Research.

4.1 Introduction

Supramolecular Nanoparticle Networks (NPN) have been employed lately as a biosensing methodology for detection of a wide range of biomolecules such as nucleic acids [1-3], proteins [4, 5] microbes [6, 7], cell-receptors [8] and even in vivo cells or tissues as a whole [9]. NPN biosensors are advantageous because they combine the intrinsic properties of the core nanoparticle material with the orthogonality and dynamic nature of the supramolecular interactions [10]. These properties can be tuned on demand to design ultrasensitive, highly selective, versatile and often on-spot biosensors [1, 2, 11-13].

The majority of supramolecular NPN biosensors are based on the formation of secondary supramolecular networks, which consist of two building blocks, functionalized nanoparticles bearing recognition moieties and the target biomolecule. In secondary NPN biosensors, the biosensing strategies can be categorized in monitoring the assembly process or the concomitant disassembly of NPN [2] caused for example by competitor molecules [3, 14] enzyme cleaving of linkers [14], or other physicochemical triggers [3, 15, 16]. The next step for improving the tunability and selectivity of biosensors, is the transition from secondary to ternary supramolecular NPN [17, 18] where NPN form due to sequential binding events of three orthogonal building blocks. The three building blocks are functionalized nanoparticles and bifunctional bridging molecules orthogonal to both the nanoparticle ligand and the target biomolecule.

The wide occurrence of lectins in nature (plants, animals, bacteria and viruses) with numerous biological roles is subject of study in various scientific fields such as plant biology, immunology, food science and clinical biochemistry [6, 17, 19-24]. NPN biosensors [25-27] have been extensively applied to unravel the occurrence, pattern recognition and biological role of multivalent sugar-specific-binding proteins called lectins [28]. For example, NPN have been used for plant lectin classification [20] discriminating each lectin from a mixture of lectins. Clinically some of the theranostic applications of lectins include bacterial detection, [6, 21] HIV inhibition, [23] and cancer detection [19]. In food science, NPN-based assays have been developed for the detection and screening of toxic and allergenic lectins [24]. Thus, developing label-free, easy to use and highly selective lectin-based biosensors has an enormous potential use in many scientific fields.

Samanta et al have recently shown an elegant approach applying ternary supramolecular networks for isolation of lectins using magnetic nanoparticles; fluorescent labels were separately added to follow and characterize the process [17]. Herein a quantum-dot based sugar-selective fluorescent lectin sensor is reported, which assembles in-situ upon addition of a sugar-specific lectin. The building blocks of the sensor are β-cyclodextrin-capped CdTe quantum dots (β-CD-QD) with maximum emission wavelength

at 671 nm, tetraethylene glycol-tethered mannose-adamantane linkers (ADTEGMan) and Concanavalin A (ConA). ConA was chosen as a model lectin since it is a very well-studied, tetravalent mannose-binding lectin with various biomedical applications [6, 29-31]. The success of this sensor lies in the dual orthogonal molecular interactions of the ADTEGMan linker. The linker exhibits binding not only with the β-CD-QD but also with the lectin. Thus, the sensor self-organizes in-situ, forming ternary supramolecular networks, only when the lectin is present. Consequently, upon addition of ConA in a mixture β-CD-QD and ADTEGMan, the fluorescence intensity decreases, as the networks form, flocculate and sediment (Figure 4-1).

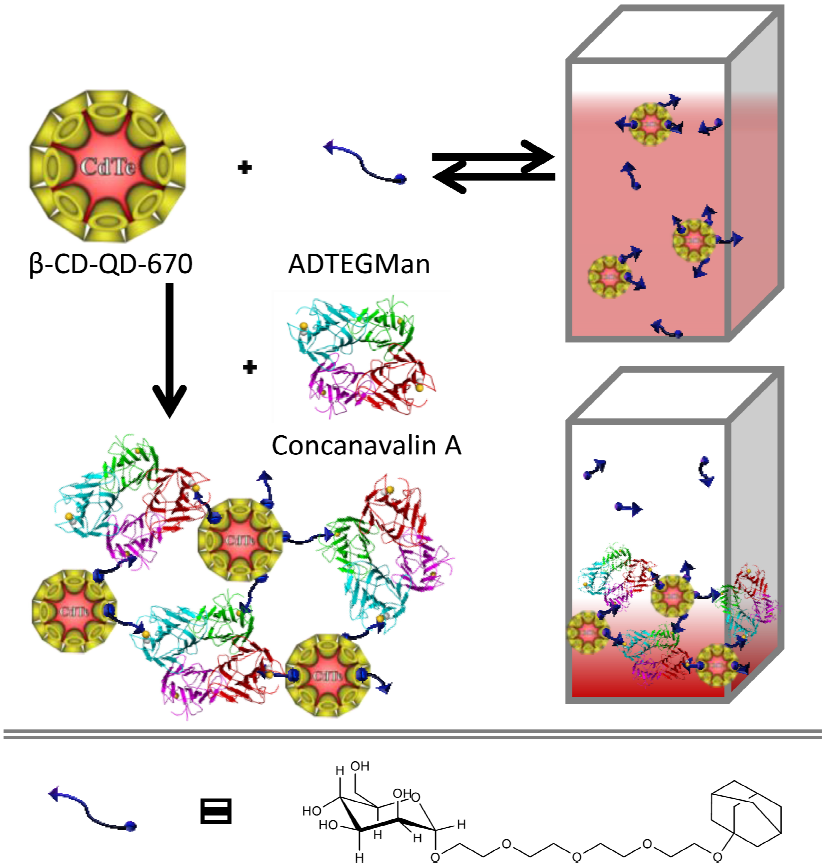

Figure 4-1: Representation of formation of ternary supramolecular network upon addition of ConA to a solution of β-CD-QD and ADTEGMan; once formed the NPN sediment and the solution loses fluorescence

In the past, when designing and using lectin biosensors, sedimentation of NPN was considered rather unwanted because the detection was based typically on SPR signal or UV-Vis absorption [32, 33]. Moreover, identification and isolation of lectins was possible upon application of a magnetic field [17]. Recently, however, there have been a few examples in literature, where flocculation and sedimentation was induced on purpose

for developing a new generation of sensors. Based on nanoparticle flocculation assays, Wee et al. presented a rapid, qualitative DNA sensor [1]. In another case, demonstrated by Earhart et al., the inhibition effect of a glycoprotein on the flocculation kinetics of nanoparticle-Concanavalin A networks, allowed for screening the biochemical activity of the synthesized nanoparticles [34].

Therefore, the lectin sensor was designed such as controlled assembly, flocculation and sedimentation of ternary supramolecular networks leads to qualitative and quantitative detection [35]. This is the first example of ternary supramolecular networks that quantitatively detect biomolecules by flocculation assay reported in literature. On-spot detection by naked-eye or UV illumination is also possible up to a concentration of 10^{-8} M of ConA.

4.2 Experimental

Water-soluble CdTe quantum dots capped with thioglycolic acid [36] exhibiting emission at 670±10 nm were purchased from Plasmachem (Germany). Dolichos biflorus (DBA), Ricinus communis I (RCA_{120}), Soyabean Agglutinin (SBA) and Wheat Germ agglutinin (WGA) were purchased from Vector Labs. Concanavalin A was purchased from Sigma Aldrich with and without fluorescent label. Five fluoresceins were estimated to be attached on Concanavalin A by comparing it to the fluorescence of free fluorescein. For binding studies samples were prepared in PBS buffer saline 0.01 M with Mg^{2+} 0.015 mM, Mn^{2+} 0.011 mM, Ca^{+2} 0.011 mM and 0.008 % w/v NaN_3.

β-CD-QDs were synthesized by exchanging carboxyl-terminated monothiol ligands of the capped quantum dots with heptakis-thiolated β-CD after overnight stirring in water [37]. Purification of β-CD-QD is performed by spin-filtration. Heptakis-thiolated β-CD used for the ligand exchange is synthesized in two steps and ADTEGMan in three steps comprising only one column purification. Both building blocks are synthesized by modified protocols reported elsewhere; see supporting information for details [38-40].

For characterizing the modified β-CD-QDs 1H NMR, DOSY NMR and TEM was used, see supporting information. For monitoring and characterizing the network formation, flocculation and sedimentation DLS, steady-state fluorescence and TEM was used.

For the quantitative assay at different lectin concentration, 8.0×10^{-8} M of β-CD-QD and ADTEGMan at 1.4×10^{-5} M was used. For obtaining quantitative fluorescence data, the quantum dot emission peak at 671 nm was monitored in time, as the networks form, flocculate and precipitate. For the selectivity experiments four different lectins (Dolichos biflorus (DBA), Ricinus communis I (RCA_{120}), Soyabean Agglutinin (SBA) and Wheat Germ

agglutinin (WGA)) were used. In these experiments, the quantum dot fluorescence at 671 nm was monitored in time. For calculating the binding stoichiometry, fluorescein labeled Concanavalin A was used and the fluorescence emissions of quantum dots, at 671 nm and also at 519 nm the fluorescein attached on Concanavalin A was monitored.

4.3 Results and Discussion

The synthesis of ADTEGMan involved three steps (see SI, Figure S 4-1). First, bromoadamantane was coupled to tetraethylene glycol, then a peracetylated mannose was attached and last deprotection of the mannose moiety yielded the final linker. The synthesis of heptakis-thiolated β-CD used for the ligand exchange involved two steps, first the bromination of β-CD and then thiolation with thiourea (see SI, Figure S 4-2). For the quantum dot modification with β-CD, a ligand exchange reaction was performed by adding excess of heptakis-thiolated β-CD. The reaction successfully exchanges coordinating monothiol ligands such as thioglycolic acid with thiols of higher valency [41].

Verification of the ligand exchange was performed by 1H NMR and DOSY NMR. By 1H NMR broad cyclodextrin peaks are observed, indicating the confinement of cyclodextrin on the nanoparticle surface.

The size of the core of the modified β-CD-QD was characterized by TEM and found to be 2.2 nm (see SI, Figure S 4-4). According to DOSY NMR, the broadened cyclodextrin peaks of the proton spectrum correspond to nanoparticles with a hydrodynamic radius of 3.0 nm, proving that the cyclodextrins are covering the nanoparticle surface (see SI, Figure S 4-4). Considering that cyclodextrin has a half-height of 0.8 nm, the hydrodynamic radius obtained by the DOSY agrees perfectly with the expected theoretical radius size (2.2 nm+0.8 nm=3.0 nm). The fluorescence emission β-CD-QD is at 671 nm by exciting at 450 nm.

For developing a supramolecular sensor, the choice of the amounts and respective ratios of the amounts between all building blocks is crucial. The estimation of the number of cyclodextrins was done by the following rationale. Every quantum dot (r=2.2 nm) has a surface area of approximately a sphere, thus 61 nm^2 and, in an ideal monolayer, every cyclodextrin (r=0.45 nm) occupies a surface area of a circle, thus 0.64 nm^2. Considering that the packing of circles on a sphere is approximately 90% [42], then every quantum dot is considered to bear ideally 86 cyclodextrins, if there is no steric hindrance. For the quantitative assay, β-CD-QD and linker concentrations were optimized in order to obtain fast response times upon addition of lectins (see SI, Figure S 4-6 and Figure S 4-7). After optimization, in all cases 8.0 x 10^{-8} M of β-CD-QD and ADTEGMan at 1.4 x 10^{-5} M were used. Since 146 of cyclodextrins are estimated to be on one quantum dot, the ratio of the effective concentration of β-CD and ManTEGAD is 0.4, there is therefore

an excess of linker. The binding strength of the adamantane-cyclodextrin interactions is $7.2x10^4$ M^{-1} [38] and the binding strength of each sugar binding lectin site with mannose is around $8.2x10^3$ M^{-1} [43]. Hence, the cross-linker ADTEGMan engages in two supramolecular asymmetric binding interactions.

As a proof of principle for the network formation, flocculation and sedimentation, normal photographs and TEM micrographs were recorded from blank samples containing only β-CD-QD (Figure 4-2a) and on networks of β-CD-QD, ADTEGMan and ConA formed after five-hour incubation (Figure 4-2b).

Photographs under UV illumination are given of a solution of β-CD-QD and ADTEGMan (Figure 4-2a right) and the same solution after networks formed upon addition of ConA (Figure 4-2b right). Before addition of ConA all luminescent Quantum Dots are clearly in solution, whilst loss of fluorescence from solution and concomitant sedimentation of fluorescent assemblies at the bottom after incubation with ConA is evident. Qualitative detections are possible up to a concentration of 10^{-8} M, where by naked eye brown-red precipitates or red fluorescent precipitates upon UV illumination.

The TEM micrographs in Figure 4-2b (left) do not provide the exact size of the ternary supramolecular networks formed after addition of ConA as they were obtained from resuspended solutions by mild vortexing. The NPN are smaller than the network size determined by DLS, vide infra, but they still clearly show the difference between blank samples and the networks.

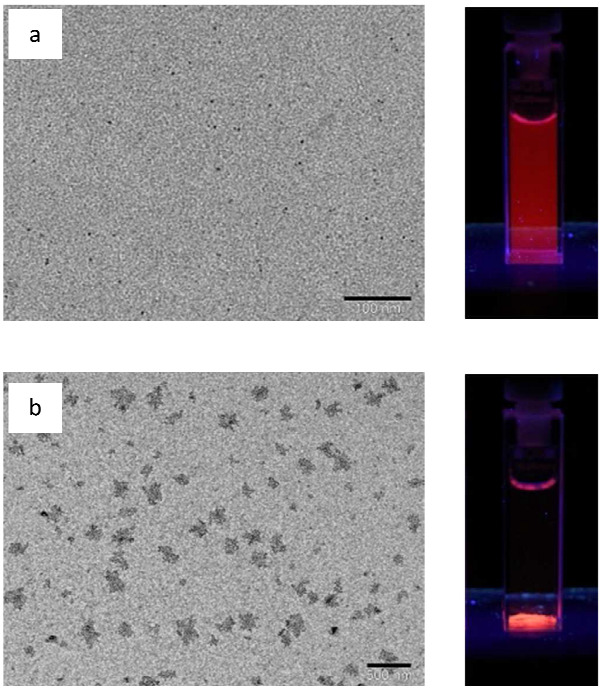

Figure 4-2: TEM images of β-CD-QD (scale bar 100 nm) (a) and suspension of sedimented networks of β-CD-QD, ADTEGMan and ConA after 24h incubation (scale bar 500 nm) (b). The photos on the upper and bottom right belong to the mixture of β-CD-QD and ADTEGMan before, respectively, after the addition of ConA and are illuminated from the bottom by a UV lamp.

For quantitative detection and further investigation of the process, flocculation assays were performed by monitoring the QD-fluorescence intensity over time upon adding different amounts of ConA (1.6×10^{-6} - 3.2×10^{-8} M) (Figure 4-3A).

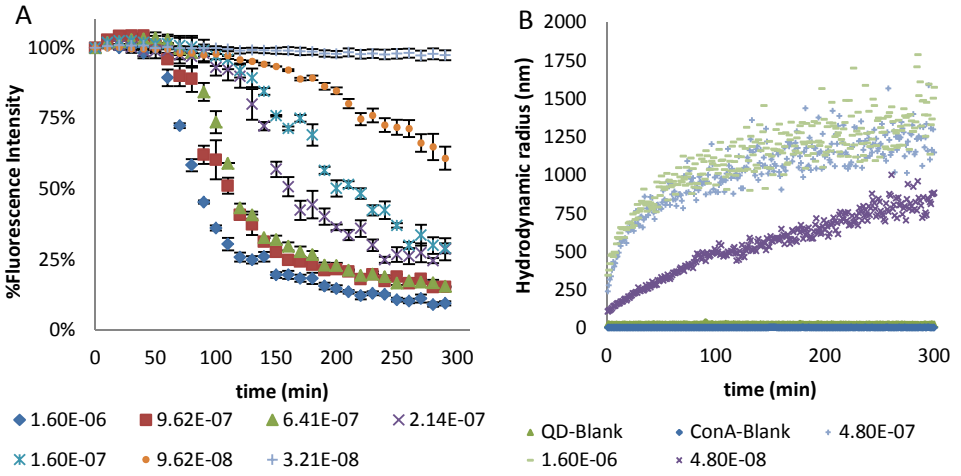

Figure 4-3: Fluorescence flocculation assays at different concentrations of ConA (A.) DLS measurements monitoring the kinetics of network formation induced by ConA at different concentrations in terms of hydrodynamic radius (B).

The assays reveal sigmoidal binding kinetics with a lectin concentration dependent rate [35]. At first, a lag phase is observed, where small assemblies are formed. Then a growth phase follows, where small aggregates assemble further into big aggregates, which eventually sediment. At last, equilibrium is reached when the majority of big assemblies have already sedimented. With increasing lectin concentration, the assembly and sedimentation rate increase, while the time of lag phase and time to reach equilibrium (plateau) both decrease. Observation in-situ of the fluorescent sediments along with the quantitative information from the flocculation assays suggest that the networks form and stay in solution until a critical size is reached, which leads eventually to sedimentation.

To further study and investigate the flocculation process, the kinetics of network formation in terms of hydrodynamic radius (R_H) by DLS at three representative levels of concentration were monitored (Figure 4-3B). The changes in hydrodynamic radius provide size information of the flocculates over time due to the selective, sequential, orthogonal assembly of β-CD-QD, ADTEGMan and ConA in solution. When ConA is added to a solution of β-CD-QD and ADTEGMan, an immediate increase in hydrodynamic radius (R_H) is observed while the R_H of control samples (ConA and β-CD-QD) is constant throughout the experimental time. With increasing ConA concentration, the initial R_H value increases, while the time point of slope change and for the plateau to be reached is decreased. After the addition of 1.6×10^{-6}, 4.8×10^{-7} and 4.8×10^{-8} of ConA, the initial R_H (at time zero of the flocculation kinetics) are 346, 240 and 108 nm respectively and increase within time. In the cases of 1.6×10^{-6} and 4.8×10^{-7} M of ConA added, plateau is reached while in the case of 4.8×10^{-8} of ConA plateau is not reached within 5 hours. For 1.6×10^{-6}

M of ConA, a slope change around 20 minutes is observed, which is in good agreement with the observed time point when fluorescence intensity starts to decrease. For 4.8 x 10^{-7} M, the slope change is around 40 minutes and the evolution profile of R_H over time is constantly below the one of 1.6 x 10^{-6} M. Judging from hydrodynamic radius curves obtained in time at two concentrations; 1.6 x 10^{-6} and 4.8 x 10^{-7} M, the critical sedimentation radius R_H is estimated to be approximately 0.9 μm. The critical sedimentation radius is regarded as the point of slope change.

To demonstrate the orthogonality of the sensor, control tests of five-hour incubated samples of β-CD-QD with ConA (without linker), and β-CD-QD with ADTEGMan (without ConA) were performed, by monitoring the fluorescence intensity decrease of the quantum dots at 671 nm (Figure 4-4). The results clearly show that ConA is detected only due to orthogonal assembly of β-CD-QD, ADTEGMan and the lectin. If one of the three building blocks is missing, no change in fluorescence is observed.

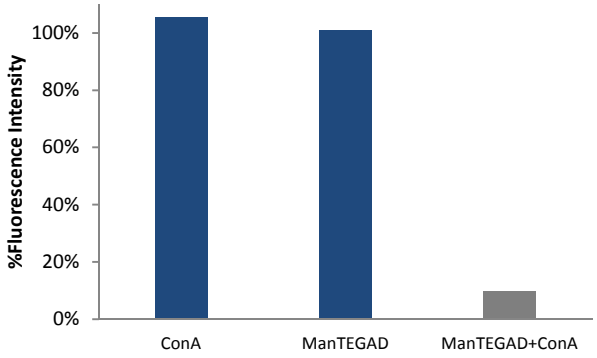

Figure 4-4: Fluorescence intensity % of β-CD-QD after 5 hours incubation time of different control samples demonstrating orthogonality of the sensor. The concentration of β-CD-QD is 8.0 x 10^{-8} M and concentration of ConA is 1.6 x 10^{-6} M. In blue are the control samples, in grey is the Concanavalin A positive test sample.

Subsequently, selectivity was tested by monitoring the fluorescence intensity decrease of the quantum dots at 671 nm against of five-hour incubated samples containing four different lectins. The four lectins used for the selectivity tests were Dolichos Biflorus (DBA), Ricinus Communis I (RCA_{120}), Soyabean Agglutinin (SBA) and Wheat Germ agglutinin (WGA) (Figure 4-5). DBA, RCA_{120}, SBA and WGA recognize mainly galactosamine, galactose, galactose/galactosamine, glucosamine sequences [43].

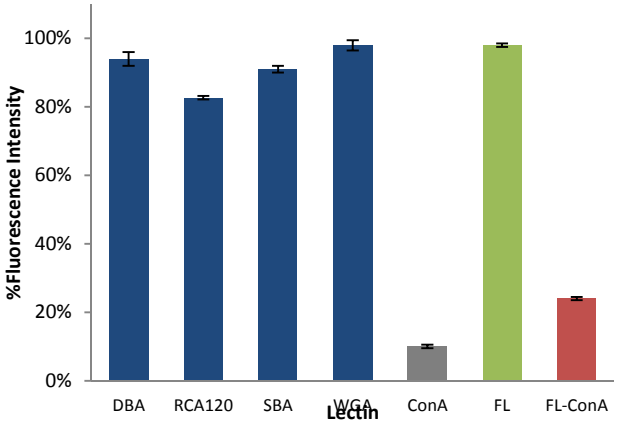

Figure 4-5: Fluorescence intensity % of β-CD-QD remaining in solution at 671 nm or Fluorescein at 519 nm remaining in solution after 5 hours incubation time of different control samples. The concentration of β-CD-QD is 8.0×10^{-8} M and concentration of lectins is 1.6×10^{-6} M. In blue are the control samples, in grey is the β-CD-QD signal (671 nm) tested with non-labeled Concanavalin A (positive test A), in red is the β-CD-QD signal (671 nm) tested with fluorescently labeled Concanavalin A (positive test B) and in green is the fluorescein fluorescence signal (519 nm) attached on ConA.

Whilst is known that monosaccharides bind not as specifically and strongly as complex polysaccharides [20, 44], the selectivity of the ternary NPN for ConA against DBA, SBA, and WGA is excellent with minimal intensity loss over 5 hours of incubation. RCA_{120} seems to exhibit weak quantum dot binding and flocculation, since there is approximately 17% fluorescence intensity loss after 5 hours of incubation. The sensor response to RCA_{120} is attributed to similar specificity of the lectin towards mannose, glucose, galactose as reported [20, 44, 45] and possibly influenced by other parameters as well, such as the lectin geometry and size. In comparison to previously reported selectivity studies, these results are similar and in some cases even significantly improved [4, 46, 47]. The improved selectivity is attributed to the fact that even if nonspecific interactions or weak nanoparticle-lectin interactions occur, these do not lead to sedimentation of quantum dots. In the case non-specific or weak binding does lead to flocculation and sedimentation, like RCA_{120}, the kinetics are much slower than the ConA kinetics, yielding again to better selectivity.

Binding stoichiometry between β-CD-QD and ConA mediated by ADTEGMan linkers is a fundamental parameter for the success of the sensor, since, at least two, and maximum four binding lectin sites need to be engaged in network formation. To quantify the binding stoichiometry between β-CD-QD and ConA mediated by ADTEGMan linkers, fluorescently labeled ConA which bears five fluorescein molecules was used and the fluorescence intensity change of fluorescein at 519 nm emission wavelength in respect to fluorescence intensity change of β-CD-QD at 671 nm was analyzed (Figure 4-5). In the case

of fluorescein-labeled ConA, slightly different kinetics were observed, compared to the non-labeled ConA kinetics, which probably occur due to the proximity of the bulky fluorescein molecules to the mannose binding sites of ConA [48]. This allowed us to quantify the β-CD-QD/ConA ratio that is engaged in the network formation. The amount of Concanavalin A engaged in the networks is 2%, since the fluorescein signal intensity (519 nm) decreased by 2% five hours after the lectin was added in solution, as seen in Figure 4-5. Consequently the amount of lectin engaged in the networks is: 1.60×10^{-6} M x 0.02 $=3.2 \times 10^{-8}$ M. The β-CD-QD concentration is by 76% engaged, when fluorescein-labeled-Concanavalin A is added, thus 4.0×10^{-8} M x 0.76 $=3.04 \times 10^{-8}$ M. The quantified the ratio of β-CD-QD/ConA is approximately one, which means that on average all four binding sites of Concanavalin A bind through an ADTEGMan to a quantum dot.

To quantify the amount of ConA present in solution, the dependency of flocculation kinetics on lectin concentration was analyzed. As shown before in Figure 4-3, the process of flocculation and sedimentation follow sigmoidal binding kinetics with a lectin concentration dependent rate. To quantify, the analysis was performed at a certain time point, where the quantum dot fluorescence intensity values of samples containing different amounts of lectin were plotted against lectin concentration. At the beginning of the growth phase, a linear dependence is found. For example at 100 minutes the following linear response curve %FI =-416271C+1.0176, R^2 = 0.9974 was obtained. At later times (equilibration regime), kinetics exhibit a power law dependence on lectin concentration. The lower detection limits of this sensor are constrained by the concentration of β-CD-QD in solution and are approximately 4.0×10^{-8} M.

4.4 Conclusion

A sensitive, versatile, and selective supramolecular sensor for qualitative and quantitative detection of ConA with a limit of quantitation of 4.0×10^{-8} M was presented. Key feature is the formation and controlled flocculation of supramolecular nanoparticle networks based on orthogonal ternary interactions of simple building blocks. The sensor is easy to use, since β-CD-QD and ADTEGMan only have to be mixed in fixed concentrations. Moreover, on-spot, qualitative detection is possible by observing the formation of fluorescent sediments by naked-eye or UV illumination. Quantitative data can be extracted at different time points either in the linear regime (~100 minutes) or later in the power-law regime (> 160 minutes). The sensing response times can be tuned on demand simply by changing the linker or β-CD-QD concentration and their respective ratios (see SI, Figure S 4-6 and Figure S 4-7).

The presented supramolecular methodology is well suited for detection of ConA and can be extended to the detection of other lectins in solution. Hence it could be used

for sensing other multivalent mannose binding lectins. Apart from detecting other mannose binding lectins, also other sugar binding lectins can be detected, if different sugar linkers are synthesized.

Main advantage of a ternary supramolecular system against covalent systems with two components is its dynamic, self-organizing character based on the sequential binding and self-organization of three orthogonal components. Sequential binding from quantum dots to linkers and from linkers to lectins, leads to selective flocculation and sedimentation excluding in most cases weak or non-specific binding. Preliminary tests show that ConA can also be detected in human serum, although the partial inhibition of the ConA flocculation kinetics, require a recalibration of the sensor (see SI, Figure S 4-8), which is currently further pursued. Altogether, this study opens new opportunities for the development of a new generation of sensors for sensing multivalent biomacromolecules in vitro.

4.5 References

1. Wee, E.J., et al., Re-purposing bridging flocculation for on-site, rapid, qualitative DNA detection in resource-poor settings. Chem Commun (Camb), 2015. 51(27): p. 5828-31.
2. Valentini, P. and P.P. Pompa, Gold nanoparticles for naked-eye DNA detection: smart designs for sensitive assays. RSC Advances, 2013. 3(42): p. 19181.
3. Witten, K.G., et al., Glyco-DNA–Gold Nanoparticles: Lectin-Mediated Assembly and Dual-Stimuli Response. Small, 2011. 7(14): p. 1954-1960.
4. Hu, X.L., et al., Colorimetric and plasmonic detection of lectins using core-shell gold glyconanoparticles prepared by copper-free click chemistry. ACS Appl Mater Interfaces, 2015. 7(3): p. 1874-8.
5. Chapman, R., et al., Multivalent Nanoparticle Networks Enable Point-of-Care Detection of Human Phospholipase-A2 in Serum. ACS Nano, 2015. 9(3): p. 2565-2573.
6. Richards, S.-J., et al., Discrimination between bacterial phenotypes using glyco-nanoparticles and the impact of polymer coating on detection readouts. Journal of Materials Chemistry B, 2014. 2(11): p. 1490.
7. Marin, M.J., et al., Glyconanoparticles for the plasmonic detection and discrimination between human and avian influenza virus. Organic & Biomolecular Chemistry, 2013. 11(41): p. 7101-7107.
8. Souza, G.R., et al., Networks of gold nanoparticles and bacteriophage as biological sensors and cell-targeting agents. Proceedings of the National Academy of Sciences, 2006. 103(5): p. 1215-1220.
9. Liu, Y., J.-J. Yin, and Z. Nie, Harnessing the collective properties of nanoparticle ensembles for cancer theranostics. Nano Research, 2014. 7(12): p. 1719-1730.
10. Verma, A. and V.M. Rotello, Surface recognition of biomacromolecules using nanoparticle receptors. Chemical Communications, 2005(3): p. 303-312.

11. Kameta, N., M. Masuda, and T. Shimizu, Two-step naked-eye detection of lectin by hierarchical organization of soft nanotubes into liquid crystal and gel phases. Chem Commun (Camb), 2015. 51(31): p. 6816-9.
12. Cheng, J., et al., Phosphorylation triggered poly-nanoparticle assembly for naked-eye distinguishable T4 polynucleotide kinase detection. RSC Adv., 2014. 4(100): p. 56731-56735.
13. de la Rica, R. and M.M. Stevens, Plasmonic ELISA for the detection of analytes at ultralow concentrations with the naked eye. Nat Protoc, 2013. 8(9): p. 1759-64.
14. de la Rica, R., et al., Multivalent Nanoparticle Networks as Ultrasensitive Enzyme Sensors. Angewandte Chemie, 2011. 123(25): p. 5822-5825.
15. Krings, J.A., et al., Light-responsive aggregation of [small beta]-cyclodextrin covered silica nanoparticles. Journal of Materials Chemistry A, 2014. 2(25): p. 9587-9593.
16. Stevens, M.M., et al., Coiled-Coil Peptide-Based Assembly of Gold Nanoparticles. Advanced Materials, 2004. 16(11): p. 915-918.
17. Samanta, A. and B.J. Ravoo, Magnetic Separation of Proteins by a Self-Assembled Supramolecular Ternary Complex. Angewandte Chemie International Edition, 2014. 53(47): p. 12946-12950.
18. Nalluri, S.K.M., et al., Light-Responsive Capture and Release of DNA in a Ternary Supramolecular Complex. Angewandte Chemie International Edition, 2011. 50(41): p. 9747-9751.
19. Basuki, J.S., et al., Magnetic nanoparticles with diblock glycopolymer shells give lectin concentration-dependent MRI signals and selective cell uptake. Chemical Science, 2014. 5(2): p. 715-726.
20. Jayawardena, H.S.N., X. Wang, and M. Yan, Classification of Lectins by Pattern Recognition Using Glyconanoparticles. Analytical Chemistry, 2013. 85(21): p. 10277-10281.
21. Reynolds, M., et al., Multivalent gold glycoclusters: high affinity molecular recognition by bacterial lectin PA-IL. Chemistry, 2012. 18(14): p. 4264-73.
22. Manikandan, B. and M. Ramar, Detection and characterization of natural and inducible lectins in human serum. Results Immunol, 2012. 2: p. 132-41.
23. Martínez-Ávila, O., et al., Multivalent Manno-Glyconanoparticles Inhibit DC-SIGN-Mediated HIV-1 Trans-Infection of Human T Cells. ChemBioChem, 2009. 10(11): p. 1806-1809.
24. Schofield, C.L., et al., Colorimetric detection ofRicinus communis Agglutinin 120 using optimally presented carbohydrate-stabilised gold nanoparticles. Analyst, 2008. 133(5): p. 626-634.
25. Yilmaz, G. and C.R. Becer, Glyconanoparticles and their interactions with lectins. Polymer Chemistry, 2015. 6(31): p. 5503-5514.
26. Marin, M.J., et al., Glyconanoparticles for colorimetric bioassays. Analyst, 2015. 140(1): p. 59-70.
27. Chen, X., O. Ramström, and M. Yan, Glyconanomaterials: Emerging applications in biomedical research. Nano Research, 2014. 7(10): p. 1381-1403.
28. Wittmann, V. and R.J. Pieters, Bridging lectin binding sites by multivalent carbohydrates. Chem Soc Rev, 2013. 42(10): p. 4492-503.

29. Ahirwar, R. and P. Nahar, Screening and Identification of a DNA Aptamer to Concanavalin A and Its Application in Food Analysis. Journal of Agricultural and Food Chemistry, 2015. 63(16): p. 4104-4111.
30. Shi, Z., et al., Antitumor effects of concanavalin A and Sophora flavescens lectin in vitro and in vivo. 2014. 35(2): p. 248-256.
31. Sánchez-Pomales, G., et al., A lectin-based gold nanoparticle assay for probing glycosylation of glycoproteins. Biotechnology and Bioengineering, 2012. 109(9): p. 2240-2249.
32. Sato, Y., et al., 12-Mercaptododecyl beta-maltoside-modified gold nanoparticles: specific ligands for concanavalin A having long flexible hydrocarbon chains. Anal Bioanal Chem, 2008. 391(7): p. 2527-32.
33. Babu, P., S. Sinha, and A. Surolia, Sugar–Quantum Dot Conjugates for a Selective and Sensitive Detection of Lectins. Bioconjugate Chemistry, 2007. 18(1): p. 146-151.
34. Earhart, C., et al., Synthesis of Carbohydrate-Conjugated Nanoparticles and Quantum Dots. Langmuir, 2008. 24(12): p. 6215-6219.
35. Soman, C. and T. Giorgio, Kinetics of molecular recognition mediated nanoparticle self-assembly. Nano Research, 2009. 2(1): p. 78-84.
36. Poderys, V., et al., Interaction of Water-Soluble CdTe Quantum Dots with Bovine Serum Albumin. Nanoscale Research Letters, 2011. 6(1): p. 9-9.
37. Alvarez, J., et al., Water-soluble platinum and palladium nanoparticles modified with thiolated [small beta]-cyclodextrin. Chemical Communications, 2000(13): p. 1151-1152.
38. Kauscher, U. and B.J. Ravoo, Mannose-decorated cyclodextrin vesicles: The interplay of multivalency and surface density in lectin–carbohydrate recognition. Beilstein Journal of Organic Chemistry, 2012. 8: p. 1543-1551.
39. Chmurski, K. and J. Defaye, An Improved Synthesis of Per(6-Deoxyhalo) Cyclodextrins Using N-Halosuccinimides —Triphenylphosphine in Dimethylformamide. Supramolecular Chemistry, 2000. 12(2): p. 221-224.
40. Rojas, M.T., et al., Supported Monolayers Containing Preformed Binding Sites. Synthesis and Interfacial Binding Properties of a Thiolated .beta.-Cyclodextrin Derivative. Journal of the American Chemical Society, 1995. 117(1): p. 336-343.
41. Perumal, S., et al., Kinetics Study of the Binding of Multivalent Ligands on Size-Selected Gold Nanoparticles. Langmuir, 2011. 27(8): p. 4456-4464.
42. Onclin, S., et al., Molecular Printboards: Monolayers of β-Cyclodextrins on Silicon Oxide Surfaces. Langmuir, 2004. 20(13): p. 5460-5466.
43. Ambrosi, M., N.R. Cameron, and B.G. Davis, Lectins: tools for the molecular understanding of the glycocode. Org Biomol Chem, 2005. 3(9): p. 1593-608.
44. Otten, L. and M.I. Gibson, Discrimination between lectins with similar specificities by ratiometric profiling of binding to glycosylated surfaces; a chemical 'tongue' approach. RSC Advances, 2015. 5(66): p. 53911-53914.
45. Zhang, J.T., et al., Two-dimensional photonic crystal sensors for visual detection of lectin concanavalin A. Anal Chem, 2014. 86(18): p. 9036-41.
46. Lim, K.R., K.-S. Ahn, and W.-Y. Lee, Detection of concanavalin A based on attenuated fluorescence resonance energy transfer between quantum dots and mannose-stabilized gold nanoparticles. Analytical Methods, 2013. 5(1): p. 64-67.

47. Bogdan, N., R. Roy, and M. Morin, Glycodendrimer coated gold nanoparticles for proteins detection based on surface energy transfer process. RSC Adv., 2012. 2(3): p. 985-991.
48. Sato, K. and J.-i. Anzai, Fluorometric determination of sugars using fluorescein-labeled concanavalin A–glycogen conjugates. Analytical and Bioanalytical Chemistry, 2006. 384(6): p. 1297-1301.

4.6 Supplementary information

Details on the ligand syntheses, nanoparticle functionalization and characterization, and binding studies are given in this section.

Ligand Syntheses.

General details. All starting materials were purchased by Sigma-Aldrich, except otherwise stated, and were used without further purification. NMR solvents were purchased by Euriso-top (France). The synthesis of ligands was performed as described previously [38].

Synthesis of 2-(2-(2-(2-(adamantan-1-yloxy)ethoxy)ethoxy)ethoxy)ethan-1-ol (1)

1-Bromoadamantane (10.7g, 50 mmol) and TEA (20 mL, 144 mmol) were dissolved in tetraethylene glycol (175 mL). The reaction mixture then was stirred overnight at 180^{o}C. After cooling to room temperature, DCM (170mL) was added to the reaction mixture. The organic layer then was washed four times with HCl (2M, 50mL) and once with brine. To the water layer, DCM (50mL) was added and then the organic layers were combined. The organic layer was dried with $MgSO_4$, filtered and concentrated by rotary evaporation. Column chromatography is optional (Ethyl acetate : Hexane, 97:3) (1) (15.6 g, 47.5 mmol, Yield: 95%)

1HNMR (500 MHz, $CDCl_3$, 300 K): δ = 1.59 (q, 6H, 20-,22-,24-H), 1.72 (d, 6H, 16, 17, 21-H), 2.12 (s, 3H, 18-,19-,23-H), 2.84 (s, 1H, OH), 3.57 (m, 6H, 7, 8, 13-H), 3.64 (d, 8H, 9-12-H), 3.70 (d, 2H, 14H).

Synthesis 2-(2-{2-[2-(adamantan-1-yloxy)ethoxy]ethoxy}ethoxy)ethyl 2,3,4,6-Tetra-O-acetyl-α-D-mannopyranoside (2)

Mannose pentaacetate (1.5 g, 3.8 mmol) was added in 10 ml DCM and 2-(2-(2-(2-(adamantan-1-yloxy)ethoxy)ethoxy)ethoxy)ethan-1-ol (1) (3.7 g, 11.4 mmol) in a 50-ml round-bottomed flask. The reaction vessel was purged with nitrogen and the mixture was cooled to 0 °C in an ice bath. Then BF_3-Et_2O (2.43 ml 15.2 mmol) was added through the addition funnel (addition takes 30 min) and the reaction was left overnight by gradually warming it up to room temperature. Then, the reaction mixture was quenched with triethylamine and 30 ml of water and the product was extracted five times with DCM (100 ml). The combined organic layers were dried over Na_2SO_4 (10 g) while stirring filtered through filter paper and the solvent was evaporated using a rotary evaporator; pale brown oil is obtained (368 mg, 0.57 mmol Yield: 15 %). Then a SiOH column was performed with 1:1 (vol/vol) hexane: ethyl acetate as the eluent.

H NMR (500 MHz, $CDCl_3$, 300 K): δ = 1.61 (q, 6H, 20-,22-,24-H), 1.77 (d, 6H, 16, 17, 21-H), 2.18 – 2.01 (m, 15H, 18-,19-,23-H, 3 x OAc), 3.88-3.58 (m, 16H,7-14-H), 4.15 – 4.06 (m, 2H, 5-,6-H), 4.28-4.36 (m, 2H, 6-H), 4.90 (d, 1H, 1-H), 5.41-5.26 (m, 3H, 2-,3-,4-H) ppm

Synthesis 2-(2-{2-[2-(adamantan-1-yloxy)ethoxy]ethoxy}ethoxy)ethyl α-D-mannopyranoside (3) (ADTEGMan)

(2) (368 mg, 0.57 mmol) was dissolved in dry methanol (5 mL) under an atmosphere of argon and a solution of NaOMe (catalytic amounts) was added. The reaction was monitored by TLC. By addition of Dowex HCR-W2 in its hydrogen form the solution was neutralized. The mixture was stirred for 15 min and was then filtered. Methanol was evaporated off to yield pure product as colorless oil (268 mg, 0.55 mmol, Yield: 96%).

H NMR (500 MHz, $CDCl_3$, 300 K): δ = 1.64 (q, 6H, 20, 22, 24-H), 1.76 (d, 6H, 16, 17, 21-H), 2.16 (s, 18, 19, 23-H), 3.84-3.56 (m, 19H, 3, 4, 5, 7-14 -H), 3.96-3.76 (m, 3H, 2-,6-H), 4.91 (s, 1H, 1-H) ppm.

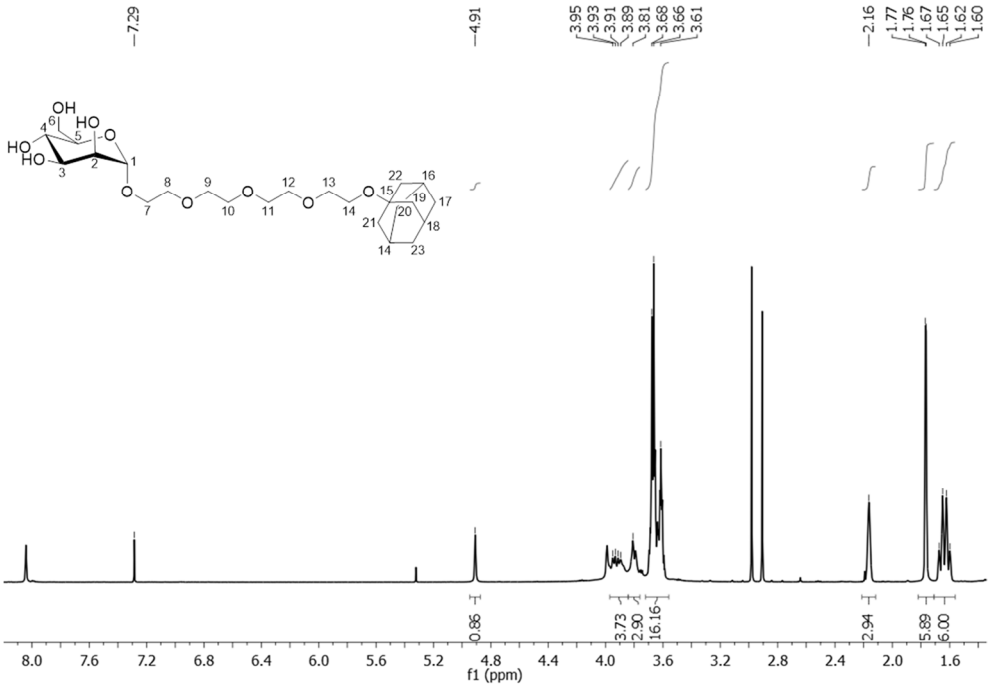

Figure S 4-1: 1H NMR spectrum of 2-(2-{2-[2-(adamantan-1-yloxy)ethoxy]ethoxy}ethoxy)ethyl α-D-mannopyranoside (3) (ADTEGMan) in $CDCl_3$.

Nanoparticle Syntheses and Characterization.

General details. Carboxy-terminated water-soluble CdTe quantum dots with 670±10 nm emission were purchased from Plasmachem (Germany).

Synthesis of heptakis(6-bromo-6-deoxy)-β-cyclodextrin.

The synthesis of heptakis(6-bromo-6-deoxy)-β-cyclodextrin was adapted from Chmurski et al [39]. 11.35 g (10 mmol) of β-cyclodextrin were dissolved in dry DMF (300 mL) under nitrogen atmosphere. N-Bromosuccinimide (24.92g, 140 mmol) and tripenylphosphine (36.72g, 140 mmol) were added. The reaction mixture was stirred for 3.5h at 75 °C. After cooling to room temperature, 100 mL of methanol were added then stirred for 30 minutes. The reaction mixture was evaporated to about 100 mL and subsequently 100 mL of methanol were added. The pH was adjusted with saturated NaOMe in methanol (PA grade) to a pH 8-9 and stirred for 30 minutes. This mixture was poured slowly in 1.6L of ice water and stirred for 10 minutes. The crude pink precipitate was filtered off and dried under vacuum. The pinkish solid was dissolved in 200 mL of methanol and stirred for 10 minutes. The solid was then filtered off, washed with methanol and dried in high vacuum. For further purification, the solid was suspended in ethanol (c.a. 200 mL) and refluxed for 2h. After cooling down the solid was filtered off, washed in ethanol and dried in high vacuum (12.3 g, 7.8 mmol, Yield: 89%).

Synthesis of heptakis-(6-thio-6-deoxy)-β-cyclodextrin

The synthesis of heptakis(6-thio-6-deoxy)-β-cyclodextrin was adapted from Rojasi et al [40]. Heptakis-(6-bromo-6-deoxy)-β-cyclodextrin (1 g, 0.635 mmol) was dissolved in DMF (10 mL); thiourea (0.320g, 4.2 mmol) was then added and the reaction mixture heated to 70°C under nitrogen atmosphere. After 19h, the DMF was removed under pressure to give yellow oil which was dissolved in water (50 mL). Sodium hydroxide was added (0.26 g) and the reaction mixture heated to a gentle reflux under a nitrogen atmosphere. After 1h, the resulting suspension was acidified with aqueous $KHSO_4$ (1g, 10 mL demi water, 0.7 M) and the precipitate filtered off, washed thoroughly with distilled water and dried. To remove the last traces of DMF, the product was suspended in water (50 mL) and the minimum amount of potassium hydroxide was added to give a clear solution. The product was then reprecipitated by acidifying with aqueous $KHSO_4$ (0.7 M). The resulting fine precipitate was carefully filtered off and dried under vacuum over P_2O_5 to yield heptakis-(6-thio-6-deoxy)-β-cyclodextrin as an off-white powder. (299.7 mg, 0.240 mmol, Yield: 38%). δ H (400 MHz, DMSO-d6): 2.13 (7 H, t, -SH), 2.76 (7 H, dd, 6a-H), 3.19 (7 H, d, 6b-H), 3.35 (14 H, d, 2, 4-H), 3.61 (7 H, t, 3-H), 3.69 (7 H, t, 5-H), 4.93 (7 H, s, 1-H), 5.97 – 5.66 (14 H, m, 2, 3-OH)

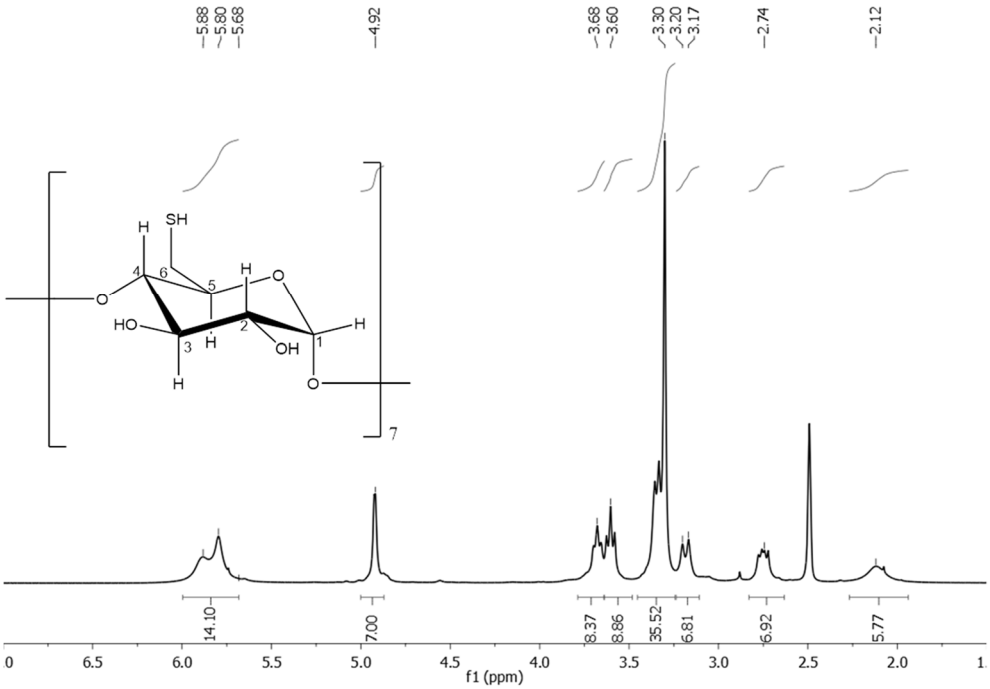

Figure S 4-2: 1H NMR spectrum of heptakis(6-thio-6-deoxy)-β-cyclodextrin in DMSO

Functionalization of carboxy-terminated quantum dots with heptakis(6-thio-6-deoxy)-β-cyclodextrin (β-CD QD). Functionalization of carboxy-terminated, monothiol protected quantum dots with heptakis(6-thio-6-deoxy)-β-cyclodextrin was performed by ligand exchange. In an aqueous solution of 1.2 x 10^{-5} M of quantum dots, 300 equivalents of heptakis(6-thio-6-deoxy)-β-cyclodextrin was added and the reaction was stirred overnight. Afterwards, the quantum dots were washed at least 5 times with deionized water by spin filtration (Amicon Ultra, 10kDa, Millipore) and were reconstituted with water to 1.2 x 10^{-5} M.

Transmission Electron Microscopy (TEM). TEM micrographs of the nanoparticles were by using a JEOL JEM1011 microscope with an acceleration voltage of 80 kV. The micrographs were processed with the program ImageJ to determine the average diameters of the nanoparticles. The average diameter is 4.44±0.8 nm after analysis of 46 nanoparticles.

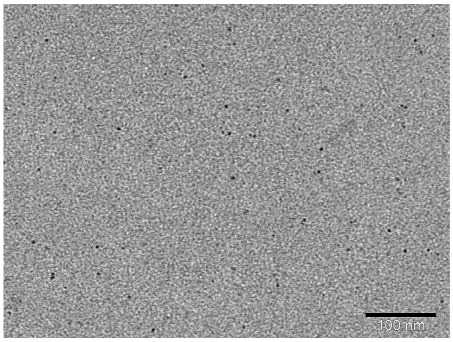

Figure S 4-3: TEM image of β-CD QD with 100 nm scale bar

DOSY NMR Spectroscopy. DOSY NMR for quantum dot measurements were performed on a 500 MHz Bruker Avance III NMR spectrometer, proton frequency 500.137 MHz, equipped with a 5 mm TXI 1H-13C/ 15N Z-GRD Z8161/ 80 probehead at 300 K. The pulse sequence was a stimulated echo bipolar gradient pulse (stebpgp1s) with the DOSY spectra acquired for each sample having 32 increments (exponential array), 32 scans, gradient pulse length (δ) 6.0 ms and big delta (Δ) 120.0 ms. Samples were prepared in D_2O (Euriso top, France) (99.96%).

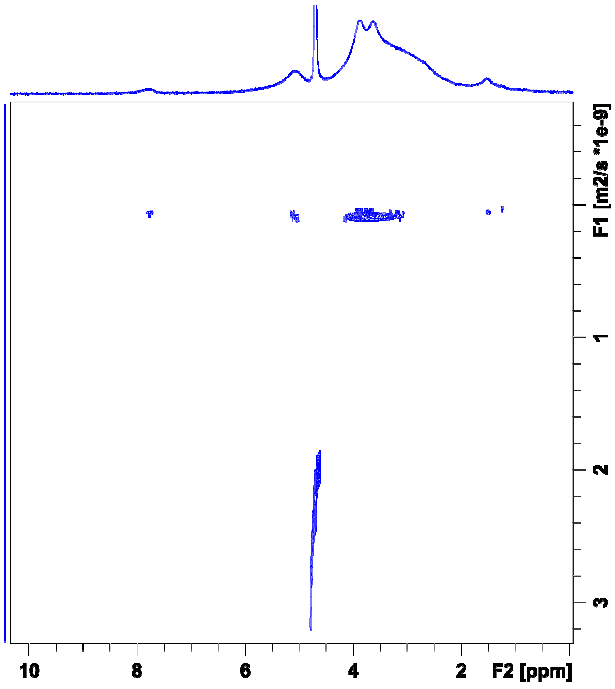

Figure S 4-4: DOSY NMR spectra of β-CD QD quantum dots after ligand exchange with heptakis(6-thio-6-deoxy)-β-cyclodextrin

Diffusion coefficients of β-CD QD were used to estimate the hydrodynamic radii of the nanoparticles by using the Stokes-Einstein Equation S 4-1) where k is the Boltzmann's constant, T is the temperature (300 K), η is the viscosity of the solvent (D2O), D is the diffusion coefficient of the β-CD QD, and Rh is the hydrodynamic radius.

$$D = \frac{k_B T}{6 \pi \eta r}$$

Equation S 4-1

Hydrodynamic radii, R_h of CdTe quantum dots after ligand exchange with heptakis(6-thio-6-deoxy)-β-cyclodextrin are estimated to 3.0 nm.

Binding Studies.

General details. For all binding studies all samples were prepared in PBS buffer saline 0.01 M with Mg^{2+} 0.015 mM, Mn^{2+} 0.011 mM, Ca^{+2} 0.011 mM and 0.008 % w/v NaN_3. Dolichos biflorus (DBA), Ricinus communis I (RCA_{120}), Soyabean Agglutinin (SBA) and Wheat Germ agglutinin (WGA) were purchased from Vector Labs. Concanavalin A was purchased from Sigma Aldrich with and without fluorescent label. Five fluoresceins are estimated to be attached on Concanavalin A by comparing it to the fluorescence of free fluorescein.

Transmission Electron Microscopy. TEM micrographs of the nanoparticle networks were by using a JEOL JEM1011 microscope with an acceleration voltage of 80 kV.

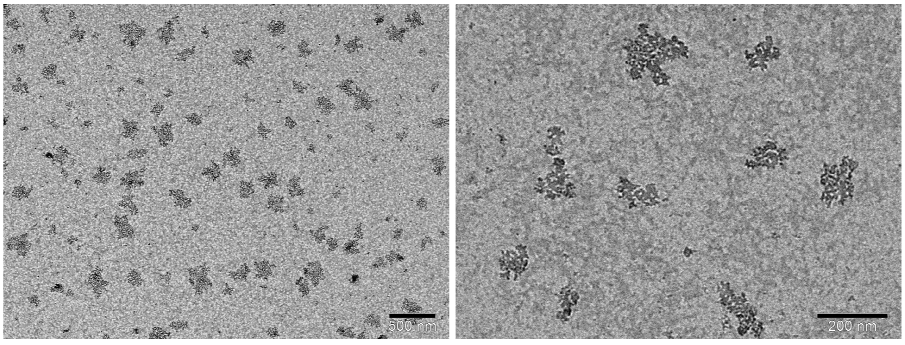

Figure S 4-5: TEM image of β-CD QD with 500 nm (left side) and 200 nm scale bar (right side)

Dynamic Light Scattering (DLS). DLS measurements were performed using an ALV instrument equipped with an ALV-7004 multiple tau digital correlator, a Uniphase Model 1145P He-Ne laser (632.8 nm with an output of 22 mW), and a 2 off ALV/Dual High QE APD Detector Unit. The position of the latter is located 90° relative to the laser source. All samples prior to measurement were filtrated with a cellulose acetate 0.1 µm disc filter (mdi, US). All measurements were processed with ALV-7004 Version 3.0 software.

Fluorescence measurements. Steady-state fluorescence measurements were done on a Cary Eclipse fluorescence spectrophotometer (Varian) at 22°C. The software used is Cary Eclipse version 1.2(147). Quartz cuvettes of 3.5 ml nominal volume (Hellma) were used for the samples and all samples were prepared to a final volume of 3.0 ml. Excitation and emission slits were at 10 nm, detection voltage was at 600 V and excitation wavelength was at 450 nm. Scans of every sample were performed every 5 or 10 minutes from 500-800 nm. All fluorescence intensity data were analyzed at maximum fluorescence emission at 671 nm.

Binding fluorescence measurements were performed twice and the measurements related to the optimization of the sensor (quantum dot and linker effect) and the selectivity were performed once.

For testing the linker dot effect the concentration of the quantum dots and Concanavalin A was kept constant at $4.0x10^{-8}$ and $1.6x10^{-6}$ M respectively. For testing the quantum dot effect the concentration of the linker and Concanavalin A was kept constant at $1.4x10^{-5}$ and $1.6x10^{-6}$ M respectively.

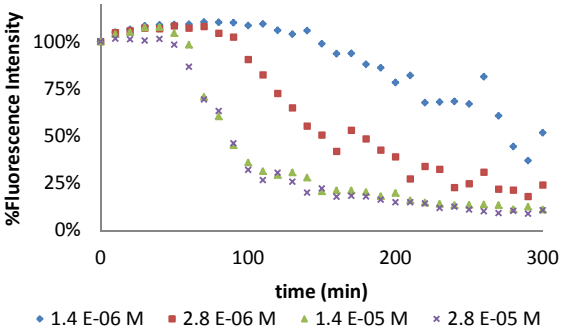

Figure S 4-6: Linker (ADTEGMan) effect on binding kinetics of Concanavalin A. (Concentration of quantum dots and Concanavalin A was kept constant at $4.0x10^{-8}$ and $1.6x10^{-6}$ M respectively)

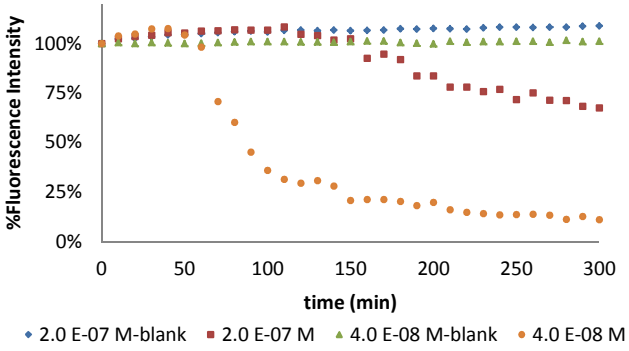

Figure S 4-7: Quantum dot effect on binding kinetics of Concanavalin A. (Concentration of ADTEGMan and Concanavalin A was kept constant at 1.4 x 10^{-5} and 1.6 x 10^{-6} M respectively)

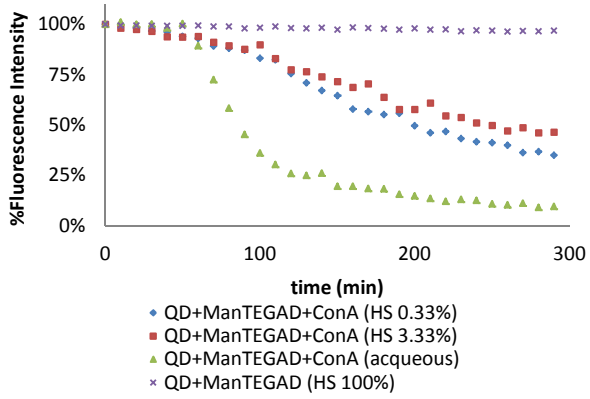

Figure S 4-8: Human serum effect on quantum dot stability and binding kinetics of Concanavalin A. (Concentration of ADTEGMan and Concanavalin A was kept constant at 1.4 x 10^{-5} and 1.6 x 10^{-6} M respectively)

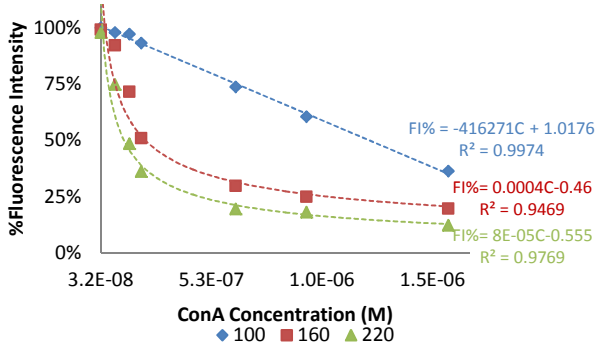

Figure S 4-9: Calibration curves for quantifying the lectin concentration at different timepoints of the flocculation kinetics (100 min, 160 min, and 220 min)

Chapter 5 Selective supramolecular lectin sensors by triadamantane sugar linkers

Abstract

In this Chapter the study of selective lectin sensing through controlled flocculation of ternary supramolecular quantum dot networks is continued. The goal is to compare the impact on lectin sensing between the use of monovalent (ADTEGMan) or trivalent (TriADTEGMan) linkers, exhibiting dynamic or non-dynamic interactions with β-cyclodextrin-capped CdTe quantum dots (β-CD-QD), respectively, and to, ultimately, prove that the non-dynamic, supramolecular systems, combine the advantages from covalent e.g. robustness, and from supramolecular systems e.g. tunability, reversibility and to compare. The building blocks of the lectin sensor are β-cyclodextrin-capped CdTe quantum dots (β-CD-QD) with maximum emission wavelength at 671 nm, tetraethylene glycol-tethered mannose-adamantane linkers, either monovalent (ADTEGMan) or trivalent (TriADTEGMan), and the mannose-binding lectins; Concanavalin A, Lens Culinaris and Galanthus Nivalis. The differences in terms of dynamics and binding were revealed by 1H NMR titrations and DOSY measurements, where the triadamantane linkers on the β-cyclodextrin quantum dots are proved to yield supramolecular, non-dynamic systems, in contrast with the dynamic, monovalent cyclodextrin-adamantane interactions. The differences in terms of dynamics between the two linkers are found to influence several features of the lectin sensors, such as flocculation kinetics, robustness, tunability and selectivity. Lastly, both types of linkers, allow for sensing and studying flocculation kinetics of other lectins, such as Galanthus Nivalis and Lens Culinaris as well. Supramolecular nanoparticle sensors are indispensable platforms for sensing lectins in solution, since they combine on-spot detection with simplicity, speed, selectivity, robustness and tunability.

Part of this Chapter is based on: M. Oikonomou, G. Viilup, K. van der Ploeg, R. Steijsijger, N. Vos and A. H. Velders, Non-Dynamic Supramolecular Quantum Dot Functionalization for Improved Lectin Sensing, Manuscript in preparation.

5.1 Introduction

Nanoparticle functionalization for biomedical sensing requires decoration of nanoparticles with ligands that have affinity for the nanoparticle surface and also bear biorecognition moieties [1, 2]. Ligand affinity for the nanoparticle surface is either achieved by chemisorption or physisorption. In either of these cases, chemisorption or physisorption, the ligand needs to be modified with biorecognition moieties, in order to exhibit affinity to biomolecules. Modification of the ligands with bioreceptors can be performed before or after the nanoparticle decoration and two main strategies are used; covalent conjugation or non-covalent assembly (Figure 5-1). Both strategies exhibit advantages and disadvantages. By covalent modification, better control and stability over a big range of concentrations and environmental conditions can be achieved. Characterization of covalently immobilized ligands is more straightforward since the nature of covalent bonds is permanent. At the same time, non-covalent strategies are harder to control and characterize, since they are based on weaker, dynamic interactions, which are equilibrium dictated. On the other hand, the dynamic nature of these interactions provides more versatile, tunable and often reversible biorecognition interactions at the nanoparticle interface. Recently, other alternative chemical strategies for nanoparticle functionalization for biomedical sensing started to being explored. Dynamic covalent functionalization [3] and non-dynamic non-covalent functionalization of surfaces [4] (Figure 5-1) has given rise to nanosystems with exciting properties such as reversibility, robustness and tunability.

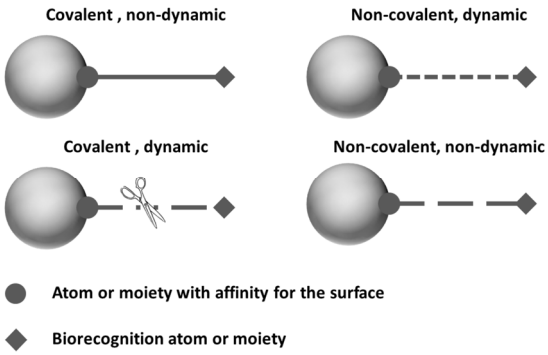

Figure 5-1: Dynamic chemistries, either covalent or non-covalent for functionalizing nanoparticles with bioreceptor ligands

Here, strongly-bound, non-dynamic, supramolecular, ligand-nanoparticle systems are explored as a functionalization strategy for biomedical sensing. For this purpose, a widely used orthogonal supramolecular pair for self-assembly is employed which is β-cyclodextrin with adamantane [5, 6]. Cyclodextrins are cyclic oligosaccharides that form inclusion complexes with many hydrophobic molecules such as adamantane [5].

Adamantane and its derivatives form 1:1 β-cyclodextrin inclusion complexes with high binding constants [7-9]. Impressive binding constants have been reported by integrating multivalency in such systems [10, 11]. According to previous research 1:1 monovalent interaction with a binding constant of $\approx 10^4$ M^{-1}, a divalent one typically has a binding constant of $\approx 10^7$ M^{-1} and a trivalent interaction can exhibit a binding constant of $\approx 10^{10}$ M^{-1} [12]. Of course, the ligand length and flexibility, as well as the surface dimensions and cyclodextrin coverage are crucial parameters that can radically change the respective binding values [13]. For example, bivalent interactions at the cyclodextrin SAMs resulted in a binding constant of 10^{10} M^{-1}, three orders of magnitude higher than that for the corresponding bivalent interaction in solution (10^7 M^{-1}) [12]. This large effect brings the discussion to the impact of regional effective concentration. An uncomplexed adamantane close to a surface has approximately double probability into interacting with a cyclodextrin in respect to the case where the cyclodextrin is in solution. The third sequential binding of adamantane in the case of the trivalent adamantane linkers would exhibit even higher binding effect, in the range of 10^{10} M^{-1} and possibly more, since on surface [4, 14]. Exciting applications that take advantage of the differences in binding strengths between monovalent, divalent and trivalent adamantane linkers on flat surfaces has been shown in the work of Hsu et al, Perl et al and Krabbenborg at al [4, 15, 16], where trivalent adamantane linkers don't exhibit exchange kinetics when free cyclodextrin is added in solution, while the divalent adamantane analogue exhibits directional movement along a concentration gradient. Based on these observations, the hypothesis that triadamantane based linkers are bound in a very strong, almost covalent fashion, on multivalent cyclodextrin nanoparticles as for example quantum dots (β-CD-QDs) is tested. These systems are expected to combine the advantages of both covalent and non-covalent chemistry, since they fall under the category of "supramolecular, non-dynamic chemistry". Non-dynamic, supramolecular systems are expected to be highly robust and at the same time still tunable. Higher stability can be achieved over a wide range of environmental conditions such as pH, salt, temperature and competitor molecules, and still maintaining, tunability, in terms of ligand density, and to a certain point, reversibility by addition of excess of free cyclodextrin. With an eye on the future, the great potential of this approach lies within the field of multiplex chemical and biological sensing. For example, this strategy could be advantageous for selectively sensing lectins. Lectins are proteins that exhibit strong and specific binding towards certain carbohydrate moieties [17]. Targeting lectins is important for diagnosis of diseases [18] and detection of microbes [19]. In this work, the advantages and pitfalls of using monovalent, dynamic and trivalent adamantane mannose linkers in nanoparticle-based lectin sensors are compared. The building blocks of the sensor are β-cyclodextrin-capped CdTe quantum dots (β-CD-QD) with emission maximum at 671 nm, tetraethylene glycol-tethered mannose-adamantane linkers, either monovalent (ADTEGMan) or trivalent (TriADTEGMan), and Concanavalin A (ConA). ConA was chosen as a model lectin since it is a very well-studied, tetravalent mannose-binding

lectin with various biomedical applications such as for bacterial and food analysis, HIV inhibitor, glycosylation probe of glycoproteins [20-23]. The success of this sensor lies in the dual orthogonal molecular interactions of the mannose-adamantane linkers. The linkers exhibits binding not only with the β-CD-QD but also with the lectin. Thus, upon addition of ConA in a mixture β-CD-QD and linker, supramolecular networks form, eventually flocculating and sedimenting (Figure 5-2).

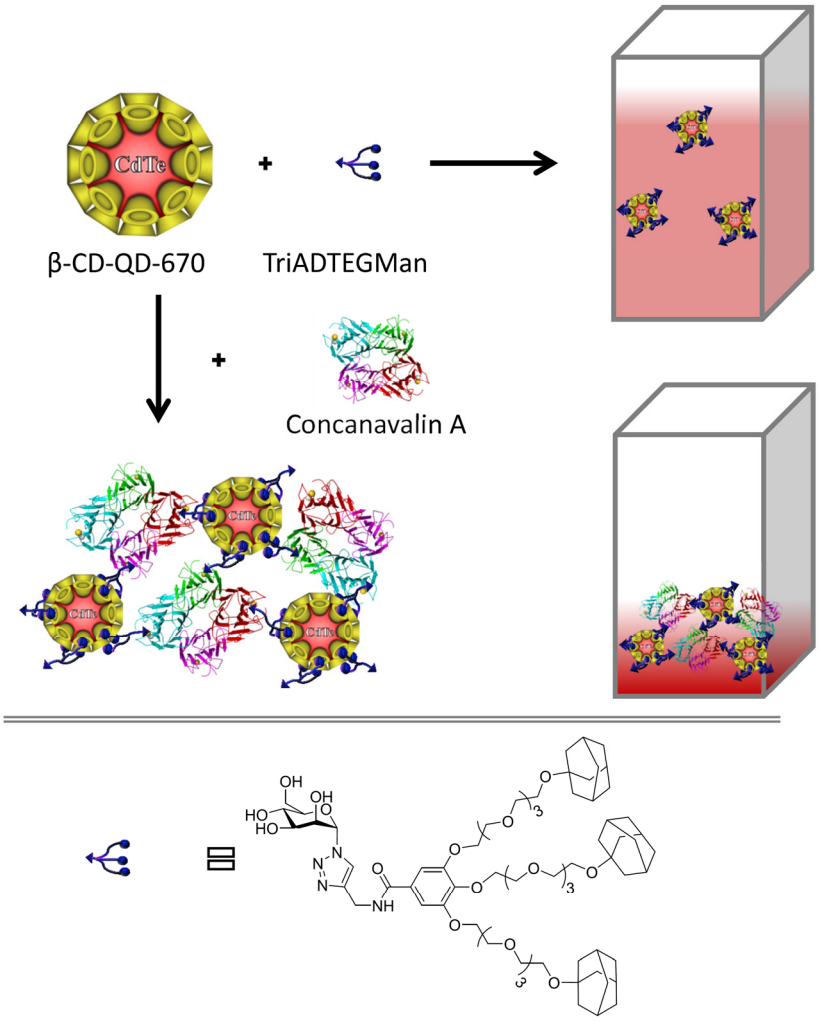

Figure 5-2: Representation of formation of ternary supramolecular network upon addition of ConA to a solution of β-CD-QD and TriADTEGMan; once formed the NPN sediment and the solution loses fluorescence

The success of this sensor lies in the dual orthogonal molecular interactions of the mannose-adamantane linkers. The linkers exhibits binding not only with the β-CD-QD

but also with the lectin. Thus, upon addition of ConA in a mixture β-CD-QD and linker, supramolecular networks form, eventually flocculating and sedimenting.

5.2 Experimental

Water-soluble CdTe quantum dots capped with thioglycolic acid exhibiting emission at 670±10 nm were purchased from Plasmachem (Germany) [24]. β-CD-QDs were synthesized by exchanging carboxyl-terminated monothiol ligands of the capped quantum dots with heptakis-thiolated β-CD after overnight stirring in water [25]. Purification of β-CD-QD is performed by spin-filtration. Heptakis-thiolated β-CD used for the ligand exchange is synthesized in two steps and ADTEGMan in three steps comprising only one column purification. Both building blocks are synthesized by modified protocols reported elsewhere [12, 26, 27] , (see SI for details and Chapter 4). For NMR binding studies, precursor compounds are employed, which were used in the synthesis prior attaching the mannose moiety.

For characterizing the modified β-CD-QDs 1H NMR, DOSY NMR and TEM was used (see SI). 1H and DOSY NMR measurements were performed on a 500 MHz Bruker Avance III NMR spectrometer, proton frequency 500.137 MHz, equipped with a 5 mm TXI 1H-13C/ 15N Z-GRD Z8161/ 80 probehead at 300 K. The pulse sequence was a stimulated echo bipolar gradient pulse (stebpgp1s) with the DOSY spectra acquired for each sample having 32 increments (exponential array), 256 scans, gradient pulse length (δ) 7.0 ms and big delta (Δ) 200.0 ms. Samples were prepared in D_2O (Euriso top, France) (99.96%).

For lectin binding studies all samples were prepared in PBS buffer saline 0.01 M with Mg^{2+} 0.015 mM, Mn^{2+} 0.011 mM, Ca^{+2} 0.011 mM and 0.008 % w/v NaN_3. Peanut Agglutinin (PNA), Ricinus communis I (RCA120), Soyabean Agglutinin (SBA), Wheat Germ agglutinin (WGA), Lens Culinaris Agglutinin (LCA) and Galanthus Nivalis Agglutinin (GNL) were purchased from Vector Labs. Concanavalin A (Con A) was purchased from Sigma Aldrich. For the fluorescent assays 2.4×10^{-7} M of β-CD-QD was used and therefore an active cyclodextrin concentration of 2.1×10^{-5} M was assumed. For obtaining quantitative data from the fluorescence assays, the quantum dot emission peak at 671 nm was monitored in time, as the networks form, flocculate and sediment. For the selectivity experiments, four different lectins (Peanut Agglutinin (PNA), Ricinus communis I (RCA_{120}), Soyabean Agglutinin (SBA) and Wheat Germ agglutinin (WGA)) were used. Also, in these experiments, the quantum dot fluorescence at 671 nm was monitored in time.

5.3 Results and Discussion

The synthesis of monovalent linkers is described in Chapter 4 and the synthesis of trivalent linkers involved six steps in order to obtain the final product (see SI). First, bromoadamantane was coupled to tetraethylene glycol and converted it into the tosylate analogue. Then, the tosylate was reacted with the gallate ester and later, the ester was hydrolyzed to obtain the respective acid (TriADTEG). For utilizing the TriADTEG linker in lectin sensing further modification with propargylamine was needed to obtain the alkyne equivalent. Then the copper catalyzed click reaction was used in order to attach a peracetylated mannose moiety. The last step involved the sugar deprotection and yielded the trivalent adamantane mannose linker (TriADTEGMan). The synthesis of heptakis-thiolated β-CD used for the ligand exchange involved two steps, first the bromination of β-CD and then thiolation with thiourea (see SI). For the quantum dot modification with β-CD, a ligand exchange protocol is followed by adding excess of heptakis-thiolated β-CD (see SI). The estimation of the number of cyclodextrins was done by the following rationale. Every quantum dot (r=2.2 nm) has a surface area of approximately a sphere, thus 61 nm^2 and, in an ideal monolayer, every cyclodextrin (r=0.45 nm) occupies a surface area of a circle, thus 0.64 nm^2. Considering that the packing of circles on a sphere is approximately 90% [28], then every quantum dot is considered to bear ideally 86 cyclodextrins, if there is no steric hindrance. To determine the stoichiometry and dynamics of binding of the β-CD-quantum dots with TriADTEG or ADTEG, 1H titrations were carried out by adding stepwise, increasing amount of β-CD-quantum dots (Figure 5-3 and Figure 5-5).

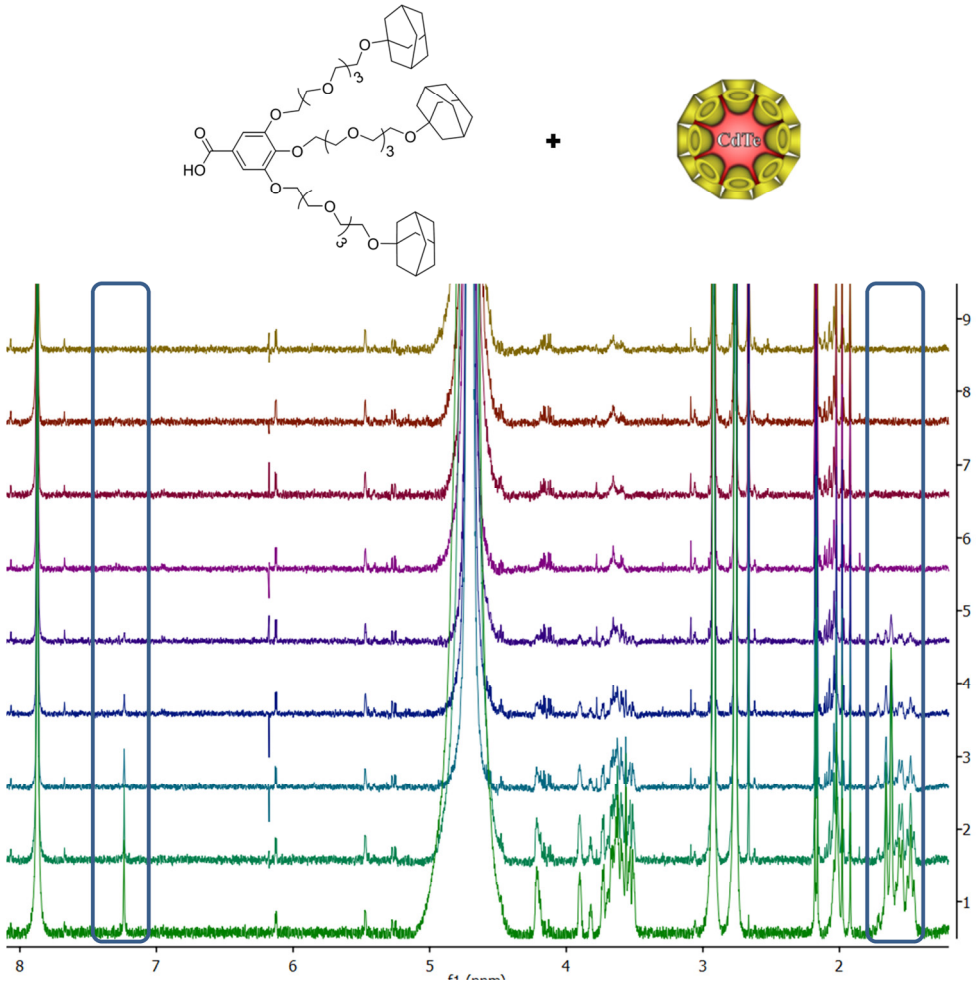

Figure 5-3: Overlay of 1H spectra with increasing, from 1 to 9, amounts of red β-CD-QDs. The ratios between TriAD and that correspond to each sample can be found in Table 5-1.

By adding, stepwise, increasing amounts of β-CD-QDs, gradual intensity loss of all linker peaks is observed in Figure 5-3 for the case of TriADTEG. This is attributed to the non-dynamic binding of the linker, in combination with its confinement close to the nanoparticle surface. For quantifying the changes observed, the integral changes at 7.24 and 1.56 ppm in respect to DMF peaks, used as internal standard, are followed (Table 5-1). The differences in the observed changes between the aromatic peak integral and the adamantane peak integral are probably due to integration accuracy, as the aromatic peak rises from the signal of only two protons, while the adamantane peak, due to spectral overlap, represents 36 protons.

Table 5-1: Series of samples measured by 1H NMR and the respective integrals and relative integral changes by stepwise addition of β-CD-QDs

Sample Nr.	Ratio TriAD and β-CD	Integral at 7.24 ppm, s, 2H	Integral at 1.43-1.70 ppm, m, 36H	ΔI %, 7.24 ppm	ΔI %, 1.56 ppm
1	-	0.0420	1.0270	-	-
2	0.22	0.0373	0.6707	88.81%	65.31%
3	0.43	0.0271	0.4267	64.52%	41.55%
4	0.65	0.0158	0.1963	37.62%	19.11%
5	0.86	0.0093	0.0754	22.14%	7.34%
6	1.08	0.0079	0.0158	18.81%	1.54%
7	1.51	0.0008	0.0027	1.90%	0.26%
8	2.16	0.0001	0.0024	0.29%	0.23%
9	3.23	0.0001	0.0020	0.24%	0.19%

Next, for determining the stoichiometry of the complexes formed on nanoparticle surfaces, the relative integral changes, I_0-I/I_0 against the ratio of effective β-CD concentration to linker concentration are plotted (Figure 5-4).

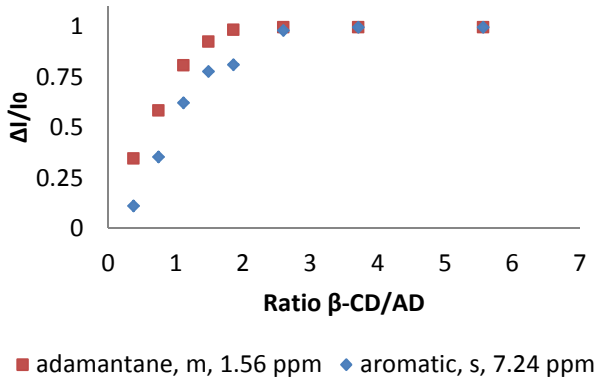

Figure 5-4: Relevant change of integrals, I_0-I/I_0, of adamantane or aromatic proton peaks by adding stepwise increasing amounts of red β-CD-QD

From Figure 5-4, it can be seen that for both data sets the slope changes at an approximate ratio, of β-CD concentration to linker, of between two and three, which strengthens the hypothesis that the linker binds in a trivalent fashion on the cyclodextrin nanoparticle surface.

The same experiments were performed for the monovalent adamantane linker (ADTEG) (Figure 5-5), in three times higher concentration of the ADTEG in respect to TriADTEG, in order to keep the effective adamantane concentration the same.

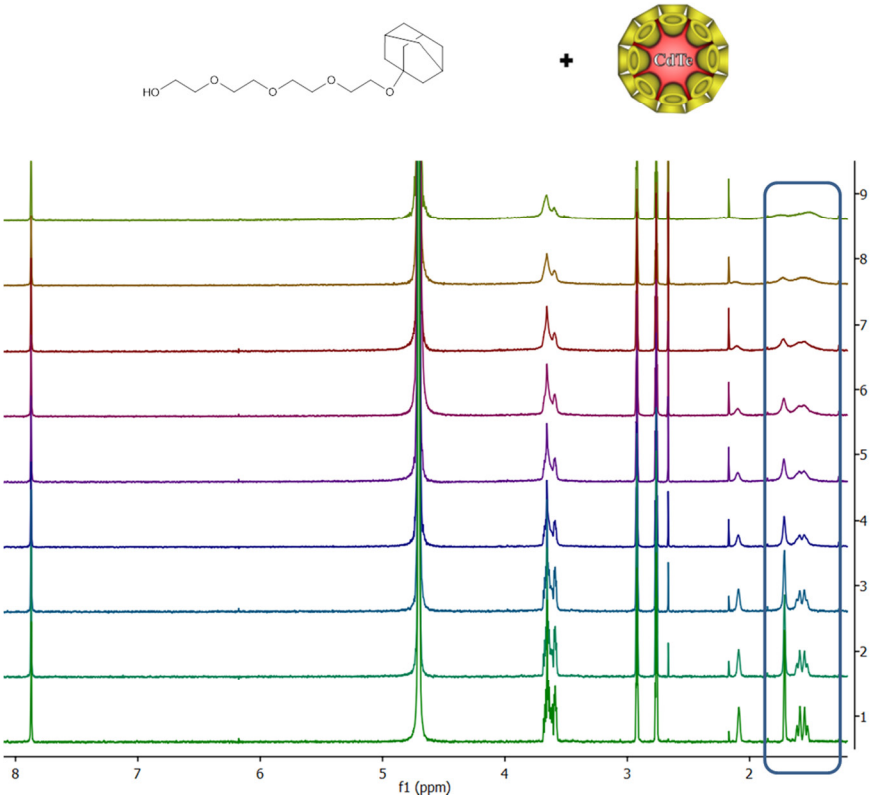

Figure 5-5: Overlay of 1H spectra with decreasing, from 1 to 9, amounts of β-CD-QDs. The concentration of ADTEG was three times more in order to have the same effective adamantane concentration in all 1H experiments.

In Figure 5-5 broadening and shifting of the adamantane peaks is found with increasing β-CD-QD but without a change in integrals in respect to the internal standard, DMF. By comparing the β-CD-QD binding effect between the two linkers on the 1H peaks, the dynamics of the binding are found to differ significantly. In the case of the ADTEG is evident that a dynamic complex is formed, whereas in the case of TriADTEG the loss of intensity is associated with a non-dynamic binding.

To further prove the non-dynamic nature of the linker binding, the diffusion coefficients, obtained by DOSY NMR, of two samples containing either TriADTEG or ADTEG at stoichiometric ratio in respect to the cyclodextrins found on the quantum dots (Figure

5-6). These experiments were repeated, with the case of monovalent adamantane linkers, where the dynamic exchange is fast on the NMR timescale and compared all results.

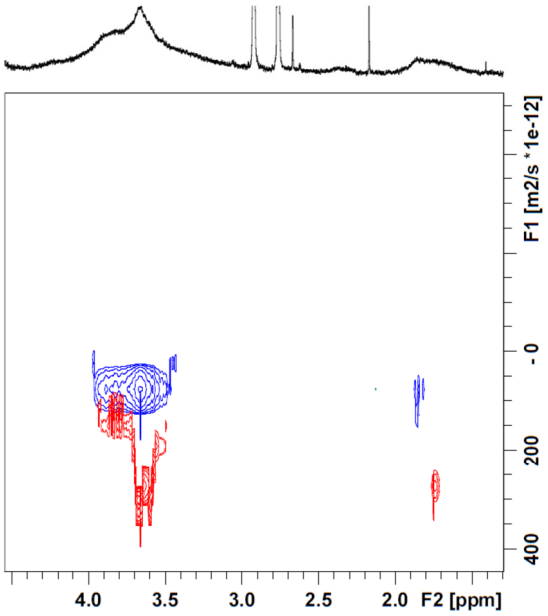

Figure 5-6: Overlay of two DOSY NMR spectra; in red is the spectrum of the ADTEG and in blue the spectrum of TriADTEG, both in stoichiometric ratio in respect to the number of cyclodextrins found on quantum dots.

As seen in Figure 5-6, the trivalent linker (TriADTEG) is found in the same diffusion line with the quantum dots, proving that the binding is non-dynamic and that the linkers are kinetically trapped on the cyclodextrin quantum dot surface. The strong, non-dynamic binding between TriADTEG and quantum dots leads to the formation of highly stable and robust complexes. On the contrary, due to dynamic binding, the monovalent linker (ADTEG) has an apparent diffusion coefficient D_{obs}, representing a weighted average of the coefficients of the free and the bound states, [29] (see also Chapter 3).

Next the reversibility and binding strength tunability on the linker-nanoparticle assemblies in the presence of free β-cyclodextrin was investigated. Addition of different amounts of free β-cyclodextrin in a constant, stoichiometric ratio of β-CD-QDs to TriADTEG, enables the study the multivalency potency of the linkers and to tune on demand the binding strength of the TriADTEG linker. Four experiments were performed by adding 110.0 mM, 11.0, 1.1 and 0.11 mM of free β-cyclodextrin, measuring a series of 1H NMR before the addition of β-cyclodextrin (Figure 5-7) and after the addition of β-cyclodextrin Figure 5-8.

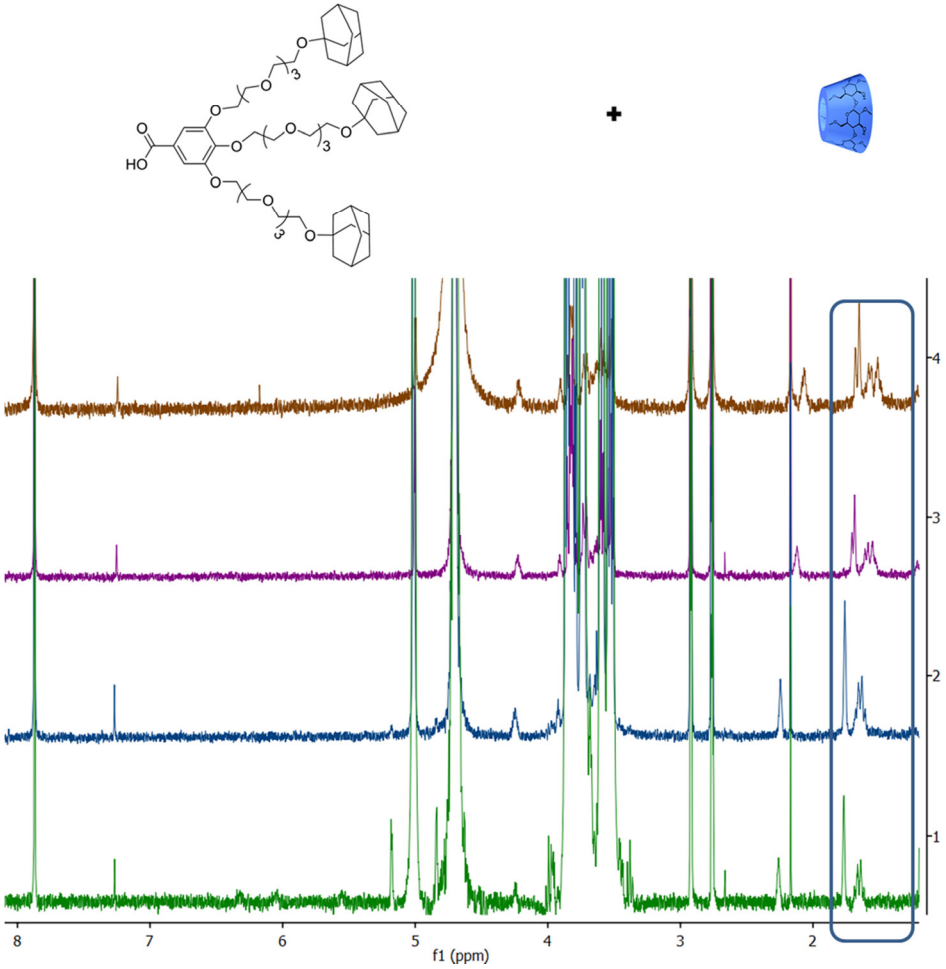

Figure 5-7: Samples containing TriAD linker (9.6 x 10^{-5} M) and from top-down increasing amount of β-cyclodextrin (Nr1: of 110.0, Nr2: 11.0, Nr3: 1.1 and Nr4: 0.2 mM) before the addition of β-CD-QDs

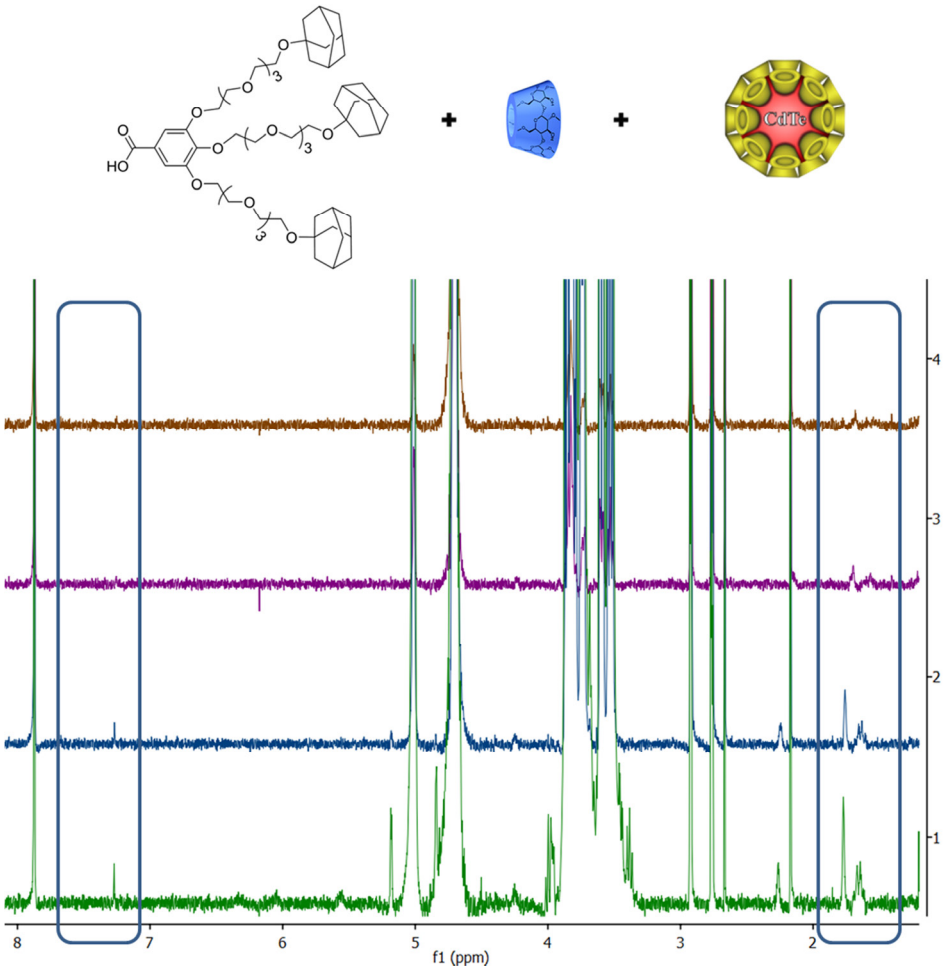

Figure 5-8: Samples containing TriAD linker (9.6 x 10^{-5} M) and from the top-down increasing amount of β-cyclodextrin (Nr1: of 110.0, Nr2: 11.0, Nr3: 1.1 and Nr4: 0.2 mM) after the addition of β-CD-QDs.

Before adding β-CD-QDs in the mixture of TriADTEG and β-cyclodextrin differences in the chemical shifts of adamantane were observed when different amounts of free β-cyclodextrin are added. As seen in Figure 5-7, when excess of β-cyclodextrin is added (Nr1, Nr2 and Nr3), only one set of quartets at 1.56 ppm and one set of doublets at 1.70 ppm is observed, whereas in the top spectrum (Nr4), two sets of quartets and two sets of doublets are found. In the fourth sample the amount of β-cyclodextrin is below the active concentration of adamantane, thus below molar stoichiometry, which means not all adamantanes are in the same chemical environment and, thus, able to complex with β-cyclodextrin. The fact that only above stoichiometry only one set of quartets and doublets is observed proves that TriAD forms 1:3 complexes in solution with β-cyclodextrin.

In Figure 5-8, the results after the addition of 5μL β-CD-QD in the samples, shown in Figure 5-7, are given. In all cases there is a gradual decrease in the integrals of the TriADTEG peaks with decreasing amount of β-cyclodextrin. The more β-cyclodextrin in solution, the less the decrease, implying that the binding can be tuned and even completely reversed with a (high) excess of β-cyclodextrin.

For a comparison between monovalent and trivalent linkers, the sensor response times to ConA (6.4 x 10^{-6} M) were tested in three linker concentration levels; below molar stoichiometry (7.3 x 10^{-6} M), at, approximately, molar stoichiometry (2.8 x 10^{-6} M) and in excess (5.7 x 10^{-5}M) in respect to the active cyclodextrin concentration (~2.1 x 10^{-5} M). The results of these experiments are shown in Figure 5-9, where the % quantum dot fluorescence intensity is followed for 500 minutes.

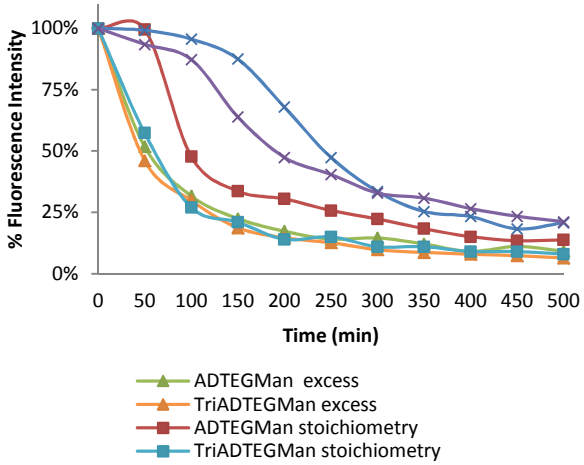

Figure 5-9: % Fluorescence intensity of β-CD-QD at 671 nm over 500 minutes to test the sensor response times to ConA (6.4 x 10^{-6} M) against three linker concentration levels; below stoichiometry (7.3 x 10^{-6} M), at, approximately, stoichiometry (2.8 x 10^{-6} M) and in excess (5.7 x 10^{-5} M) in respect to the active cyclodextrin concentration (~2.1 x 10^{-5} M).

In the case of the monovalent linker, as seen in Figure 5-9, due to the dynamic fashion of binding, there is a much larger impact of linker concentration in the flocculation kinetics. This result is correlated to all types of dynamic systems, where is crucial to use molar excess of linker, even higher than the ones shown in Figure 5-9. For example, as seen in Figure 5-9 in the case of linker excess, only 1 adamantane is found in complex with β-cyclodextrin tethered on quantum dots, calculated from the association constant equation where the association constant (Ka) between adamantane and β-cyclodextrin to be ~5 x 10^{4} M^{-1}. In the case of the trivalent linker, due to the non-dynamic fashion of binding, the impact of linker concentration is minimal, in concentration ranges close to stoichiometry and above. The comparison between the flocculation kinetics of the

monovalent and trivalent linker for every concentration level, provides insight for the dynamics and tunability. In all cases, the trivalent linker exhibits faster kinetics than the monovalent, although, when linkers are used in excess, all kinetics is comparable. The sensor based on the monovalent linker is better in terms of tunability by varying linker concentration. But, as shown in the NMR experiments (Figure 5-7 and Figure 5-8), the tunability in response times of the lectin sensor based on the trivalent linker, should be possible by the addition of free cyclodextrin in solution, prior to the addition of the β-CD-QDs. Indeed, in Figure 5-10, the tunability in response times, due to the presence of different amounts of free cyclodextrin in solution (0.3 mM, 1.5 mM and 15.0 mM), is observed.

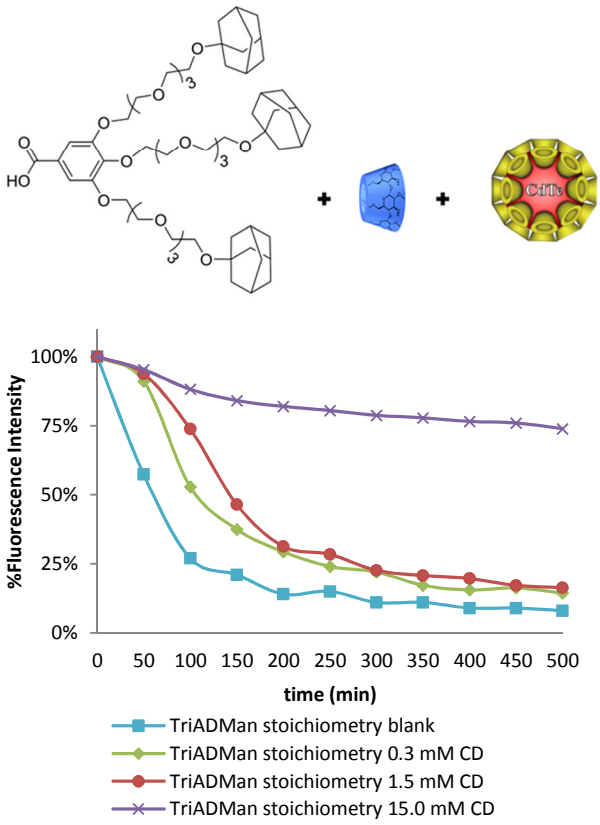

Figure 5-10: % Fluorescence intensity of β-CD-QD at 671 nm over 500 minutes to test the sensor response to Concanavalin A (6.4 x 10^{-6} M) based on the trivalent linker, when different amounts of free cyclodextrin in solution (0.0 Mm, 0.3 mM, 1.5 mM and 15.0 mM) is present.

Extending the application of ternary, supramolecular nanoparticle networks for the sensing of other lectins, the monovalent and trivalent linker, in excess in respect to the amount of cyclodextrins bound on the quantum dots, were tested against two other mannose-binding lectins (6.4 x 10^{-6} M); Galanthus Nivalis and Lens Culinaris (Figure 5-11).

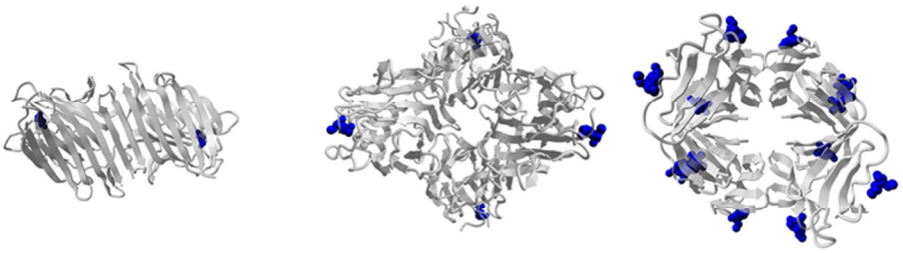

Figure 5-11: Schematic representation of Lens Culinaris (L: 16 nm, W: 9 nm), Concanavalin A (L: 13 nm, W: 7 nm) and Galanthus Nivalis (L: 14 nm, W: 7 nm) in complex with α-mannopyranoside, as adapted by http://www.ebi.ac.uk/

These results were also compared with the flocculation kinetics of ConA (Table 5-2). Galanthus Nivalis Lectin (GNL) has 12 binding sites, Lens Culinaris Agglutinin (LCA) possesses two binding sites and Concanavalin A (ConA) is a tetravalent lectin.

Table 5-2: % Fluorescence intensity of β-CD-QD at 671 nm at 500 minutes to test the sensor response to Galanthus Nivalis, Lens Culinaris and Concanavalin A (6.4×10^{-6} M) in excess or substoichiometry of TriADTEGMan or ADTEGMAN in respect to the amount of cyclodextrins bound on the quantum dots

	EXCESS (5.7×10^{-5} M)		SUBSTOICHIOMETRY (7.3×10^{-6} M)	
time=500 minutes	ADTEGMan	TriADMan	ADTEGMan	TriADMan
LCA	39%	49%	89%	73%
CONA	14%	8%	21%	21%
GNL	89%	83%	99%	86%

As seen in Table 5-2, faster responses for GNL are achieved when TriADMan is added, instead of ADTEGMan, although in all cases, the flocculation kinetics are very slow, without reaching equilibrium. For LCA, a faster response for both linkers is observed in respect to GNL flocculation kinetics. For LCA, the monovalent and the trivalent linker, either in excess or substoichiometric amounts exhibit similar kinetics. LCA flocculation kinetics is in all cases faster than GNL flocculation kinetics. Overall, for both linkers at two concentration levels, the ConA flocculation kinetics is the fastest in respect to LCA and GNL. When the linkers are used in excess, there is significant difference in response times between the trivalent and the monovalent, where the trivalent yields much faster kinetics (see also

Figure 5-9). LCA has only two binding sites in respect to ConA, so the slow kinetics is possibly due to the lesser multivalency potency of that lectin. For GNL, 12 binding sites are available for binding mannose in very close proximity. So, not all binding sites can be occupied by quantum dots and, therefore, participate in network formation

due to steric hindrance between quantum dots located in neighboring GNL binding sites. To sum up, the lectin multivalency potency is not the only parameter influencing the flocculation kinetics. Possible steric hindrance between quantum dots is possible, when lectin binding sites are situated too close to each other. For both TriADMan and ADTEGMan, excess in respect to effective cyclodextrin concentration seems to speed up network formation, flocculation and sedimentation. When dynamic interactions are employed, there is a slower response in the network formation and flocculation. However, seems to interfere less when the linkers are used in excess.

To test and compare the selectivity of the supramolecular sensors based on trivalent or monovalent adamantane linkers, four lectins, which do not bind mannose were used (Figure 5-12). Peanut Agglutinin (PNA), Ricinus communis I (RCA120) and Soyabean Agglutinin (SBA) bind galactose and galactose derivatives while Wheat Germ agglutinin (WGA) binds glucosamine and sialic acid residues [30].

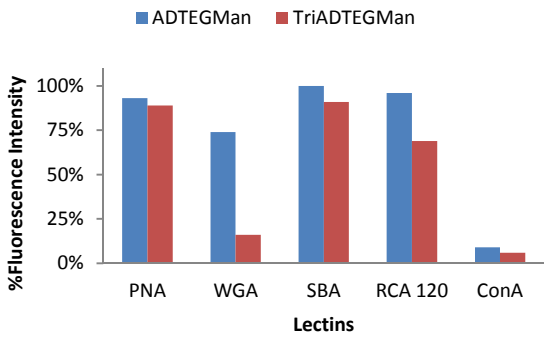

Figure 5-12: Fluorescence intensity % of β-CD-QD remaining in solution at 671 nm, after 500 minutes incubation time, for selectivity testing against Peanut Agglutinin (PNA), Ricinus communis I (RCA I), Soyabean Agglutinin (SBA) and Wheat Germ Agglutinin (WGA) . The concentration of β-CD-QD is 2.4 x 10^{-7} M, of lectins is 6.4 x 10^{-6} M and of linkers 5.7 x 10^{-5}. In blue are the samples tested with ADTEGMan and in red the samples tested with TriADTEGMan.

In Figure 5-12, comparison of the fluorescence intensity of 500-minute-incubated samples with PNA, WGA, SBA and RCA I reveals excellent selectivity of the supramolecular sensor based on the monovalent (ADTEGMan) linker for three (PNA, SBA, RCA I) out four lectins. For WGA the selectivity is still satisfactory, although the fluorescence intensity decreased significantly over time (26%). For the trivalent adamantane linker, excellent selectivity is observed for PNA and SBA, but in the case of RCA I and WGA, the sensor is much less selective, since a significant decrease in fluorescence intensity is observed (31% and 84% respectively). By comparing the selectivity results between the two linkers it can be concluded that selectivity of the supramolecular sensors based on monovalent linkers is better than when trivalent linkers

are used. Better performance of the monovalent linker, in terms of selectivity, is attributed to the fact that even if nonspecific interactions or weak nanoparticle-lectin interactions occur, these do not lead to substantial sedimentation of quantum dots, due to the dynamic nature of the adamantane- β-cyclodextrin interaction. In the case, where non-specific or weak binding does lead to flocculation and sedimentation, like RCA_{120} and WGA, the kinetics are much slower than the ConA kinetics, yielding again to better selectivity. In all cases, since the supramolecular sensors are based on flocculation kinetics, selectivity results can be time-dependent. This gives an excellent advantage in terms of selectivity and sensitivity over sensors based in analytical readouts based on equilibrium structures.

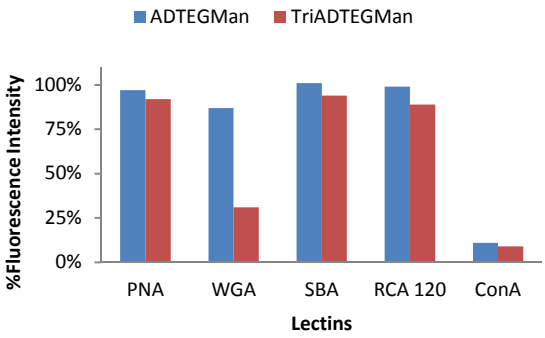

Figure 5-13: Fluorescence intensity % of β-CD-QD remaining in solution at 671 nm, after 300 minutes incubation time, for selectivity testing against Peanut Agglutinin (PNA), Ricinus communis I (RCA I), Soyabean Agglutinin (SBA) and Wheat Germ Agglutinin (WGA) . The concentration of β-CD-QD is 2.4×10^{-7} M, of lectins is 6.4×10^{-6} M and of linkers 5.7×10^{-5}. In blue are the samples tested with ADTEGMan and in red the samples tested with TriADTEGMan.

For example, if an earlier timepoint for selectivity is chosen e.g. 300 minutes, as in Figure 5-13, where the ConA kinetics have reached equilibrium (Figure 5-9), then the selectivity results are excellent for all cases except the trivalent linker-WGA lectin combination.

5.4 Conclusion

In summary, the multivalency potency of trivalent adamantane linkers on cyclodextrin nanoparticle surfaces was exploited as a supramolecular nanoparticle functionalization strategy such as for building gluconanoparticles. The triadamantane linkers bind on the cyclodextrin quantum dot surface in a non-dynamic fashion, yielding supramolecular, non-dynamic systems which are very robust. Nonetheless the binding strength of such complexes is highly tunable by the addition of free cyclodextrin in solution.

Using supramolecular chemistry strategies, either dynamic or non-dynamic, is more advantageous in respect to covalent chemistry. First, supramolecular systems can self-organize in-situ providing simplicity and speed in building-up selective lectin sensors for on-spot detection. Response times of supramolecular sensors can be easily tuned either by varying concentration or by adding competitor molecules. In terms of selectivity, both sensors give excellent results, except when tested against WGA, if the timepoint for testing selectivity is carefully chosen.

Lectin sensors which are based on the non-dynamic, supramolecular interactions of trivalent adamantane-mannose linkers with β-cyclodextrin decorated quantum dots, exhibit certain advantages over the case of their monovalent, dynamic equivalents. Not only trivalent adamantane linkers are more robust, being affected less by concentration changes, but also more faster in response times, good in selectivity, and highly-tunable by either varying their concentration or by adding cyclodextrin as competitor molecule. Lastly, both types of linkers, allow for sensing and studying flocculation kinetics of other lectins, such as Galanthus Nivalis and Lens Culinaris as well. To sum up, supramolecular nanoparticle sensors are advantageous platforms for sensing lectins in solution, since they combine on-spot detection with simplicity, speed, selectivity, robustness and tunability.

5.5 References

1. Sapsford, K.E., et al., Functionalizing Nanoparticles with Biological Molecules: Developing Chemistries that Facilitate Nanotechnology. Chemical Reviews, 2013. 113(3): p. 1904-2074.
2. Sperling, R.A. and W.J. Parak, Surface modification, functionalization and bioconjugation of colloidal inorganic nanoparticles. Philosophical Transactions of the Royal Society of London A: Mathematical, Physical and Engineering Sciences, 2010. 368(1915): p. 1333-1383.
3. Nowak, P., et al., Localized Template-Driven Functionalization of Nanoparticles by Dynamic Combinatorial Chemistry. Angewandte Chemie International Edition, 2015. 54(14): p. 4192-4197.
4. Perl, A., et al., Gradient-driven motion of multivalent ligand molecules along a surface functionalized with multiple receptors. Nat Chem, 2011. 3(4): p. 317-322.
5. Szejtli, J., Introduction and general overview of cyclodextrin chemistry. Chemical Reviews, 1998. 98(5): p. 1743-1753.
6. Wenz, G., Cyclodextrins as building blocks for supramolecular structures and functional units. Angewandte Chemie (International Edition in English), 1994. 33(8): p. 803-822.
7. Gelb, R.I., L.M. Schwartz, and D.A. Laufer, Cycloamylose complexation of adamantane derivatives. Life Sciences, 1983. 33(1): p. 83-85.
8. Hamilton, J.A., Structure of inclusion complexes of cyclomaltoheptaose (cycloheptaamylose): Crystal structure of the 1-adamantanemethanol adduct. Carbohydrate Research, 1985. 142(1): p. 21-37.

9. Jaime, C., et al., β-cyclodextrin inclusion complex with adamantane Intermolecular 1H{1H} NOE determinations and molecular mechanics calculations. Journal of Molecular Structure, 1991. 248(3-4): p. 317-329.
10. Badjić, J.D., et al., Multivalency and cooperativity in supramolecular chemistry. Accounts of Chemical Research, 2005. 38(9): p. 723-732.
11. Mulder, A., J. Huskens, and D.N. Reinhoudt, Multivalency in supramolecular chemistry and nanofabrication. Organic and Biomolecular Chemistry, 2004. 2(23): p. 3409-3424.
12. Kauscher, U. and B.J. Ravoo, Mannose-decorated cyclodextrin vesicles: The interplay of multivalency and surface density in lectin–carbohydrate recognition. Beilstein Journal of Organic Chemistry, 2012. 8: p. 1543-1551.
13. Krishnamurthy, V.M., L.A. Estroff, and G.M. Whitesides, Multivalency in ligand design. Fragment-based approaches in drug discovery, 2006. 34: p. 11-53.
14. Baldini, L., et al., Calixarene-based multivalent ligands. Chemical Society Reviews, 2007. 36(2): p. 254-266.
15. Hsu, S.-H., et al., Nonlinear Amplification of a Supramolecular Complex at a Multivalent Interface. Angewandte Chemie International Edition, 2013. 52(2): p. 714-719.
16. Krabbenborg, S.O., J. Veerbeek, and J. Huskens, Spatially Controlled Out-of-Equilibrium Host–Guest System under Electrochemical Control. Chemistry-A European Journal, 2015. 21(27): p. 9638-9644.
17. Wittmann, V. and R.J. Pieters, Bridging lectin binding sites by multivalent carbohydrates. Chemical Society Reviews, 2013. 42(10): p. 4492-4503.
18. Liu, Z., et al., Animal Lectins: Potential Antitumor Therapeutic Targets in Apoptosis. Applied Biochemistry and Biotechnology, 2012. 168(3): p. 629-637.
19. Samanta, A. and B.J. Ravoo, Magnetic Separation of Proteins by a Self-Assembled Supramolecular Ternary Complex. Angewandte Chemie International Edition, 2014. 53(47): p. 12946-12950.
20. Ahirwar, R. and P. Nahar, Screening and Identification of a DNA Aptamer to Concanavalin A and Its Application in Food Analysis. Journal of Agricultural and Food Chemistry, 2015. 63(16): p. 4104-4111.
21. Shi, Z., et al., Antitumor effects of concanavalin A and Sophora flavescens lectin in vitro and in vivo. 2014. 35(2): p. 248-256.
22. Richards, S.-J., et al., Discrimination between bacterial phenotypes using glyco-nanoparticles and the impact of polymer coating on detection readouts. Journal of Materials Chemistry B, 2014. 2(11): p. 1490.
23. Sánchez-Pomales, G., et al., A lectin-based gold nanoparticle assay for probing glycosylation of glycoproteins. Biotechnology and Bioengineering, 2012. 109(9): p. 2240-2249.
24. Poderys, V., et al., Interaction of Water-Soluble CdTe Quantum Dots with Bovine Serum Albumin. Nanoscale Research Letters, 2011. 6(1): p. 9-9.
25. Alvarez, J., et al., Water-soluble platinum and palladium nanoparticles modified with thiolated [small beta]-cyclodextrin. Chemical Communications, 2000(13): p. 1151-1152.
26. Chmurski, K. and J. Defaye, An Improved Synthesis of Per(6-Deoxyhalo) Cyclodextrins Using N-Halosuccinimides —Triphenylphosphine in Dimethylformamide. Supramolecular Chemistry, 2000. 12(2): p. 221-224.

27. Rojas, M.T., et al., Supported Monolayers Containing Preformed Binding Sites. Synthesis and Interfacial Binding Properties of a Thiolated .beta.-Cyclodextrin Derivative. Journal of the American Chemical Society, 1995. 117(1): p. 336-343.
28. Onclin, S., et al., Molecular Printboards: Monolayers of β-Cyclodextrins on Silicon Oxide Surfaces. Langmuir, 2004. 20(13): p. 5460-5466.
29. Yapar, S., et al., Dipeptide recognition in water mediated by mixed monolayer protected gold nanoparticles. Chemical Communications, 2015. 51(75): p. 14247-14250.
30. Ambrosi, M., N.R. Cameron, and B.G. Davis, Lectins: tools for the molecular understanding of the glycocode. Org Biomol Chem, 2005. 3(9): p. 1593-608.

5.6 Supplementary information

Details on the ligand syntheses, nanoparticle functionalization and characterization, and binding studies are given in this section.

Ligand Syntheses.

General details. All starting materials were purchased by Sigma-Aldrich, except otherwise stated, and were used without further purification. NMR solvents were purchased by Euriso-top (France). The synthesis of ligands was adapted from a protocol as described previously [12].

Synthesis of 2-(2-(2-(2-(adamantan-1-yloxy)ethoxy)ethoxy)ethoxy) ethyl 4-methyl-benzenesulfonate (5)

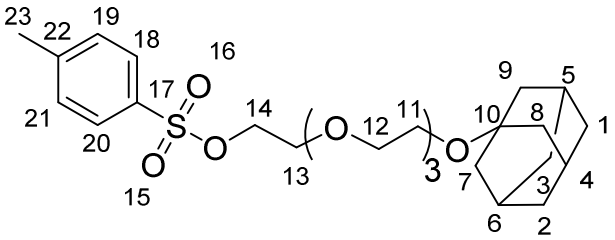

ADTEG (7.4g, 22.5 mmol) was dissolved in DCM (100 mL). 4-methylbenzenesulfonyl chloride (5.2 g, 27 mmol), TEA (3.7 mL, 27 mmol) and DMAP (180 mg 1.5 mmol) were added and the mixture was stirred overnight at room temperature. The reaction mixture was quenched with 1 M HCl (150 mL), was washed with water (2x) and with 2 M HCl (1x). The organic layer was dried with MgSO4 and was concentrated giving an oily product (5) (10.51g, 21.8 mmol Yield: 85%). Column chromatography is optional (ethyl acetate: hexane, 70:30).

1H NMR: (400 MHz, CDCl3) δ = 1.61 (q, J = 8.4 Hz, 6H, 1,2,3-H), 1.73 (dd, J = 6.5, 2.9 Hz, 6 H, 7,8,9-H), 2.45 (bs, 3H, 4,5,6-H), 3.57 – 3.69 (m, 16H, 11-14-H), 4.16 (s, 3H, 22-H), 7.41 (d, J = 8.25, 2H, 19, 21-H), 7.93 (d, J = 8.25, 2H, 18,20-H).

Synthesis of Methyl-3,4,5-tris(2-(2-(2-(2-(adamantan-1-yloxy)ethoxy)ethoxy)ethoxy)ethoxy)benzoate (2)

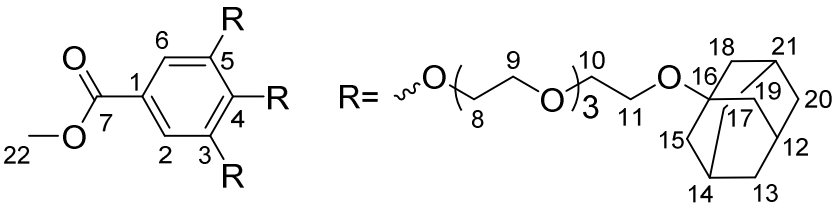

Methyl gallate (0.44 g, 2.39 mmol) was dissolved in dry acetone. Potassium carbonate (3.26 g, 23.6 mmol) and 1 (3 g, 6.2 mmol) were added. The reaction was stirred under reflux conditions and a nitrogen atmosphere for 6 days. The pink reaction mixture was filtered to remove the potassium carbonate, yielding a wine-red solution. The solvent was evaporated and the crude product was redissolved in dichloromethane and washed with water (40 mL), 1M HCl (40 mL) and again with water (50 mL). The organic layer was dried over $MgSO_4$ and the solvent was removed under reduced pressure. Column chromatography (SiO_2: ethylacetate-hexane (98:2)) was applied to remove the by-products with only one (R_f: 0.50) or two (R_f: 0.32) TEG-adamantane tails; the column was consequently flushed with dichloromethane-methanol (90:10, R_f:0.13) to give pure product as a brown oil (710 mg, 0.637 mmol, 27%).

^{1}H NMR (400 MHz, $CDCl_3$): δ = 1.54 (q, J = 9.8 Hz, 18H, 13-,19-,20- H), 1.67 (d, J = 3.0 Hz, 18H, 15-,17,18-H), 2.06 (bs, 9H, 12-,14-,21-H), 3.44 – 3.84 (m, 45H, 9-11-,22-H), 4.09 – 4.18 (m, 6H, 8-H), 7.23 (s, 2H, 2-,6-H) ppm.

Synthesis of 3,4,5-Tris(2-(2-(2-(2-(adamantan-1-loxy)ethoxy)ethoxy)ethoxy)ethoxy)benzoic acid (3)

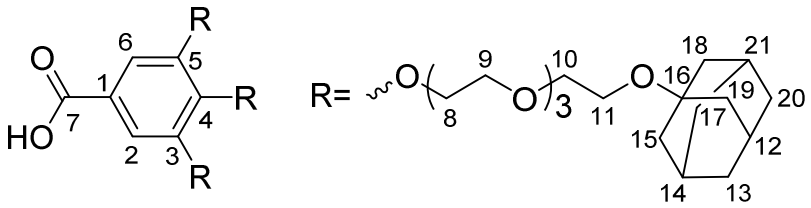

Compound 2 (0.71 g, 0.63 mmol) was added to a solution of lithium hydroxide (88.7 mg, 3.71 mmol) in water/methanol (50/50, 35 mL). The mixture was stirred for 2 days under reflux conditions. The solvents were evaporated and the residue was redissolved in dichloromethane (40 mL) and washed with HCl (2x 2M, 50 mL) and water (2x 50 mL). The organic layer was dried over $MgSO_4$ and the solvents were evaporated off to yield pure product as yellow oil (540 mg, 0.49 mmol, 77%).

^{1}H NMR (400 MHz, $CDCl_3$): δ = 1.56 (q, J = 8.4 Hz, 18H, 13-,19-,20- H), 1.70 (dd, J = 6.5, 2.9 Hz, 18H, 15-,17,18-H), 2.09 (bs, 9H, 12-,14-,21-H), 3.50 – 3.84 (m, 42H, 9-11-H), 4.14 – 4.21 (m, 6H, 8-H), 7.34 (s, 2H, 2-,6-H) ppm.

Synthesis of 3,4,5-Tris(2-(2-(2-(2-(adamantan-1-yloxy)ethoxy)ethoxy)ethoxy)ethoxy)-N-(prop-2-yn-1-yl)benzamide (4)

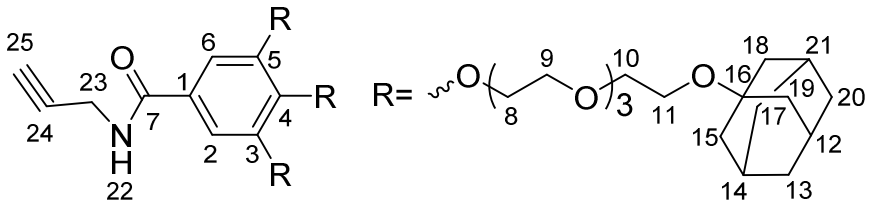

Compound 3 (1.2 g, 1.09 mmol) was dissolved in dimethylformamide (20 mL). 1-Ethyl-3-(3-dimethylaminopropyl)carbodiimide (0.621 g, 4,00 mmol) and hydroxybenzotriazole (0.534 g, 4.02 mmol) were added. The mixture was stirred for 30 minutes under a nitrogen atmosphere. Propargylamine (0.3965 g, 7.20 mmol) and n-methylmorpholine (0.4021 g, 3.98 mmol) were added. The mixture was stirred overnight under a nitrogen atmosphere. The solvents were evaporated and the mixture was redissolved in chloroform (25 mL) and washed with brine (2x 30 mL), water (2x 30 ML), saturated $NaHCO_3$ solution (2x 30 mL) and again with water (2x 30 mL). The organic layer was dried over $MgSO_4$ and the solvent was removed under reduced pressure. Column chromatography (SiO_2: dichloromethane-methanol (95:5)) was applied to yield pure product (0.32 g, 0.28 mmol, 26%).

^{1}H NMR (400 MHz, $CDCl_3$): δ = 1.60 (q, J = 11.9 Hz, 18H, 13-,19-,20- H), 1.73 (dd, J = 9.3, 2.9 Hz, 18H, 15-,17,18-H), 2.13 (bs, 9H, 12-,14-,21-H), 2.25 (t, J=2.5 Hz, 1H, 25-H), 3.53 – 3.86 (m, 42H, 9-11-H), 4.17 – 4.25 (m, 8H, 8-,23-H), 7.01 (s, 1H, 22-H), 7.18 (s, 2H, 2-,6-H) ppm.

Synthesis of 2,3,4,6-Tetra-O-acetyl-α-D-mannosepyranosyl monoazide (5)

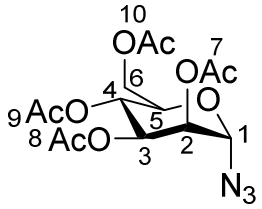

Man5Ac (1.00 g, 2.56 mmol), $SnCl_4$ (800 mg, 3.08 mmol) and Me_3SiN_3 (355 mg, 3.08 mmol) were dissolved in chloroform (10 mL). The solution was stirred overnight at RT and afterwards washed with distilled water (10 mL), brine (10 mL) and again water (10 mL). The organic layer was dried over $MgSO_4$ and the solvent was evaporated off to give $Man5AcN_3$ (5) as a brown oil (910 mg, 2.44 mmol, 95%).

^{1}HNMR: (400 MHZ, $CDCl_3$, 298 K) δ = 1.73-1.91 (4s, 12H, 7-, 8-, 9-, 10-H), 3.91 (m, 2H, 4-, 5-H), 4.02 (m, 1H, 2-H), 4.89 (s, 1H, 3-H), 4.98 (m, 2H, 6-H), 5.17 (bs, 1H, 1-h).

Synthesis of N-((1-(2,3,4,6-tetra-O-acteyl-α-D-mannosepyranosyl)-1H-1,2,3-triazol-4-yl)methyl)-3,4,5-tris(2-(2-(2-(2-(adamantan-1-yloxy)ethoxy)ethoxy)ethoxy)ethoxy)-N-(prop-2-yn-1-yl)benzamide (6)

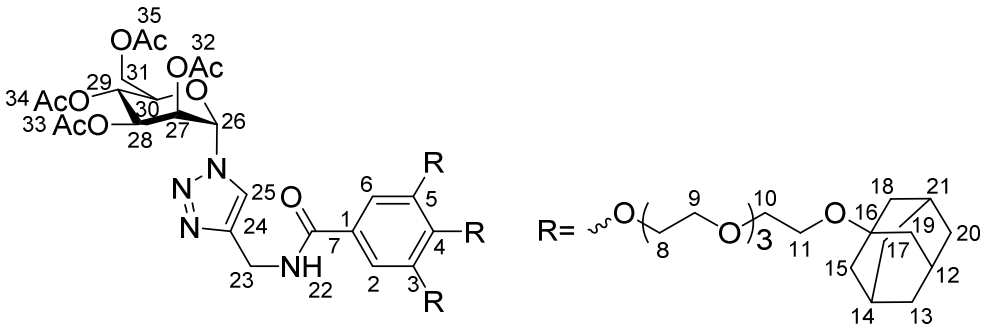

Compound 4 (151 mg, 0.13 mmol) and compound 5 (865 mg, 0.21 mmol) were dissolved in dimethylformamide. Catalytic amounts of copper(I)iodide were added and the suspension was stirred overnight at 60° C. Afterwards the solvent was evaporated and the mixture was redissolved in chloroform. The solution was washed with brine (50 ml) and water (2x 50 mL). The organic layer was dried with $MgSO_4$ and the solvent was removed under reduced pressure. The crude product was purified via column chromatography (SiO_2: dichloromethane-methanol (90:10)) and was obtained as a slight yellow waxy solid (30 mg, 0.01 mmol, 8%).

1H NMR (400 MHz, CDCl3): δ = 1.41-1.68 (m, 18H, 13-,19-,20-H), 1.71 (dd, J = 9.2, 2.7 Hz, 18H, 15-,17-,18-H), 1.86-2.34 (m, 22H, 12-, 14-, 21-, 32-, 33-, 34-, 35-H), 2.95-4.43 (m, 50H, 9-, 10-, 11--H, 31-H), 4.56 -4.69 (m, 1H, 30-H), 4.69-4.85 (m, 1H, 29-H), 5.20-5.43 (m, 1H, 28-H), 5.87 (m, 1H, 27-H), 5.95 (t, J = 4.2 Hz, 1H, 26-H), 7.16 (d, J = 13.9 Hz, 2H, 2-,6-H), 7.80-7.91 (m, 1H, 25-H) ppm.

Synthesis of N-((1-(α-D-mannosepyranosyl)-1H-1,2,3-triazol-4-yl)methyl)-3,4,5-tris(2-(2-(2-(2-(adamantan-1-yloxy)ethoxy)ethoxy)ethoxy)-N-(prop-2-yn-1-yl)benzamide (7)

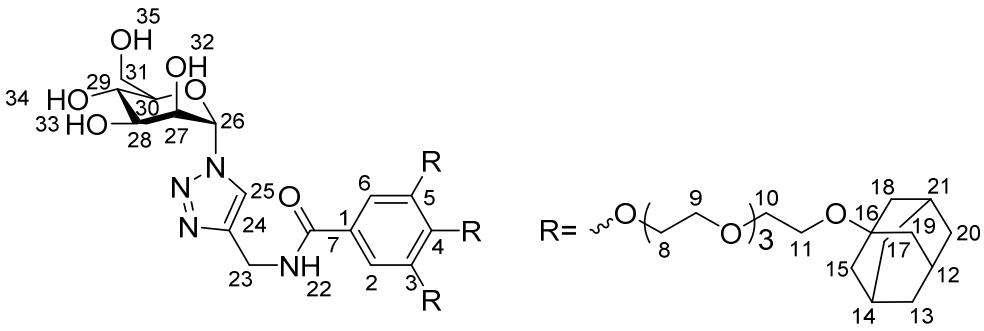

Compound 7 (30 mg, 0.01 mmol) was dissolved in dry methanol and a solution of NaOMe (catalytic amounts) in methanol was added. The mixture was stirred at room temperature until TLC signaled a complete conversion. Afterwards the solution was neutralized by addition of Dowex HCR-W2 ion exchange resign in hydrogen form. The suspension was stirred for 15 minutes and was then filtered. The crude product was purified via column chromatography (SiO_2: dichloromethane-methanol (90:10)) and was obtained as a white powder (10 mg, 0.005 mmol, 37%).

1H NMR (500 MHz, $CDCl_3$): δ = 1.57-1.72 (m, 18H, 13-,19-,20-H), 1.72-1.78 (m, 18H, 15-,17-,18-H), 2.09-2.19 (m, 9H, 12-,14-,21-H), 3.34-3.37 (m, 2H, 23-H), 3.48-3.96 (m, 50H, 8-, 9-, 10-, 11-, 29-, 30-H), 4.09-4.11 (dd, J = 8.4, 3.6 Hz, 1H, 28-H), 4.23- 4.25 (m, 3H, 22-,31-H), 4.60-4.72 (m, 1H, 27-H), 5.98 (d, J = 2.6 Hz, 1H, 26-H), 7.29 (s, 2H, 2-,6-H), 7.62 (dd, J = 15.7, 10.0 Hz, 1H, 23-H), 7.80-7.91 (m, 1H, 25-H), 8.15 (s, 1H, 22-H) ppm.

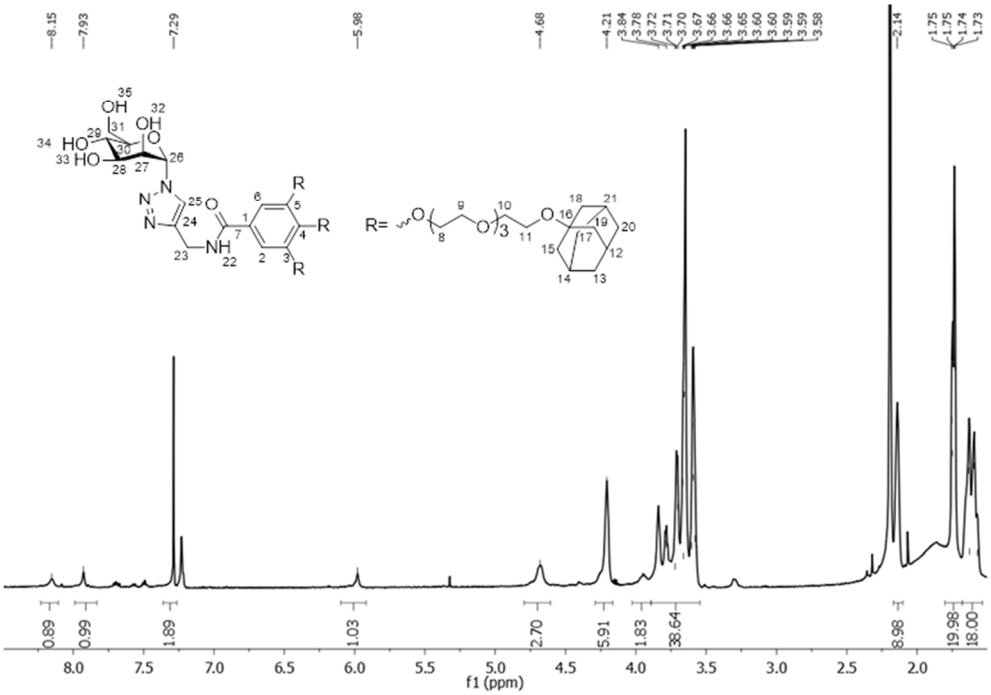

Figure S 5-1: 1H NMR spectrum of N-((1-(α-D-mannosepyranosyl)-1H-1,2,3-triazol-4-yl)methyl)-3,4,5-tris(2-(2-(2-(2-(adamantan-1-yloxy)ethoxy)ethoxy)ethoxy)ethoxy)-N-(prop-2-yn-1-yl)benzamide in $CDCl_3$

Nanoparticle Syntheses and Characterization.

General details. Carboxy-terminated water-soluble CdTe quantum dots with 670±10 nm emission were purchased from Plasmachem (Germany).

Synthesis of heptakis(6-bromo-6-deoxy)-β-cyclodextrin. The synthesis of heptakis(6-bromo-6-deoxy)-β-cyclodextrin was adapted from Chmurski et al [26].

Synthesis of heptakis-(6-thio-6-deoxy)-β-cyclodextrin. The synthesis of heptakis(6-thio-6-deoxy)-β-cyclodextrin was adapted from Rojasi et al [27].

Functionalization of carboxy-terminated quantum dots with heptakis(6-thio-6-deoxy)-β-cyclodextrin (β-CD QD). Functionalization of carboxy-terminated quantum dots with heptakis(6-thio-6-deoxy)-β-cyclodextrin was performed by ligand exchange. In an aqueous solution of 1.2 x 10^{-5} M of quantum dots, 300 equivalents of heptakis(6-thio-6-deoxy)-β-cyclodextrin was added and the reaction was stirred overnight. Afterwards, the quantum dots were washed at least 5 times with deionized water by spin filtration (Amicon Ultra, 10kDa, Millipore) and were reconstituted with water to 1.2 x 10^{-5} M.

Binding Studies.

DOSY NMR Spectroscopy.

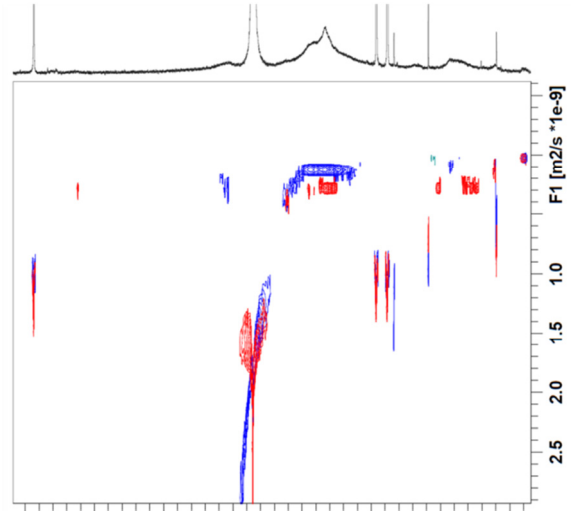

Figure S 5-2: Overlay of two DOSY NMR spectra; in red is the spectrum of the free TriADTEG and in blue the spectrum of TriADTEG in stoichiometric ration in respect to the number of cyclodextrins found on quantum dots.

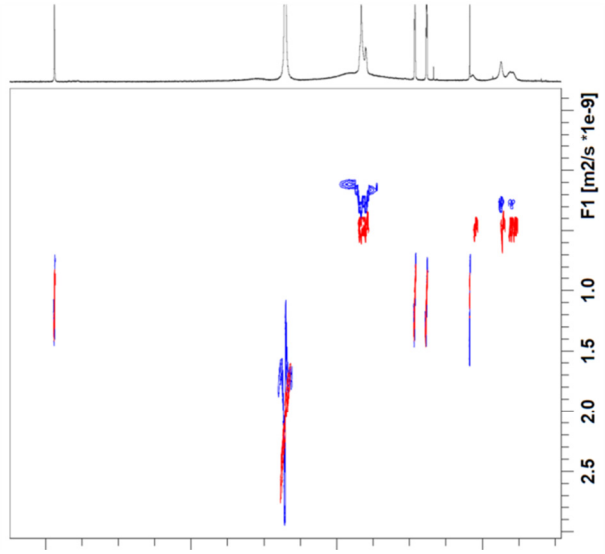

Figure S 5-3: Overlay of two DOSY NMR spectra; in red is the spectrum of the free ADTEG and in blue the spectrum of ADTEG in stoichiometric ration in respect to the number of cyclodextrins found on quantum dots.

Fluorescence measurements. Steady-state fluorescence measurements were done on a Cary Eclipse fluorescence spectrophotometer (Varian) at 22°C. The software used is Cary Eclipse version 1.2(147). Quartz cuvettes of 3.5 ml nominal volume (Hellma)

were used for the samples and all samples were prepared to a final volume of 3.0 ml. Excitation and emission slits were at 10 nm, detection voltage was at 600 V and excitation wavelength was at 450 nm. Scans of every sample were performed every 5 or 10 minutes from 500-800 nm. All fluorescence intensity data were analyzed at maximum fluorescence emission at 671 nm.

Chapter 6 General discussion

Abstract

In this thesis, the motivation was to progressively discover and understand molecular interactions that govern natural systems and beyond, and the goal was to acquire the ability to design, direct and control complex matter. Special focus was put on implementing and controlling supramolecular ligand interactions on nanoparticle surfaces with an emphasis on biomolecule sensing. This Chapter summarizes the most important findings of every chapter. By linking all the findings of this thesis, the questions answered are evaluated and a general conclusion is reached. With an eye on the future, some observations to extend the discussion further and beyond this thesis are added and new questions arisen are identified. Finally, a conclusion is reached by providing insight, guidelines and suggestions on designing and controlling multivalent, supramolecular interactions on the nanoparticle bionanointerface, between nanomaterials, ligands and biomolecules.

6.1 Introduction

The motivation was to progressively discover and understand molecular interactions that govern nanoscale natural systems and beyond, and the goal was to acquire the ability to design, direct and control complex matter. In this context, supramolecular ligand interactions on nanoparticle surfaces were designed and implemented with an emphasis on biomolecule sensing.

In this Chapter, the most striking findings of this thesis are linked and evaluated to reach a general conclusion. Three main topics are addressed:

- NMR as a tool in Nanotechnology to study reactions and supramolecular interactions between molecules, nanoparticles and biomacromolecules.
- Supramolecular Orthogonal Interactions at nanoparticle surfaces.
- Applications of Supramolecular Orthogonal Interactions for biomolecule recognition and sensing.

With an eye on the future, some observations regarding these topics are added in order to extend the discussion further and beyond this thesis and to identify new questions arisen.

Coming to the conclusion, general guidelines and future outlook on designing and controlling multivalent, supramolecular interactions on the nanoparticle interface are provided.

6.2 NMR as a tool in Nanotechnology

Throughout this thesis, reactions and supramolecular interactions between molecules, nanoparticles and biomacromolecules were investigated by 1H-, 2D- and Diffusion Ordered SpectroscopY (DOSY NMR) for qualitative and mostly quantitative analysis [1-6].

6.2.1 NMR for kinetic processes at the nanoscale

In Chapter 2 the development of an acquisition technique, named p-DOSY, was achieved in order to improve diffusion accuracy in concentration evolving systems. Although, a model reaction of known kinetics, in specific the glucose anomerization, was

used, this technique can be implemented also for other kinetic processes. To monitor kinetic processes with DOSY NMR, typically a series of DOSY NMR measurements are acquired throughout the duration of the process. DOSY measurements, at high analyte concentration, last for a few minutes and can last for several hours if analyte concentration is very low. Chemical reactions expand over many orders of magnitude, from femtoseconds to years. The timescale of the kinetic process itself in comparison to the timescale of each DOSY measurement has to be matched. If each, single DOSY measurement is longer than the timescale of the kinetic process itself, no kinetic experimental observations can be acquired. If the timescale of the reaction is considerably longer than the timescale for each DOSY measurement, then accuracy is not heavily affected, since concentration changes with the timescale of the DOSY measurement are negligible. Taking the relation between these two timescales under consideration, the window of observation for kinetic processes by p-DOSY NMR is limited to kinetic processes that last from minutes to hours (Figure 6-1).

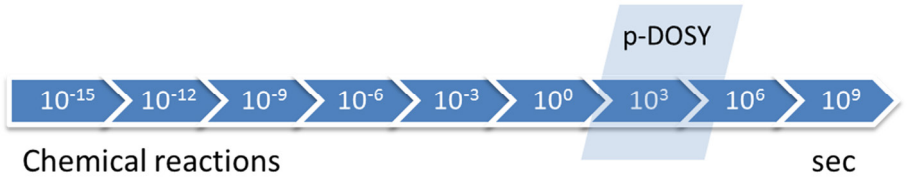

Figure 6-1: Timescale of chemical reaction kinetics in relation to the observation window that can be monitored by acquiring a series of p-DOSY measurements

At the nanoscale most kinetic processes such as for the monitoring of time-dependent synthesis of nanoparticles [7, 8], nanoparticle functionalization reactions [9], ligand exchange on nanoparticles [10], aggregation [11], and self-assembly [12, 13] processes are found in the window of observation by the p-DOSY, which enables nanotechnologists to fundamentally understand the underlying factors and mechanisms of such processes. Lastly, the lower level in the window of observation of kinetic processes by the p-DOSY could be lowered, if permutation of gradient strengths could be integrated in the single-scan DOSY NMR techniques [14-20].

6.2.2 NMR for nanoparticle surface analysis

A key aspect in Nanotechnology is the analysis and understanding of the nanoparticle surface chemistry. By NMR spectroscopy, the main features of the nanoparticle surface such as ligand identity [9, 21], quantity [21, 22], and arrangement [23]can be resolved. In this thesis, thiol-based, ligand exchange reactions were performed in order to obtain nanoparticles with functional monolayers. Qualitatively, verification of ligand exchange can be verified by comparing 1H NMR spectra, before and after the ligand

exchange, as conducted in Chapter 3 and Chapter 4. In between these measurements, a cleaning step is typically involved for the removal of excess of unreacted and exchanged ligand from solution. Especially for gold nanoparticles, there is also the possibility to degrade them by iodine decomposition [22] and determine the exact ligand number and composition by 1H NMR, as shown in Chapter 3. An alternative approach for verification of ligand exchange on nanoparticles would be the use of DOSY NMR for monitoring in situ the ligand exchange [10]. This approach is advantageous, because it reveals kinetic aspects of the ligand exchange reactions and does not, necessarily, require a cleaning step in between. An additional advantage is that from the DOSY measurements quantitative information about the hydrodynamic size of the nanoparticle can be acquired. There are though, some practical issues, such as the frequent overlap of the ligand peaks when free in solution and also on the nanoparticles. To overcome this problem, advanced acquisition [17, 24] and processing [25-28] techniques should be used. Since ligand exchange is a reaction between nanoparticles and ligands, thus a concentration evolving system, the use of the p-DOSY acquisition technique is recommended. Concerning the processing and analysis of diffusion data, in cases of overlapping signals, two approaches can be taken. If, the number of components, that constitute the overlapping signal are known, a multiexponential fit [29] for the decay curves could be used, as shown in Chapter 3. If the number of components is unknown or concentration changes are involved, then advanced processing software can improve the diffusion accuracy such as the MAXimum ENTropy analysis [25] (Chapter 2). By DOSY MAXimum ENTropy analysis, no assumption of the number of exponential components in a mixture is made, nor of their monodispersity, while this is the case for other software such as the CONTIN [27].

Apart from NMR, a lot of other techniques have been employed in order to define the nanoparticle surface chemistry. Among these techniques are Inductively Coupled Plasma Mass Spectrometry (ICPMS), Optical Emission Spectroscopy (ICPOES), Auger Electron Spectroscopy [AES] and X-ray Photoelectron Spectroscopy [XPS]); ion-based methods (Secondary Ion Mass Spectrometry [TOF-SIMS] and Low Energy Ion Scattering [LEIS]); Scanning Probe Microscopy (SPM), including Atomic Force Microscopy (AFM) and Scanning Tunneling Microscopy (STM) and ThermoGravimetric Analysis (TGA) [30]. While most of these techniques are powerful in measuring the amount of ligands on the nanoparticles, they lack in providing information in the molecular level. Other techniques, giving information in the molecular level and of the amount of ligands on the nanoparticle surface, are fluorescence-based methods and Raman, but they require molecular labeling or alteration of the ligands. Consequently, 1H- and DOSY NMR spectroscopy are indispensable methods for elucidating ligand identity, quantity and arrangement on nanoparticle surfaces. For quantitative ligand identification, though, an in-between decomposition step could be required.

6.2.3 NMR for nanoparticle size and shape elucidation

Size and shape are also important nanoparticle properties, influencing the surface chemistry of the nanoparticle. By knowing the nanoparticle size and shape, the available surface area of the nanoparticle can be calculated, and, if the number of ligands is known, the packing of the ligands in a monolayer can be defined (Chapter 3). The packing of ligands on the nanoparticle surface, influences nanoparticle solubility, stability and recognition (binding capacity). In Chapter 3 and Chapter 4, Transmission Electron Microscopy (TEM) and DOSY NMR are employed as the main techniques for calculating monolayer packing and surface area [31, 32]. By TEM, the core size of the nanoparticles and, by DOSY, the nanoparticle hydrodynamic radius is measured. By subtracting the core radius from the hydrodynamic radius, the monolayer height can be estimated. Using the core radius, also the nanoparticle surface area can be calculated. For example, in Chapter 3 and Chapter 4, the surface area can be approximated by the surface area of a sphere, thus $4\pi r_{core}^2$, by using the nanoparticle core radius obtained by TEM. Knowing the surface area of the core and the surface area a ligand occupies on the nanoparticle, the theoretical amount of ligands on surface can be calculated. In Chapter 3, the theoretical calculations are found to be very close to the experimental data from the decomposition studies. In Chapter 4 the cyclodextrin surface area is approximately the area of a circle (πr^2) and the theoretical amount of cyclodextrins per nanoparticle, seems to agree well with the findings in Chapter 5, when ligand titrations were performed. One would thus conclude that TEM and DOSY are complimentary techniques, excellent for determining the size, shape and concomitant surface properties of nanoparticles.

Apart from TEM and DOSY, Dynamic Light Scattering (DLS) [33-35] is also an appropriate technique for measuring size and shape at the nanoscale, and could be coupled to TEM and DOSY, or to be used instead of DOSY. Nevertheless, this technique was not thoroughly explored in this thesis.

6.2.4 NMR for investigating supramolecular interactions

Non-covalent weak forces that instigate molecular nanoparticle assemblies through intermolecular hydrogen bonds, aromatic π–π stacking, hydrophobic and electrostatic interactions [36], are the basis to fundamentally understand, design and control complex matter [37-40]. In such interactions, the number of molecules, their orientation, and their association strength should be determined. In Chapter 5, through 1H NMR titrations between a triadamantane or monoadamantane ligand and β-cyclodextrin nanoparticles, the dynamic nature, number of ligands and their orientation was quantified. The non-dynamic nature of the trivalent adamantane linker, as well as the number of adamantanes per β-cyclodextrin, was revealed, when addition of β-

cyclodextrin quantum dot in a constant amount of linker, altered the integrals of the linker peaks. The dynamic nature of the monovalent adamantane linker was manifested, when addition of β-cyclodextrin quantum dot in a constant amount of linker, resulted in altered chemical shifts of the linker peaks and not in integral change. In addition, these experiments confirmed qualitatively the binding of both linkers with the quantum dots, since the characteristic peak broadening [41] increased with increasing amount of β-cyclodextrin quantum dots in solution. Lastly, addition of free cyclodextrin in solution, and concomitant addition of β-cyclodextrin quantum dots gave information about the binding strength between the trivalent linkers and the quantum dots. In Chapter 5, DOSY NMR was performed only to confirm and support the observations made by 1H NMR. Despite the valuable proton information acquired in Chapter 5, the main limitation of 1H NMR was demonstrated in Chapter 3; titrations between ligand and nanoparticles could not be repeated for the peptide-nanoparticle system due to signal overlap of the peptide and nanoparticle peaks. Another (NMR spectroscopic) technique had therefore to be employed. DOSY NMR, known as NMR chromatography, was considered the most appropriate to study selective peptide binding towards gold nanoparticles. DOSY NMR is known as a principal technique to investigate weak binding of small molecules on significantly bigger receptors such as macromolecules, biomacromolecules and nanoparticles [1, 5, 42]. The success of DOSY NMR in weak binding experiments relies on the size difference between ligand and nanoparticles. The bigger the size difference, the more pronounced the change in ligand diffusion due to binding and therefore the more accurate the results. During the DOSY measurements, the problem of signal overlap became again evident, but it was successfully solved by using biexponential fitting [29] with a fixed diffusion for the nanoparticles as determined by blank gold nanoparticle experiments for fitting the peptide decays. Lastly, in Chapter 3, DOSY NMR measurements provided clear evidence for the interaction between the different peptides and the gold nanoparticles. The number of interacting peptides per nanoparticle, their binding strength and their selectivity towards different mixed nanoparticle monolayers was elucidated.

Apart from 1H- and DOSY NMR, other techniques for elucidation of the interactions could be employed. From the NMR toolbox, SaTuration Difference (STD) NMR [43] would probably be a good choice. STD-NMR is based on saturation transfer due to nuclear Overhauser effect from a receptor to a ligand. The advantage of this technique relies on the fact that on an STD spectrum only the proton signals of a binding ligand will appear. Other non-binding ligands present in solution will not receive any saturation transfer; thus they will not appear in the STD spectrum. The bigger the intensity of a ligand peak in an STD spectrum, the stronger the binding. Moreover, the orientation of binding can also be determined, since only the signals of the protons, that are in close contact to the receptor (≤5 Å) and receive magnetization transfer, will appear in the saturation difference spectrum and from those, the ones that are closer to the receptor will exhibit

higher intensity, due to a more efficient saturation transfer. STD NMR is appropriate for measuring weak binding such as dissociation constants ranging from 10^{-8} to 10^{-3} M. From, non-spectroscopic techniques, Isothermal Titration Calorimetry (ITC) [44, 45] would also be appropriate in order to measure binding strength. ITC measures the heat absorbed or generated when molecules interact. ITC is most useful for measuring dissociation constants in the 10^{-5} to 10^{-8} M range. The biggest disadvantages of ITC are long experimental times and use of relatively big volumes of concentrated solutions, typically in the range of 10^{-3} to 10^{-6} M.

While a wide range of binding affinities can be measured by the above mentioned techniques for weakly binding molecules with a fast association-dissociation rates, to detect strong- binding ligands with slow dissociation rates, such as the trivalent adamantane linkers developed in Chapter 5, can only be performed by the use of competition assays [46, 47]. Competition-based experiments utilize a competitor molecule, with known binding constant with fast exchange between the bound and free state. Addition of the strong-binding ligand, would lead in displacement of the weakly bound competitor, which is monitored as a change towards the free state in the observed physicochemical parameter (chemical shift for 1H NMR, diffusion for DOSY NMR, disappearance in the STD spectrum etc.).

To conclude, NMR spectroscopy is a valuable tool to investigate physicochemical of rather complex systems, found in various energetic landscapes. For reacting systems, as shown in Chapter 2, where concentration evolving systems move towards equilibrium, a new acquisition DOSY technique was presented in order to overcome diffusion inaccuracies and to, subsequently, facilitate nanotechnologists with the study of such systems. In Chapter 3, dynamic, non-covalent equilibrium interactions between peptides and gold nanoparticles were studied, leading to the discovery of novel, selective, nanoparticle based peptide receptors. In Chapter 5, dynamic and non-dynamic, supramolecular interactions on nanoparticle surfaces were compared, in order to design and optimize novel, selective, nanoparticle based, lectin sensors.

6.3 Supramolecular orthogonal interactions at nanoparticle surfaces

In this thesis, various multivalent systems and orthogonal supramolecular interactions on nanoparticle surfaces are described. Supramolecular interactions of several orthogonal pairs were investigated; a) quaternary ammonium with carboxylic acids (Chapter 3) b) crown ether with primary amines (Chapter 3) c) phenyl groups with other aromatic groups (Chapter 3) d) adamantane with cyclodextrins (Chapter 4 & Chapter 5) and e) mannose with mannose binding lectins (Chapter 4 & Chapter 5). These interactions

differed in binding strength and multivalency. In Chapter 3 gold nanoparticle peptide receptors were developed, employing synergetic, trivalent interactions, of different orthogonal pairs with relatively weak individual binding constants. In Chapter 4, two orthogonal pairs were employed for sequential self-organization and flocculation of ternary supramolecular nanoparticle networks between cyclodextrin-capped quantum dots, asymmetric mannose-adamantane cross-linkers and the lectin, Concanavalin A. The cross-linker molecules consisted monovalent adamantane-mannose moieties. The adamantane is orthogonal and binds strongly to β-cyclodextrin, while mannose is orthogonal and binds weakly to the tetravalent lectin, Concanavalin A. In contrast to the other chapters, in Chapter 5, the non-dynamic, supramolecular binding of trivalent adamantane linkers, which bind in an almost covalent fashion on β-cyclodextrin quantum dots, was investigated. By attaching mannose moieties on the trivalent adamantane, ligands were engaged for sensing, not only the tetravalent lectin, Concanavalin A, as in Chapter 4, but also a bivalent and a dodecavalent lectin.

In this section, the collective nanostructure properties emerging from multivalent ligand interactions at nanoparticle surfaces are presented. In simplified examples of multivalent interactions, such as unrestricted homobivalent systems (Figure 6-2b), the outcome is expected, as only a result of thermodynamics [48, 49]. In the case of restricted systems as shown in Figure 6-2a, the calculation of binding stoichiometry and affinity is more complex, since it is dependent not only on the outcome of thermodynamics between ligand-receptor interactions but also on rigidity, length, orientation, and proximity between binding sites.

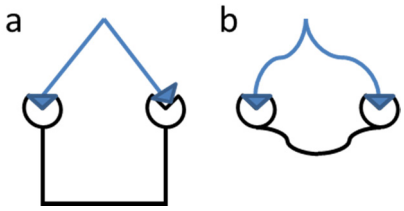

Figure 6-2: Schematic representation of homobivalent a) restricted and b) unrestricted supramolecular, multivalent interactions

The outcome of more complex interactions in solution, such as asymmetric hetero- polyvalent interactions or cross-linking ligands in ternary interactions, is already harder to predict [48, 49]. Even higher complexity rises when the above mentioned interactions take place on nanoparticle surfaces [49, 50]. Key factors influencing multivalent interactions on nanoparticle surfaces are surface curvature of the nanoparticles and length and rigidity of ligands [48, 49]. In the case of cross-linkers, not only the linker length and rigidity influence, but also the orientation of interactions and size of the other two components in the ternary system [49]. Taking the previously

mentioned factors into account, let's look at a simplified schematic overview of the interactions studied in Chapter 3, Chapter 4 and Chapter 5.

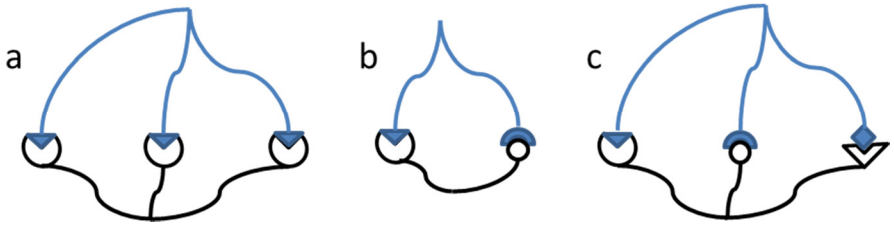

Figure 6-3: Schematic overview of the supramolecular, multivalent systems studied in this thesis, (a) represents trivalent adamantane linkers interacting with β-cyclodextrin quantum dots (Chapter 5), (b) represents dipeptide interactions with nanoparticles bearing quaternary ammonium and crown ether, NP_{QC}, or nanoparticles with quaternary ammonium and benzene group, NP_{QP} , (Chapter 3)and (c) represents the interactions of glycine-phenylalanine with a combination of all three functional groups $NP_{QPC,}$ on the nanoparticle surface (Chapter 3).

In Figure 6-3, the ternary interactions between system (a) with lectins, studied in Chapter 5, are not depicted. Concerning the amount of ligands bound on the nanoparticle surface for the systems described under (a) and (c), there is a noticeable difference in the results. In Chapter 3 the number of peptides bound on gold nanoparticles bearing all three combinations of ligand (c) is 3.6, while the number of triadamantane ligands bound on the cyclodextrin nanoparticle surface, described in Chapter 5, is close to 35. The nanoparticle size difference between these cases is approximately 1 nm, (6.2 nm for the quantum dots and 5.0 for the gold nanoparticles), yielding 1.5 times bigger surface area in the case of quantum dots in respect to the gold nanoparticles. Despite the differences in surface area, the difference in numbers of the bound molecules is so big, leading to the conclusion that there are other factors influencing these numbers. Surface curvature and even surface defects could possibly influence more the binding events in the case of dipeptide binding of gold nanoparticles. In addition, both ligands can be considered flexible and in the same size range, but the orientation of interactions is different. In the case of the dipeptide interactions with gold nanoparticles the peptides lie in a horizontal fashion and therefore cover bigger surface area, whilst in the case of the trivalent linkers the interactions are perpendicular. Lastly, the trivalent interactions described in Chapter 3 are heterovalent whereas the ones of Chapter 5 are homovalent. If the thiols on the gold nanoparticles are not in dynamic exchange, then the ligand arrangement on the surface influences more the case of heterovalent binding than the homovalent.

Comparing the multivalent interactions of the nanoparticle systems described in Chapter 3 and depicted as (a), (b) and (c) in Figure 6-3, interesting conclusions regarding additivity or cooperativity can be drawn, since surface curvature and area, peptide length and rigidity are very similar. First, the binding strength of the individual interactions differs significantly. Quaternary ammonium capped nanoparticles yield high binding constants,

while no additive or cooperative effect is observed for nanoparticles bearing quaternary ammonium together with either crown ether or aromatic groups. In the case of the nanoparticles bearing all three combinations, the result is surprising since the binding constant is double for glycine-phenylalanine in comparison to all previous cases and in comparison to glycine-glycine, leading to the assumption that there might be a peptide template effect. These results differ from Schneider at al. [51], where a small, rigid synthetic receptor bearing all three groups combinations was synthesized. No clear effect from the combination between quaternary ammonium combined either with crown ether or phenyl group was observed in contrast to Schneider's receptor. When all three interactions are combined, then stronger and selective binding is observed, an observation opposite to Schneider's findings where no added effect was seen by the addition of the aromatic group. The reason for the observed differences lies in the flexibility/orientation of the peptides as well as in possible ligand rearrangements on the nanoparticle surface. Possibly, Schneider's system is largely impacted by steric hindrance of the different peptide side groups.

Continuing with a comparison between the monovalent interactions between adamantane-β-cyclodextrin quantum dots and the system depicted as (a) in Figure 6-3 and described in Chapter 4 and Chapter 5, by increasing the adamantane multivalency from one to three, a transition between dynamic and non-dynamic supramolecular interactions is generated. It is known from literature, that bivalent interactions at the cyclodextrin SAMs resulted in a binding constant of 10^{10} M^{-1}, three orders of magnitude higher than that for the corresponding bivalent interaction in solution (10^{7} M^{-1}) [52]. This large effect brings the discussion to the impact of regional effective concentration. An uncomplexed adamantane close to a surface has approximately double probability into interacting with a cyclodextrin in respect to when the cyclodextrin is in solution. The third sequential binding of adamantane in the case of the trivalent adamantane linkers would exhibit even higher binding effect, in the range of 10^{10} M^{-1} and possibly more, since on surface [53, 54], and would lead to the non-dynamic systems observed in Chapter 5. Interestingly, non-dynamic systems described in Chapter 5 are highly robust and at the same time still tunable, when free cyclodextrin is present in solution before the quantum dots are added [53, 55].

In Chapter 4 and Chapter 5 another interesting aspect of multivalent systems is studied; the case of asymmetric linker molecules. Monovalent adamantane and trivalent adamantane ligands were coupled with mannose, in order to cross-link β-cyclodextrin quantum dots with mannose binding lectins forming ternary superstructures. A significant difference from the systems described previously is the size of the three components, where lectins and quantum dots are in the same size range and the linker significantly smaller. This is the reason for the fact that, despite the high amount of cyclodextrins on the nanoparticle surface (~86), each quantum dot can bind maximally four Concanavalin A

lectins by employing four linkers. One may then wonder why excess of linkers and lectin should be present in solution. The answer lies in the dynamic nature of the interactions between cyclodextrin and adamantane and between mannose and Concanavalin A, where faster kinetics exhibit the more the system is saturated with its components (Chapter 4). In the case of the strong-binding adamantane ligands (Chapter 5), the observed self-organization and flocculation kinetics are almost twice as fast, when stoichiometric ratios between adamantanes and β-cyclodextrin are used, as a result of the non-dynamic nature of the linker-quantum dot interactions. Moving towards sensing of other lectins than Concanavalin A, two factors can be identified for obtaining ternary supramolecular networks that flocculate. These factors are lectin valency, size and geometry [56, 57](Figure 6-4). For example, when the trivalent linkers were employed for the sensing of Lens Culinaris, almost no flocculation was observed. This result is attributed to the fact that Lens Culinaris is a bivalent lectin with poorer cross-linking capacity. In the case of lectins with higher valency, such as Galanthus Nivalis Agglutinin, faster kinetics than Concanavalin A would be expected. This expectation does not correspond to reality, though, due to lectin geometry and orientation of the mannose binding sites. Galanthus Nivalis, another mannose binding lectin, is almost the same size as of Concanavalin A, and despite its twelve binding sites, exhibits slower flocculation kinetics than Concanavalin A. The reason could be the fact that its binding sites are in close proximity with each other, not being all able to bind through a linker with a quantum dot, leading to a weaker crosslinking effect.

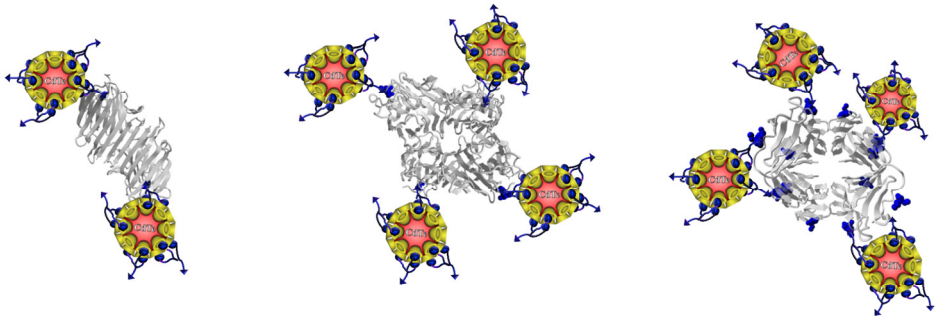

Lens Culinaris complex Concanavalin A complex Galanthus Nivalis complex

Figure 6-4: Schematic representation of quantum dot- trivalent adamantane-mannose-lectin complexes with Lens Culinaris, Concanavalin A and Galanthus Nivalis.

To sum it up, one main challenge in Nanotechnology is to create non-covalent systems that are selective, adaptive and yet at the same time robust [58]. To meet this challenge, three different strategies were established [59]. The first strategy consisted of complementing a strong orthogonal interaction with one or two extra secondary interactions (Chapter 3). This strategy resulted in selective binding of a dipeptide containing an aromatic group. The second strategy involved monitoring of kinetics of

sequential binding of three different components instead of monitoring a two component assembly (Chapter 4). This strategy is advantageous for selectively detecting biomolecules of medium selectivity, such as lectins which can bind more than one monosaccharide with different binding strengths. The lectin binding strength defines, though, the flocculation kinetics. Weakly binding lectins won't induce in most cases network formation and flocculation, but in case they do, the kinetics is substantially slower than when stronger binding monosaccharides are involved. That means that the selectivity of these systems is time-dependent. The third strategy used very strong-binding linkers at the nanoparticle surface, yielding robust yet tunable nanostructures. Tuning of binding strength with the addition of free cyclodextrin in solution varies the binding strength of the linker-nanoparticle complex. Tuning the binding strength, by adding excess of free cyclodextrin, leads to more dynamic but less robust systems. When no free cyclodextrin is present, the non-dynamic nature of the complex induces fast flocculation with high robustness but less selectivity. The third strategy is a fine example of versatility and tunability of supramolecular materials, where is up to the scientist's choice to obtain different collective properties either in thermodynamic equilibrium or not.

6.4 Applications for biomolecule recognition and sensing

Throughout the thesis, special focus was put on translating kinetics, dynamics and supramolecular interactions into detecting biomolecules or their properties. In all chapters of this thesis, biomolecule recognition and sensing in complex systems was studied. The term complex mixture defines mixtures of different components at equilibrium, towards equilibrium and out-of-equilibrium [40]. This thesis provides methods and techniques for recognizing and sensing small biomolecules such as sugars, medium size molecules such as dipeptides and bigger biomolecules such as proteins. In Chapter 2, the anomerization reaction of glucose, as a system towards equilibrium, led to the diffusion separation and discrimination of glucose anomers. In Chapter 3 gold nanoparticle receptors for selective dipeptide recognition are presented and in Chapter 4 and Chapter 5 selective lectin detection is achieved by using sequential assembly by dynamic and non-dynamic supramolecular interactions.

In Chapter 2, in an effort to improve diffusion accuracy, a simplified model was used for representing systems not at equilibrium. By the permutated DOSY, p-DOSY, glucose anomers could be separated through their diffusion coefficient. As future application, p-DOSY can be used for monitoring reactions of complex bionanotechnological systems such as the kinetics of multiple substrates catalyzed by enzyme-conjugated nanoparticles. In addition, the formation and evolution of dynamic combinatorial libraries [60] and drug-release kinetics from nanoparticles [61] could be

analyzed. In conclusion, p-DOSY is a great spectroscopic tool, enabling nanotechnologists to study systems with kinetic characteristics.

In Chapter 3, one of the few selective receptors for dipeptides containing an aromatic group was developed. In the future more supramolecular interactions could be introduced, such hydrogen bonding [62] or chiral receptors [63] for selective recognition of other types of peptides. Of high-interest would also be multivalency-based peptide recognition that could be implemented by utilizing the nanoparticles synthesized in Chapter 3.For example, the dipeptide lysine-lysine bears two amine groups and it would be expected to bind with higher affinity to the quaternary ammonium nanoparticles. For dipeptide sensing another strategy that could be explored is the one followed in Chapter 4, thus to use the peptides as cross-linkers between two types of nanoparticles. For example, the dipeptide glycine-glycine could be detected by forming supramolecular bridges between quaternary ammonium nanoparticles and crown ether nanoparticles.

In Chapter 4 & 5 the selective detection of mannose-binding proteins was achieved. The interesting part of the lectin sensors developed is the detection method used. While many nanotechnologists consider flocculation an unwanted property of matter [11], here, flocculation of nanostructures was lectin induced and led to qualitative and quantitative Concanavalin A detection [64]. The outcome of this research provides insight on how to detect multivalent biomolecules, but also gives a taste in how to control complex matter by using biomolecules as nanotechnological tools.

In Chapter 5, it was evident that that there is an interplay between selectivity and fast detection; between dynamic and non-dynamic systems. By employing monoadamantane linkers the response time increases up to when stoichiometric ratios of adamantanes to β-cyclodextrin is used, but in the same time non-specific binding is neglected. The opposite occurs for the triadamantane linkers. To find a balance between these extreme cases, the addition of free cyclodextrin can be used to obtain intermediated binding strengths (between monovalent and trivalent binding), where selectivity and fast response are optimal.

In conclusion, for detection of biomolecules in complex mixtures, sensitive spectroscopic techniques such as NMR and fluorescence facilitate the detection of the target biomolecule in a complex mixture. To design sensors that target multivalent molecules such as peptides or lectins, not only multivalency and binding strengths have to be taken into account, but as well size, shape, geometry and binding site orientation and spatial organization of nanoparticles, ligands and biomolecules [48-50, 54, 56, 59, 65, 66]. Moreover, flocculation assays of supramolecular nanoparticle-based systems are still in their infancy [64], although they have proven to be very useful for biosensing. Flocculation assays could be also detected by other techniques, such as SPR for gold nanoparticles,

DOSY NMR for the case of small aggregates, flow cytometry and DLS [1, 5, 30, 34, 67, 68]. Lastly, biomolecules should not only be sensing targets of nanomaterials, but also the opposite, nanomaterials could be templated by biomolecules [69, 70].

6.5 Final conclusion and future outlook

In this thesis, the motivation was to progressively discover and understand molecular interactions that govern natural systems and beyond, and the goal was to acquire the ability to design, direct and control complex matter. Special focus was out on implementing and controlling supramolecular ligand interactions on nanoparticle surfaces with an emphasis on biomolecule sensing.

The most important findings regarding the first main topic of this thesis; which was the use of NMR spectroscopy as a tool in Nanotechnology to study various chemical systems, are:

Permutation of the gradient strength arrays is a robust technique, with future potential in nanotechnology, allowing diffusion identification and separation of components of transient species (Chapter 2).

DOSY NMR is the most appropriate technique for studying binding interactions of small ligand and nanoparticles due to the inherent size differences of the system. It can be used for binding studies of asymmetric mixed- ligand monolayers, cooperative binding, dynamic supramolecular interactions, very- high ligand binding affinity on nanoparticle surfaces and competition binding (Chapter 3, Chapter 4 and Chapter 5).

Regarding the second topic of this thesis; entitled as supramolecular orthogonal interactions addressing especially aspects of multivalency on nanoparticle surfaces, the following general conclusions are derived:

Weak, secondary binding interactions can yield selective nanoparticle systems (Chapter 3).

Orthogonal, sequential assembly of ternary systems mediated by small cross-linkers is a good strategy for constructing and controlling superstructures (Chapter 4).

Non-dynamic non-covalent interactions are the opposite of dynamic covalent interactions on nanoparticle surfaces, being both quite advantageous (Chapter 5).

The last topic addressed in this thesis, which was the translation of molecular mechanisms, recognition principles and supramolecular interactions in biomolecule

detection, provided useful insight for the design and development of nanoparticle based sensors.

The introduction of asymmetric supramolecular interactions, in terms of binding strength, such as mixed ligand monolayers or adamantane-sugar cross-linkers improves the selectivity of nanoparticle based sensors (Chapter 4 and Chapter 5).

Nanoparticle flocculation induced by the presence of a biomolecule is a good strategy for detecting multivalent biomolecules (Chapter 4 and Chapter 5).

During this research future aspects were identified and new questions were born.

While nanotechnology stays more on the applied field of science, the fundamental aspects of its applications should not be overlooked. The mechanisms and thermodynamics behind flocculation kinetics are not yet clear, constituting a rather new, underexplored field of research [13]. Moreover, instead of driving a system to flocculation, it would be interesting to obtain nanoparticle crystals using lectins or other biomolecules as bridges [71].

Fundamental parameters influencing biomolecule or ligand binding on nanoparticles such as size, shape, flexibility and orientation should be further investigated [48-50, 54, 56, 59, 65, 66]. For the nanoparticles studied in Chapter 3, the effect of peptide length was not examined. Longer peptides, such as glycine-glycine-phenylalanine (longer equivalent to glycine-phenylalanine used in Chapter 3) and different structures, such as phenylalanine – phenylalanine could be screened. Moreover, if the peptides would be long enough, maybe they would not only orientate towards one nanoparticle, but they would probably act as crosslinkers, forming supramolecular nanoparticle networks. Lastly, a selective peptide receptor or sensor could be based on the multivalency of multiple-charged peptides such as lysine-lysine-lysine which bears four amine groups. Looking many steps ahead, more complex mixed ligand monolayers can be designed, where more than three interactions take place [36]. Regarding the nanoparticle-based systems studied on Chapter 4 and Chapter 5, it would be of interest to study the effect of nanoparticle size on the lectin sensing. Smaller nanoparticles are probably crosslinked better with lectins, due to less steric hindrance between them when bound on lectins. Smaller nanoparticles would probably enable the extension of the flocculation assays to other sugar-binding lectins.

Instead of first designing nanoparticles that are expected to exhibit, in theory, interactions with biomolecules, biomolecule as templates could be used for the functionalization of nanoparticles [69, 70]. This would allow gaining fundamental insight of supramolecular interactions and binding and has also applications for screening libraries

of potential binders, crucial for drug discovery and design. Coming back to Chapter 5, the use of trivalent adamantane linkers with different sugar sequences in combination with a possible lectin template effect would allow for the selective functionalization of the nanoparticles, which could either be isolated from solution with physical methods or self-separate by flocculation and concomitant precipitation.

In Chapter 4 and Chapter 5, rather slow flocculation kinetics of supramolecular nanoparticle networks were explored for selective lectin sensing. There are two main routes for controlling the kinetics; either through the relative concentration of ligands to cyclodextrin, or, in the case of non-dynamic supramolecular interactions by adding free cyclodextrin in solution [53, 55]. Extending this fact to other sensing systems with very fast flocculation kinetics, such as kinetics of enzymes, quantification inaccuracies could be surpassed by fine tuning of the above mentioned parameters.

Analytical techniques such as NMR, TEM, DLS and fluorescence, have been underexplored as detection tools and are currently mostly used for material characterization [72]. On one hand this is justified due to the expense and large size of this type of equipment. Nonetheless, these techniques are quite sensitive with low detection units and could be still used in medical centers and research labs for the detection of target molecules such as biomolecules, water contaminants, bacteria and other. In this thesis, fluorescent flocculation assays were developed for the detection of lectins. Nonetheless, the flocculation kinetics could have been monitored also by DOSY, TEM or by DLS. There is an excellent example in literature, where quantification of the amount of lectin is performed by analyzing the assembly growth in size with increasing lectin concentration [72]. In-situ TEM is also an excellent tool for studying three-dimensional, in-time assembly processes [12].

Looking many steps ahead and towards biosensing, obstacles such as nanoparticle reproducibility, stability and selective sensing of targets in complex mixtures such as in human fluids need to be resolved[73]. To overcome stability and selective sensing, supramolecular, non-dynamic interactions on nanoparticles, seem to provide a solution by being be more robust than other systems and still quite adaptive[58]. To overcome reproducibility of the number and density of the ligands on the nanoparticle surface, supramolecular, non-dynamic interactions on nanoparticles could provide again an appropriate solution because the amount and density of the ligands on the nanoparticle can be better controlled. Selectivity problems, though, are mostly target specific and should be addressed separately for each individual application.

In conclusion, supramolecular ligand interactions on nanoparticle surfaces is a flourishing topic in the field of Nanotechnology. While the (inter)molecular principles governing supramolecular natural interactions are to a high extent recognized, and

artificial analogues and models can be synthesized, Nanotechnology still lacks considerably in controlling complex matter. To address this, more orthogonal supramolecular pairs need to be designed[36] and integrated in nanomaterial based systems. Also, advanced particle designs, with defined ligand orientation and binding sites, such as Janus or patchy particles need to be engaged to improve the control of flocculation or assembly kinetics. Other aspects influencing assembly and binding such as size, and shape and multivalency need also further investigation.

6.6 References

1. Cohen, Y., L. Avram, and L. Frish, Diffusion NMR spectroscopy in supramolecular and combinatorial chemistry: An old parameter - New insights. Angewandte Chemie - International Edition, 2005. 44(4): p. 520-554.
2. Friebolin, H. and J.K. Becconsall, Basic one-and two-dimensional NMR spectroscopy. 1993: VCH Weinheim.
3. Funasaki, N., et al., NMR Chemical Shift References for Binding Constant Determination in Aqueous Solutions. The Journal of Physical Chemistry B, 2001. 105(30): p. 7361-7365.
4. García, J., L.G. Martins, and M. Pons, NMR Spectroscopy in Solution, in Supramolecular Chemistry. 2012, John Wiley & Sons, Ltd.
5. Gounarides, J.S., A. Chen, and M.J. Shapiro, Nuclear magnetic resonance chromatography: Applications of pulse field gradient diffusion NMR to mixture analysis and ligand-receptor interactions. Journal of Chromatography B: Biomedical Sciences and Applications, 1999. 725(1): p. 79-90.
6. Hens, Z. and J.C. Martins, A Solution NMR Toolbox for Characterizing the Surface Chemistry of Colloidal Nanocrystals. Chemistry of Materials, 2013. 25(8): p. 1211-1221.
7. Lee, S.-W., et al., Effect of Temperature on the Growth of Silver Nanoparticles Using Plasmon-Mediated Method under the Irradiation of Green LEDs. Materials, 2014. 7(12): p. 7781.
8. Leng, W., P. Pati, and P.J. Vikesland, Room temperature seed mediated growth of gold nanoparticles: mechanistic investigations and life cycle assesment. Environmental Science: Nano, 2015. 2(5): p. 440-453.
9. Cure, J., et al., Monitoring the Coordination of Amine Ligands on Silver Nanoparticles Using NMR and SERS. Langmuir, 2015. 31(4): p. 1362-1367.
10. Doyen, M., K. Bartik, and G. Bruylants, UV–Vis and NMR study of the formation of gold nanoparticles by citrate reduction: Observation of gold–citrate aggregates. Journal of Colloid and Interface Science, 2013. 399: p. 1-5.
11. Xie, H., et al., Critical Flocculation Concentrations, Binding Isotherms, and Ligand Exchange Properties of Peptide-Modified Gold Nanoparticles Studied by UV−Visible, Fluorescence, and Time-Correlated Single Photon Counting Spectroscopies. Analytical Chemistry, 2003. 75(21): p. 5797-5805.
12. Liu, Y., et al., In Situ Visualization of Self-Assembly of Charged Gold Nanoparticles. Journal of the American Chemical Society, 2013. 135(10): p. 3764-3767.

13. Soman, C. and T. Giorgio, Kinetics of molecular recognition mediated nanoparticle self-assembly. Nano Research, 2009. 2(1): p. 78-84.
14. Loening, N.M., J. Keeler, and G.A. Morris, One-Dimensional DOSY. Journal of Magnetic Resonance, 2001. 153(1): p. 103-112.
15. Millet, O. and M. Pons, A New Method for Measuring Diffusion Coefficients by 2D NMR using Accordion Spectroscopy. Journal of Magnetic Resonance, 1998. 131(1): p. 166-169.
16. Pudakalakatti, S.M., et al., Rapid Characterization of Molecular Diffusion by NMR Spectroscopy. Chemistry – A European Journal, 2014. 20(48): p. 15719-15722.
17. Shrot, Y. and L. Frydman, Single-scan 2D DOSY NMR spectroscopy. Journal of Magnetic Resonance, 2008. 195(2): p. 226-231.
18. Steinbeck, C.A. and B.F. Chmelka, Rapid 1H{13C}-Resolved Diffusion and Spin-Relaxation Measurements by NMR Spectroscopy. Journal of the American Chemical Society, 2005. 127(33): p. 11624-11635.
19. Thrippleton, M.J., N.M. Loening, and J. Keeler, A fast method for the measurement of diffusion coefficients: one-dimensional DOSY. Magnetic Resonance in Chemistry, 2003. 41(6): p. 441-447.
20. Urbanczyk, M., W. Kozminski, and K. Kazimierczuk, Accelerating Diffusion-Ordered NMR Spectroscopy by Joint Sparse Sampling of Diffusion and Time Dimensions. Angewandte Chemie-International Edition, 2014. 53(25): p. 6464-6467.
21. Yapar, S., et al., Dipeptide recognition in water mediated by mixed monolayer protected gold nanoparticles. Chemical Communications, 2015. 51(75): p. 14247-14250.
22. Hostetler, M.J., et al., Alkanethiolate Gold Cluster Molecules with Core Diameters from 1.5 to 5.2 nm: Core and Monolayer Properties as a Function of Core Size. Langmuir, 1998. 14(1): p. 17-30.
23. Liu, X., et al., Determination of monolayer-protected gold nanoparticle ligand–shell morphology using NMR. 2012. 3: p. 1182.
24. Lucas, L.H., W.H. Otto, and C.K. Larive, The 2D-J-DOSY experiment: resolving diffusion coefficients in mixtures. Journal of Magnetic Resonance, 2002. 156(1): p. 138-145.
25. Delsuc, M. and T. Malliavin, Maximum entropy processing of DOSY NMR spectra. Analytical Chemistry, 1998. 70(10): p. 2146-2148.
26. Huo, R., R. Wehrens, and L. Buydens, Improved DOSY NMR data processing by data enhancement and combination of multivariate curve resolution with non-linear least square fitting. Journal of Magnetic Resonance, 2004. 169(2): p. 257-269.
27. Huo, R., et al., Assessment of techniques for DOSY NMR data processing. Analytica chimica acta, 2003. 490(1): p. 231-251.
28. Nilsson, M., The DOSY Toolbox: A new tool for processing PFG NMR diffusion data. Journal of Magnetic Resonance, 2009. 200(2): p. 296-302.
29. Nilsson, M., et al., Biexponential fitting of diffusion-ordered NMR data: practicalities and limitations. Analytical chemistry, 2006. 78(9): p. 3040-3045.
30. Lin, P.-C., et al., Techniques for physicochemical characterization of nanomaterials. Biotechnology advances, 2014. 32(4): p. 711-726.
31. Canzi, G., A.A. Mrse, and C.P. Kubiak, Diffusion-ordered NMR spectroscopy as a reliable alternative to TEM for determining the size of gold nanoparticles in organic solutions. The Journal of Physical Chemistry C, 2011. 115(16): p. 7972-7978.

32. Pyrz, W.D. and D.J. Buttrey, Particle Size Determination Using TEM: A Discussion of Image Acquisition and Analysis for the Novice Microscopist. Langmuir, 2008. 24(20): p. 11350-11360.
33. Pecora, R., Dynamic light scattering measurement of nanometer particles in liquids. Journal of nanoparticle research, 2000. 2(2): p. 123-131.
34. Jans, H., et al., Dynamic Light Scattering as a Powerful Tool for Gold Nanoparticle Bioconjugation and Biomolecular Binding Studies. Analytical Chemistry, 2009. 81(22): p. 9425-9432.
35. Khlebtsov, B.N. and N.G. Khlebtsov, On the measurement of gold nanoparticle sizes by the dynamic light scattering method. Colloid Journal, 2011. 73(1): p. 118-127.
36. Saha, M.L., et al., Orthogonality in discrete self-assembly - survey of current concepts. Chemical Society Reviews, 2013. 42(16): p. 6860-6909.
37. Jean-Marie, L., Supramolecular chemistry: from molecular information towards self-organization and complex matter. Reports on Progress in Physics, 2004. 67(3): p. 249.
38. Busseron, E., et al., Supramolecular self-assemblies as functional nanomaterials. Nanoscale, 2013. 5(16): p. 7098-7140.
39. Hu, X.-Y., et al., Dynamic Supramolecular Complexes Constructed by Orthogonal Self-Assembly. Accounts of Chemical Research, 2014. 47(7): p. 2041-2051.
40. Mattia, E. and S. Otto, Supramolecular systems chemistry. 2015. 10(2): p. 111-119.
41. Badia, A., et al., Structure and dynamics in alkanethiolate monolayers self-assembled on gold nanoparticles: a DSC, FT-IR, and deuterium NMR study. Journal of the American Chemical Society, 1997. 119(11): p. 2682-2692.
42. Pastor, A. and E. Martínez-Viviente, NMR spectroscopy in coordination supramolecular chemistry: A unique and powerful methodology. Coordination Chemistry Reviews, 2008. 252(21–22): p. 2314-2345.
43. Viegas, A., et al., Saturation-Transfer Difference (STD) NMR: A Simple and Fast Method for Ligand Screening and Characterization of Protein Binding. Journal of Chemical Education, 2011. 88(7): p. 990-994.
44. Cedervall, T., et al., Understanding the nanoparticle–protein corona using methods to quantify exchange rates and affinities of proteins for nanoparticles. Proceedings of the National Academy of Sciences, 2007. 104(7): p. 2050-2055.
45. Joshi, H., et al., Isothermal titration calorimetry studies on the binding of amino acids to gold nanoparticles. The Journal of Physical Chemistry B, 2004. 108(31): p. 11535-11540.
46. Liu, S., et al., The Cucurbit[n]uril Family: Prime Components for Self-Sorting Systems. Journal of the American Chemical Society, 2005. 127(45): p. 15959-15967.
47. Moghaddam, S., et al., New Ultrahigh Affinity Host−Guest Complexes of Cucurbit[7]uril with Bicyclo[2.2.2]octane and Adamantane Guests: Thermodynamic Analysis and Evaluation of M2 Affinity Calculations. Journal of the American Chemical Society, 2011. 133(10): p. 3570-3581.
48. Krishnamurthy, V.M., L.A. Estroff, and G.M. Whitesides, Multivalency in ligand design. Fragment-based approaches in drug discovery, 2006. 34: p. 11-53.
49. Fasting, C., et al., Multivalency as a Chemical Organization and Action Principle. Angewandte Chemie International Edition, 2012. 51(42): p. 10472-10498.
50. Mulder, A., J. Huskens, and D.N. Reinhoudt, Multivalency in supramolecular chemistry and nanofabrication. Organic and Biomolecular Chemistry, 2004. 2(23): p. 3409-3424.

51. Hossain, M.A. and H.-J. Schneider, Sequence-Selective Evaluation of Peptide Side-Chain Interaction. New Artificial Receptors for Selective Recognition in Water. Journal of the American Chemical Society, 1998. 120(43): p. 11208-11209.
52. Kauscher, U. and B.J. Ravoo, Mannose-decorated cyclodextrin vesicles: The interplay of multivalency and surface density in lectin–carbohydrate recognition. Beilstein Journal of Organic Chemistry, 2012. 8: p. 1543-1551.
53. Perl, A., et al., Gradient-driven motion of multivalent ligand molecules along a surface functionalized with multiple receptors. Nat Chem, 2011. 3(4): p. 317-322.
54. Baldini, L., et al., Calixarene-based multivalent ligands. Chemical Society Reviews, 2007. 36(2): p. 254-266.
55. Hsu, S.-H., et al., Nonlinear Amplification of a Supramolecular Complex at a Multivalent Interface. Angewandte Chemie International Edition, 2013. 52(2): p. 714-719.
56. Lindhorst, T.K. and S. Kubik, Supramolecular Approaches to the Study of Glycobiology, in Supramolecular Chemistry. 2012, John Wiley & Sons, Ltd.
57. Wittmann, V. and R.J. Pieters, Bridging lectin binding sites by multivalent carbohydrates. Chemical Society Reviews, 2013. 42(10): p. 4492-4503.
58. Rybtchinski, B., Adaptive Supramolecular Nanomaterials Based on Strong Noncovalent Interactions. ACS Nano, 2011. 5(9): p. 6791-6818.
59. Barnard, A. and D.K. Smith, Self-Assembled Multivalency: Dynamic Ligand Arrays for High-Affinity Binding. Angewandte Chemie International Edition, 2012. 51(27): p. 6572-6581.
60. della Sala, F. and E.R. Kay, Reversible Control of Nanoparticle Functionalization and Physicochemical Properties by Dynamic Covalent Exchange. Angewandte Chemie, 2015. 127(14): p. 4261-4265.
61. Sethi, M., et al., Effect of drug release kinetics on nanoparticle therapeutic efficacy and toxicity. Nanoscale, 2014. 6(4): p. 2321-2327.
62. Cha, X., K. Ariga, and T. Kunitake, Molecular recognition of aqueous dipeptides at multiple hydrogen-bonding sites of mixed peptide monolayers. Journal of the American Chemical Society, 1996. 118(40): p. 9545-9551.
63. Voyer, N., Chiral recognition ability of peptide-based molecular receptors. Chemical Communications, 1997(23): p. 2329-2330.
64. Wee, E.J.H., et al., Re-purposing bridging flocculation for on-site, rapid, qualitative DNA detection in resource-poor settings. Chemical Communications, 2015. 51(27): p. 5828-5831.
65. Badjić, J.D., et al., Multivalency and cooperativity in supramolecular chemistry. Accounts of Chemical Research, 2005. 38(9): p. 723-732.
66. Pieters, R.J., Maximising multivalency effects in protein-carbohydrate interactions. Organic & Biomolecular Chemistry, 2009. 7(10): p. 2013-2025.
67. Estévez, M.C., et al., Highly fluorescent dye-doped silica nanoparticles increase flow cytometry sensitivity for cancer cell monitoring. Nano Research, 2009. 2(6): p. 448-461.
68. Valentini, M., et al., Diffusion NMR Spectroscopy for the Characterization of the Size and Interactions of Colloidal Matter: The Case of Vesicles and Nanoparticles. Journal of the American Chemical Society, 2004. 126(7): p. 2142-2147.
69. Nowak, P., et al., Localized Template-Driven Functionalization of Nanoparticles by Dynamic Combinatorial Chemistry. Angewandte Chemie International Edition, 2015. 54(14): p. 4192-4197.

70. Whitesides, G.M., Bioinspiration: something for everyone. Interface Focus, 2015. 5(4): p. 20150031.
71. Abe, S. and T. Ueno, Design of protein crystals in the development of solid biomaterials. RSC Advances, 2015. 5(27): p. 21366-21375.
72. Wang, X., O. Ramstrom, and M. Yan, Dynamic light scattering as an efficient tool to study glyconanoparticle-lectin interactions. Analyst, 2011. 136(20): p. 4174-4178.
73. Howes, P.D., R. Chandrawati, and M.M. Stevens, Bionanotechnology. Colloidal nanoparticles as advanced biological sensors. Science (New York, N.Y.), 2014. 346(6205): p. 1247390.

Chapter 8 Summary

Manipulating and understanding matter at the nanoscale describes best the interdisciplinary field of nanotechnology. Nanotechnology is a new branch of science (physics, chemistry, biology and engineering) that deals with molecules and structures at the nanometer scale; typically 1-100 nm. To put it in perspective; A nanometer is one billionth of a meter as the size of a tennis ball is one billionth of the size of the earth. The reduction of size and quantities, that the field of Nanotechnology explores, enabled us to first understand, then combine, and manipulate the smallest units of matter, the atoms.

Nanotechnology is entering, currently a new era, which is described by Jean-Marie Lehn as the era of "complex matter". Complex matter is the combination of nanomaterials that together give rise to superstructures, "structures beyond nanostructures". The latest and most exciting advancements in nanotechnology employ superstructures for the design and development of smart and functional devices and materials and give a taste of the exciting future of nanotechnology.

In this thesis, the motivation was to progressively discover and understand molecular interactions that govern nanoscale natural systems and beyond, and the goal was to acquire the ability to design, direct and control complex matter. In this context, supramolecular ligand interactions on nanoparticle surfaces were designed and implemented with an emphasis on biomolecule sensing. Three main topics were addressed:

1. NMR as a tool in Nanotechnology to study reactions and supramolecular interactions between molecules, nanoparticles and biomacromolecules.

2. Supramolecular Orthogonal Interactions at nanoparticle surfaces.

3. Applications of Supramolecular Orthogonal Interactions for biomolecule recognition and sensing.

NMR spectroscopy is an excellent tool for monitoring in-situ chemical reactions. In particular, DOSY measurement is well suited to characterize transient species by the determination of their sizes. However, in Chapter 2, a difficulty, in the DOSY experiments performed in out-of-equilibrium systems, is brought to light. Taking into account, that the basis of a single DOSY measurement is the analysis of the exponential decay of the signal with increasing gradient strength, concentration evolution, within a single measurement, creates a bias, which can lead to erroneous interpretations in the diffusion coefficient estimation. This was observed for the test case of the anomerization of glucose. To average out the bias within a single DOSY measurement, a series of stimulated echo

spectra with pulse gradient strengths, sampled in a permutated manner, was proposed to be measured. This approach, named as p-DOSY does not require changes in the pulse sequences nor in the processing software, and restores completely the full accuracy of the measure. Permutation of the series of pulse gradient strengths within a single DOSY measurement, distributes randomly the concentration variation over the whole range of gradients, actually transforming an experimental bias into an additional random noise. The analysis of the permutated experiment leads to a less precise measure (larger error-bars) but eventually more accurate (less systematic error). Altogether, the DOSY experiment with a randomized list of gradients (the permutated DOSY or p-DOSY) is an unbiased experiment in the presence of an evolving system, in contrast to conventional DOSY. It is perfectly suited for the analysis of chemical reactions and kinetic processes of systems away from equilibrium. It can be used to monitor the rate of reaction kinetics, to characterize in-operando transient systems or to observe kinetics of assembly phenomena and dynamics effects. Specifically, in Nanotechnology, p-DOSY is an excellent tool for monitoring reactions on nanoparticle surfaces, such as end-group modification and ligand exchange reactions. Moreover, by p-DOSY, assembly kinetics or aggregation of nanoparticles could be studied by observing the shift of the diffusion coefficient to lower values. The robustness of p-DOSY can also be used to protect diffusion results from any experimental artifact, such as temperature shift or spectrometer drift when such artifacts are known and cannot be easily compensated for. As it does not add any burden in the acquisition step nor at the processing step, spectroscopists are recommended to use p-DOSY in these experimental cases.

In Chapter 3, the goal was to implement orthogonal selective interactions in order to design nanoparticle based peptide receptors. For this purpose, mixed monolayer protected gold nanoparticles (AuNPs) were decorated with the α,ω-functionalized thiols containing as recognition elements a terminal trimethylalkyl ammonium group, an 18-crown-6 moiety, and a phenyl group, respectively. To evaluate binding affinities, the suitability of 1H NMR chemical shift titrations method was tested. Small but clearly visible downfield shifts of peptide signals were observed when increasing the AuNP concentration, indicating an interaction between the dipeptide and the nanoparticles. The extent of these shifts combined with pronounced overlaps with AuNP signals did not allow using this method for the quantification of binding strength, however. Turning to DOSY NMR spectroscopy to gain insight into the correlation of surface composition and peptide affinity was considered the most appropriate solution. The evaluation of binding equilibria that are fast on the NMR timescale by DOSY NMR spectroscopy is based on the reduction of the diffusion coefficient of a small molecule once it binds to a larger receptor. The resulting diffusion coefficient D_{obs} represents a weighted average of the coefficients of the free and the bound states. The fraction χ of bound substrate on AuNPs was calculated for all combinations of peptides (Gly-Gly and Gly-Phe) with AuNPs. The χ value for Gly-Phe

with the AuNPs containing all three functional groups was found to be 78%, twice or more times higher than all other combinations. To evaluate peptide binding quantitatively, DOSY NMR titrations were performed with AuNPs capped either with quaternary ammonium or a combination of the latter with crown ether and aromatic groups. The resulting χ values were plotted against peptide concentration and the obtained curves were fitted to Langmuir isotherms. The adsorption equilibrium constants K thus obtained amount to 4770 ± 1180 M^{-1} for NP_Q and 8260 ± 1480 M^{-1} for NP_{QPC} (for other synthetic batches of these AuNPs equilibrium constants of 3880 ± 860 M^{-1} and 6090 ± 1380 M^{-1} were observed, respectively), clearly confirming the increase of peptide affinity upon combining the three ligands on the nanoparticle surface. The Langmuir treatment also yielded the maximum concentration of bound peptides as a second fitted parameter, which showed that AuNPs bind 3 peptide molecules on average. In conclusion, this work shows that combining different functional groups on the surface of AuNPs affords receptors for low molecular weight compounds, in this case for peptides. The individual functional groups on these AuNPs contribute to substrate recognition by presenting specific binding sites and/or surface arrangements suitable for substrate binding. The attractiveness of the presented approach lies in the ease with which the receptors can be prepared once a library of functional thiols is available and its enormous flexibility. The sensitivity of DOSY NMR to the inherent size differences between ligands and receptors, often encountered in nanoparticle molecular recognition systems, turns DOSY NMR into an excellent candidate for the elucidation of supramolecular interactions on nanoparticle interfaces.

Chapter 4 explores the possibility to employ asymmetric sugar-adamantane linkers, exhibiting different supramolecular interactions, for crosslinking cyclodextrin nanoparticles with multivalent proteins called lectins into ternary, supramolecular NanoParticle Networks (NPN). The three building blocks are β-cyclodextrin-capped CdTe quantum dots, tetraethylene glycol-tethered mannose-adamantane cross-linkers (ADTEGMan) and the tetravalent lectin Concanavalin A. Only when lectin is present, sequential binding events take place; from quantum dot to linker and from linker to lectin, leading to self-organization in-situ of the sensor through the formation of ternary supramolecular networks. The main goal of this Chapter was to selectively detect a tetravalent lectin called Concanavalin A by monitoring the loss of fluorescence signal of quantum dots in solution over time, caused by controlled network formation and consecutive flocculation and sedimentation. Observing by naked eye or by UV illumination the color of the supernatant or whether fluorescent precipitates have sedimented at the bottom of the vial or not, leads qualitative lectin detection. Monitoring the fluorescence intensity loss in due to controlled network formation, flocculation and sedimentation, leads to quantitative lectin detection. By selecting on specific time point, e.g. at 100 min, a linear correlation between lectin concentration and fluorescent intensity is observed. To

conclude, the sensor is easy to use, since quantum dots are functionalized in one step, mannose-adamantane linker is afforded in two steps and only mixing is required for the sensor build-up. The sensing response times can be tuned on demand simply by changing the linker or β-CD-QD concentration and their respective ratios. The sensor shows excellent selectivity because even if non-specific interactions or weak nanoparticle-lectin interactions occur, these do not lead to sedimentation of quantum dots. Altogether, this study can be extended for sensing of other mannose-binding lectins and opens new opportunities for the development of a new generation of sensors for sensing multivalent biomacromolecules in vitro.

Chapter 5 continues and extends the study of selective lectin sensing through controlled formation, flocculation and precipitation of ternary supramolecular quantum dot networks. In this chapter, asymmetric tetraethylene glycol-based mannose-tri-adamantane linkers (TriADTEGMan) were employed, which, due to their multivalency potency, are bound in a non-dynamic fashion on the nanoparticle surface in aqueous solutions. The goal was to compare flocculation kinetics, tunability in response times and specificity of lectin sensors that employ either trivalent or monovalent adamantane mannose linkers (ADTEGMan) and to prove that these sensors combine advantages from covalent e.g. stability, and from supramolecular systems e.g. tunability, reversibility. By 1H NMR titrations and DOSY measurements, the triadamantane linkers bound on the β-cyclodextrin quantum dots yield supramolecular, non-dynamic systems, in contrast with the dynamic, monovalent cyclodextrin-adamantane interactions. Nonetheless, the binding strength of such complexes can be tuned by addition of free cyclodextrin in solution prior to quantum dot addition. Consequently, these sensors combine the advantages of both covalent and non-covalent chemistry, and they therefore fall under the category of "supramolecular, non-dynamic chemistry". The advantages and pitfalls of this strategy were revealed when the NPN flocculation kinetics of the triadamantane-based sensor with the monovalent case were compared for Concanavalin A. In the case of the TriADTEGMan, the network formation, flocculation and sedimentation becomes significantly faster, allowing to sense and study the flocculation kinetics of other lectins (Galanthus Nivalis and Lens Culinaris) as well. Nevertheless, interplay between selectivity and fast response was found. When TriADMan is used, the flocculation is faster, but the selectivity is poorer, and the exact opposite holds for the monovalent case.

Chapter 6 summarizes the most important findings of every chapter. By linking all the findings of this thesis, the questions answered are evaluated and a general conclusion is reached. With an eye on the future, some observations to extend the discussion further and beyond this thesis are added and new questions arisen are identified. Finally, a conclusion is reached by providing insight, guidelines and suggestions on designing and controlling multivalent, supramolecular interactions on the nanoparticle bionanointerface, between nanomaterials, ligands and biomolecules.

Samenvatting

Het begrijpen en manipuleren van materie op de nanoschaal is de beste beschrijving van het interdisciplinaire veld van de nanotechnologie. Nanotechnologie is een nieuwe discipline binnen de technische en natuurwetenschappen, en houdt zich bezig met moleculen en structuren op de nanometerschaal, typisch 1-100 nm. In perspectief, een nanometer is een miljardste deel van een meter en verhoudt zich als de grootte van een tennisbal ten opzichte van de grootte van de aarde. De kleine lengteschalen en hoeveelheden die in de nanotechnologie gebruikt worden, hebben ons in staat gesteld om de kleinste eenheden van materie, de atomen, te begrijpen, combineren en manipuleren.

Op dit moment staat de nanotechnologie aan het begin van een nieuw tijdperk, welke beschreven wordt door Jean-Marie Lehn als het tijdperk van “complexe materie”. Complexe materie is de combinatie van nanomaterialen die tezamen superstructuren vormen, “Structuren die meer zijn dan nanostructuren”. De meest actuele en interessante voortgangen in de nanotechnologie zijn in het gebruik van superstructuren voor het ontwerpen en ontwikkelen van slimme en functionele apparaten en materialen. Dit belooft een interessante toekomst voor de nanotechnologie.

De motivatie voor deze thesis was om op een progressieve manier te ontdekken en begrijpen hoe moleculaire interacties natuurlijke en niet-natuurlijke systemen op de nanoschaal dirigeren. Het doel was om de mogelijkheid te verkrijgen om complexe materie te ontwerpen, sturen en controleren. In deze context werden supramoleculaire ligand interacties op het oppervlak van nanodeeltjes ontworpen en geïmplementeerd, met een nadruk op de detectie van biomoleculen. Hiervoor werden drie hoofdonderwerpen opgesteld:

1. Kernspinresonantie (NMR) als methode in de nanotechnologie om reacties en supramoleculaire interacties tussen moleculen, nanodeeltjes en biomacromoleculen te bestuderen.

2. Supramoleculaire orthogonale interacties op het oppervlak van nanodeeltjes.

3 Toepasbaarheid van supramoleculaire orthogonale interacties voor biomolecuul herkenning en detectie.

NMR spectroscopie is een uitstekende methode om in-situ chemische reacties te volgen. In het bijzonder zijn DOSY metingen adequaat voor de karakterisatie van tijdelijke producten door het bepalen van hun grootte. Echter, in Hoofdstuk 2 wordt een tekortkoming van DOSY experimenten voor bestuderen van niet-equilibrium systemen aan

het licht gebracht. In acht nemende dat de basis van een enkel DOSY experiment de analyse van het exponentiele verval van het signaal is bij toenemende gradiënt sterkte. Concentratie evolutie gedurende een experiment kan dan een afwijking in het signaal geven, wat leidt tot verkeerde interpretatie van de schatting van de diffusie coëfficiënt. Dit is waargenomen bij de anomerisatie van glucose moleculen. Om de afwijking in een enkel DOSY experiment te minimaliseren, is een serie metingen van gestimuleerde echo spectra met puls gradiënt sterktes in een gerandomiseerde manier voorgesteld. Deze aanpak, genaamd p-DOSY, vereist geen veranderingen in de pulssequentie of in de analyse software, en herstelt volledig de nauwkeurigheid van de meting. Permutatie van de puls gradiënt sterkte serie in een enkel DOSY experiment geeft een willekeurige distributie van de concentratievariatie binnen het bereik van de gradiënt, waardoor de experimentele afwijking verandert in toename van de achtergrond ruis. De analyse van het permutatieexperiment leid tot een minder precieze meting (grotere standaardafwijkingen), maar ook een meer accurate meting (kleinere systematische afwijkingen). In vergelijking met een conventioneel DOSY experiment, is een DOSY experiment met een gerandomiseerde lijst van gradiënten (permutatie DOSY of p-DOSY) een meer accuraat experiment voor een evoluerend systeem. Het werkt uitstekend voor de analyse van chemische reacties en kinetische processen van niet-equilibrium systemen. Het kan gebruikt worden om reactiekinetiek te meten, om in-operando tijdelijke systemen te karakteriseren en voor de observatie van kinetische assemblage fenomenen en dynamische effecten. Voor de nanotechnologie is p-DOSY een uitstekende methode voor het bestuderen van reacties op de oppervlakten van nanodeeltjes, zoals eindgroep modificatie en liganduitwisseling reacties. Eveneens kan met p-DOSY de assemblage kinetiek van aggregerende nanodeeltjes bestudeerd worden, door de verandering van de diffusie coëfficiënt naar lagere waardes. De robuustheid van p-DOSY kan ook gebruikt worden om diffusie resultaten te beschermen tegen experimentele artefacten, zoals veroorzaakt door temperatuursveranderingen of spectrometer afwijkingen. Wanneer zulke artefacten bekend zijn, kan hiervoor simpel worden gecompenseerd. Omdat er geen extra hinder is in de acquisitie stap, noch in de verwerking van de data, wordt spectroscopisten aangeraden de p-DOSY methode te gebruiken voor de hierboven genoemde systemen.

In hoofdstuk 3 was het streven om selectieve orthogonale interacties te implementeren op het oppervlak van nanodeeltjes, om zo peptidereceptoren te ontwikkelen op nanodeeltjes. Hiervoor zijn goud-nanodeeltjes (AuNPs) beschermd door een gemengde monolaag, uitgerust met α,ω-gefunctionaliseerde thiolen met, respectievelijk, een terminale trimethylalkyl ammonium groep, een 18-kroon-6 groep of een phenyl groep als herkenningselement voor de peptiden. Om de bindingsaffiniteiten te bepalen, werd de geschiktheid van de 1H NMR chemische verschuiving titratie methode getest. Kleine, maar duidelijk zichtbare, downfield verschuivingen van peptidesignalen

werden waargenomen wanneer de AuNP concentratie werd verhoogd, wat een indicatie is voor de interactie tussen de dipeptiden en de nanodeeltjes. De grootte van deze verschuiving, gecombineerd met de duidelijke overlap met AuNP signalen, maakte het onmogelijk om deze methode te gebruiken om de bindingssterkte te bepalen. Het gebruik van DOSY NMR spectroscopie om inzicht te krijgen in de correlatie tussen de oppervlakte compositie en peptideaffiniteit, werd daarom gekozen als beste methode. Evaluatie van bindingsevenwichten met DOSY NMR spectroscopie, voor evenwichten die snel zijn op de NMR-tijdschaal, is mogelijk door gebruik te maken van de afname van de diffusie coëfficiënt van een klein molecuul, wanneer deze bindt aan een groter molecuul. De resulterende diffusiecoëfficiënt Dobs is een weergave van het gewogen gemiddelde van de coëffienten van de gebonden en ongebonden vormen van het molecuul. De fractie χ van gebonden substraat op AuNPs is berekend voor alle peptidecombinaties (Gly-Gly en Gly-Phe) met de AuNPs. De χ waarde voor Gly-Phe met de AuNPs met alle drie de functionele groepen op het oppervlak, werd bepaald op 78%, twee of meer keer hoger dan alle andere combinaties. Om de peptide binding kwantitatief te evalueren, werden DOSY NMR titraties uitgevoerd met AuNPs, welke beschermd werden door quaternaire ammonium of een combinatie hiervan met kroonethers en aromatische groepen. De χ waarden die hieruit volgden, zijn uitgezet tegen de peptideconcentraties en gefit aan Langmuir-isothermen. De adsorptie equilibrium constanten (K), werden zo bepaald op 4770 ± 1180 M^{-1} voor NPQ en 8260 ± 1480 M^{-1} voor NPQPC (andere K voor synthetische monsters met AuNPs waren 3880 ± 860 M^{-1} and 6090 ± 1380 M^{-1}, respectievelijk), wat een duidelijke bevestiging is van de toenemende affiniteit van de peptiden voor de combinatie van de drie liganden op het oppervlak van de nanodeeltjes. Het gebruik van Langmuir-isothermen gaf ook de maximum concentratie van gebonden peptiden als een twee-parameter-fit, waarmee werd bepaald dat de AuNPs gemiddeld genomen drie peptidemoleculen binden. De conclusie van dit werk is dat het combineren van verschillende functionele groepen op het oppervlak van AuNPs, receptoren creëert voor moleculen met een laag molecuulgewicht, in dit geval dipeptiden. De individuele functionele groepen op deze AuNPs dragen bij aan de substraatherkenning door geschikte bindingsmotieven en/of structurering van het oppervlak voor substraatbinding. Het aantrekkelijke van deze aanpak is het gemak waarmee een receptor gemaakt kan worden wanneer er een serie van functionele thiolen voor handen is en de enorme flexibiliteit van het AuNP platform. De gevoeligheid van DOSY NMR voor de inherente grootteverschillen tussen ligand en receptor, welke vaak voorkomen in moleculaire herkenningssystemen gebaseerd op nanodeeltjes, maakt DOSY NMR een uitstekende kandidaat voor het ophelderen van supramoleculaire interacties op het oppervlak van nanodeeltjes.

Hoofdstuk 4 onderzoekt de mogelijkheid om asymmetrische suiker-adamantane moleculen met verschillende supramoleculaire interactie-motieven te gebruiken om verbindingen te vormen tussen nanodeeltjes met cyclodextrines op het oppervlak en

multivalente eiwitten genaamd lectines, om zo drie-component supramoleculaire nanodeeltje-netwerken (NPN) te vormen. De drie bouwstenen hiervoor zijn β-cyclodextrine-gefunctionaliseerde CdTe quantum dots, tetraethylene glycol-gebonden mannose-adamantane brugliganden (ADTEGMan) en de tetravalente lectine Concanavalin A. Alleen wanneer de lectine aanwezig is, vinden sequentiële bindingsevenementen plaats; tussen quantum dot en brugligand en tussen brugligand en lectine, wat leidt tot de zelforganisatie in-situ van een sensor, door de vorming van drie-component supramoleculaire netwerken. Het doel van dit hoofdstuk was om selectief de tetravalente lectine Concanavelin A te detecteren, door het volgen van de afname van hetfluorescent signaal van de quantum dots in oplossing over tijd, veroorzaakt door de gecontroleerde vorming van een netwerk, met als gevolg flocculatie en sedimentatie. Observatie met het oog van fluorescent neerslag is een kwalitatieve methode om lectine te detecteren. Het verlies van fluorescentie intensiteit als gevolg van het gecontroleerd vormen, flocculeren en sedimenteren van netwerken volgen, is een kwantitatieve methode om lectine te bepalen. Door de keuze voor een specifiek tijdspunt, zeg 100 minuten, kan een lineaire correlatie worden gevonden tussen de lectine concentratie en de fluorescentie intensiteit. De sensor is makkelijk te gebruiken, omdat quantum dots in één stap gefunctionaliseerd kunnen worden, mannose-adamantane brugliganden worden in twee stappen gesynthetiseerd, en de sensor wordt opgebouwd simpelweg door de componenten te mixen. De detectie-respons tijd van de sensor is simpel instelbaar door ofwel de linker of de β-CD-QD concentratie aan te passen. De sensor heeft uitstekende selectiviteit, zelfs als niet-specifieke interacties of zwakke interacties tussen de nanodeeltjes en lectine voorkomen, dan leidt dat niet tot sedimentatie van de quantum dots. Uiteindelijk kan deze studie worden uitgebreid naar de detectie van andere manose bindende lectines en het geeft de mogelijkheid tot de ontwikkeling van een nieuwe generatie sensoren, voor de detectie van multivalente biomacromoleculen in vitro.

Hoofdstuk 5 is een vervolg op, en uitbreiding van, de studie naar het selectief detecteren van lectines door gecontroleerde vorming, flocculatie en precipitatie van drie-component supramoleculaire quantum dot netwerken. In dit hoofdstuk worden asymmetrische tetraethylene glycol brugliganden met een mannose en drie adamantane eindgroepen (TriADTEGMan) gebruikt, welke door hun potentie tot multivalentie worden gebonden op een niet-dynamische manier aan het oppervlak van de nanodeeltjes in waterige oplossing. Het doel was om een vergelijking te maken van de flocculatie-kinetiek, de instelbaarheid van de response-tijd en specificiteit van lectine sensoren die ofwel monovalente of trivalente adamantane mannose linkers (ADTEGMan) gebruiken. Hiermee wilden wij aantonen dat de sensoren met de trivalente brugliganden de voordelen van covalente (e.g. stabiliteit) en supramoleculaire (e.g. instelbaarheid en reversibiliteit) systemen combineren. Met behulp van 1H NMR titraties en DOSY NMR metingen is aangetoond dat de drie adamantane groepen van de trivalente brugliganden binden aan

β-cyclodextrine quantum dots, waardoor supramoleculaire, niet-dynamische systemen ontstaan, in tegenstelling tot de dynamische systemen die ontstaan met de monovalente brugliganden. Echter, de bindingssterkte van zulke complexen kan worden gereguleerd door vrij cyclodextrine aan de oplossing toe te voegen voordat de quantum dots worden toegevoegd. Hiermee combineren deze sensoren de voordelen van zowel covalente als niet covalente chemie en daarom behoren zij tot de categorie “supramoleculaire, niet-dynamische chemie”. De voor- en nadelen van deze strategie werden ontdekt toen de NPN flocculatie kinetiek werd vergeleken van de monovalente en de trivalente sensoren voor Concanavelin A. In het geval van de TriADTEGMan, is de netwerkformatie, flocculatie en sedimentatie significant sneller, waardoor wij in staat waren om ook de flocculatiekinetiek van andere lectines (Galanthus Nivalis en Lens Culinaris) te bepalen. Desalniettemin werd een samenspel tussen selectiviteit en een snelle respons gevonden. Wanneer TriADMan werd gebruikt, was de flocculatie sneller maar de selectiviteit minder, met de monovalente linker werd juist een langzamere flocculatie bepaald, maar met een betere selectiviteit.

Hoofdstuk 6 is de samenvatting van de meest belangrijke ontdekkingen in ieder hoofdstuk. Alle vindingen in deze thesis zijn aan elkaar gekoppeld en de beantwoordde vragen zijn geëvalueerd, waarna een algemene conclusie wordt gegeven. Met het oog op de toekomst nodigen sommige observaties uit tot discussies die verder gaan dan dit proefschrift en nieuwe vragen worden geformuleerd. Tenslotte wordt een conclusie bereikt die inzicht, duiding en suggesties geeft voor het ontwerpen en controleren van multivalente supramoleculaire interacties op het bio-nanooppervlak van nanodeeltjes tussen nanomaterialen, liganden en biomoleculen.

Acknowledgements

Within these few pages lies the essence of my whole PhD thesis and even more. My relationships, past and new, are part but also go above and beyond this thesis.

Four years ago, I met with Aldrik, who came in an “all-in-one” package; my supervisor, PI for the MC DYNAMOL network and promotor! Aldrik, I am grateful to you because “with great power comes great responsibility” and you took up all these roles with bravery, investing a lot of time, energy and talking(!) to develop me further and integrate me into the scientific world. What I appreciate the most is the freedom you gave me, in my research and for my personal development. To deliver this research we both went above and beyond ourselves in a creative way, and I am truly happy, thankful and proud of that. Thank you for helping me “write” the best chapter of my life, up to now.

A special place in my heart is there for my students, Gerli, Kevin, Naomi and Remco, who, deserve a big thank you! In many different ways, you contributed greatly by supporting me and by believing in our research.

I would like to thank the co-authors of my papers, together with whom, I had the honor to publish this research. My first paper came with you, Mark, and this is an honor for me. Our collaboration was so smooth, that research and publishing seemed almost as a piece of cake. Of course we could not have made it without the help of Aldrik and Fijs and many others. My second paper and first, first-author paper, came with you, Marc-André and Julia, and I am grateful to you because our collaboration launched my career in the NMR world. Serap and Stefan, from the beginning I saw great potential in our collaboration and in publishing our work. Thank you, for your trust in my NMR skills, and for such open and friendly collaboration. My last publication, up to now, was with you Junyou and Aldrik. Junyou, I enjoy discussing and exchanging scientific ideas with you and that’s why this can go on for hours! I know I will always have a good friend in Shanghai!

Many thanks to Nadege, Serap, Piotr, Colm and Christos for the memorable moments during your visit in Wageningen and the lab.

Thanks to all my officemates, Dmitry, Junus, Rui, Camilla and Anton! Dmitry and Junus I appreciate your advice and guidance, when I was still a newbie in the lab.

As the first PhD of the group I witnessed it blossoming and this was one of my most valuable experiences. Shortly after me came Rui, Junyou, Jan Bart and Vittorio and later on Stan, Anton, Pieter, Camilla, Gerben and Julia. And oh what great fun it was! Together with some legendary BioNT students, like Suzanne, Kevin and Oscar there was so

much fun, jokes and positive energy, which almost made me not to want to go back home. We all had great chemistry together, literally and metaphorically!

While BioNT was my group, PCC was my other (support) group. Within this big group I only encounter friendly faces, which helped keeping my motivation high. Mara, Josie and Anita, thank you, the value of your help and support is priceless! It also always came with a smile! The PCC members welcomed, discussed and supported greatly my research. That is why I kept on going to the group meetings, even though we had already have started our own at BioNT. Martien and Frans, you were one of the first people talking to me on my first day in Wageningen in the coffee room, I still remember how this immediately made me feel so welcome. Many thanks to you all: Aljosha, Anton, Antsje, Armando, Bert, Cecilia, Celine, Chris, Christian, Diane, Dirk, Dmitry, Duc, Esio, Evan, Frank, Frans, Gosia, Gosia, Hande, Hanne, Hannie, Hans, Harke, Helene, Herman, Huanhuan, Ilse, Inge, Jacob, Jan Maarten, Jasper, Jeroen, Joanne, Johan, Joris, Joshua, Juan, Junus, Kamuran, Katarzyna, Lennart, Lione, Liyakat, Maarten, Marcel, Marleen, Martien, Merve, Mieke, Monika, Nadia, Natalia, Paulo, Peter, Prachi, Rahim, Ran, Remco, Rene, Renko, Rojman, Ronald, Ruben, Sabine, Soumi, Surrender, Simeon, Thao, Ties, Tingting, Willem and Wolf.

Not only did I have PCC but also ORC, having supported my (synthesis) work greatly. Many thanks to all the people of the group and especially Han, Ton, Tom, Maurice, Frank, Barend and Pepijn and to my lab mates Rik, Sidhu, Rui, Christie, Peter, Judith, Maboubeh, Wouter, Umesh and Radostina.

And my being nested in warm groups has literally no end. Another one, was the FP7 ITN DYNAMOL network. Within this network, I learned the most important lesson during my PhD, which is that research in multidisciplinary fields of science is achieved better by groups of talented scientists than by individual geniuses. I found the true meaning of science, which is communication and team work, of course, when I met all of you. Thank you Aldrik, Ana, Anna, Christos, Colm, Elwin, Frank, Gérard, Ivan, Jonathan, Julian, Kay, Kitjanit, Laura, Marco, Milko, Olof, Piotr, Quan, Rui, Serap, Sijbren, Sreejith, Stefan, Uli and Will.

Now, it is time to switch to Greek since I want to thank from the heart my family and friends.

Ειρήνη, Νίκο, Ρούλα, Κώστα, Μαρία και Θωμά, είστε πραγματικοί φίλοι, με έσας χαίρομαι να μοιράζομαι τα όνειρα μου. Η φιλία σας με τιμά τόσα χρόνια τώρα και ελπίζω να συνεχίσει να με τιμά. Λουκά σε ευχαριστώ πολύ, μου στάθηκες απεριόριστα τα πρώτα χρόνια του διδακτορικού μου.

Στους γονείς μου, στην μνήμη της γιαγιάς μου αλλά και στην υπόλοιπη οικογένεια είναι αφιερωμένο το διδακτορικό αυτό, μιας που το ευχαριστώ μοιάζει να μην είναι αρκετό για να σας αποδώσω το μέγεθος της ευγνωμοσύνης μου.

Jeroen, thank you, you stood by me in such a great way that even during the gloomiest days we would have still many reasons to laugh and to enjoy life. Many thanks also to your family, Bert, Lies, Omi and Thijs, who always take good care of me.

Jeroen, my PhD thesis is dedicated to my family and memory of my grandmother, but my future is dedicated to you and to Rafael and Arthur. Rafael you taught me Dutch and then it was my turn to try to teach it to Arthur. Arthur, when you spoke one of your first words, ijsbeer, at the zoo in Rhenen, I felt I was exploding out of happiness and pride. Thanks to both of you, Dutch, is the language that talks to my heart. Ik hou van jullie en ik wens jullie het allerbeste! Jeroen, Rafael and Arthur, my everyday miracles, I learned from you that love is found in unexpected places, at unexpected moments, in unexpected numbers! We, all together, shall go on with love, harmony and happiness!

Maria Oikonomou,

Bennekom,

26/01/2016

.

About the author

The author of this thesis was born on April 24 1984 in Amarousio, Attika. She completed her secondary education in 2002 at Othisi Highschool, Stamata, Attikis. In the same year, she undertook undergraduate studies in chemistry at the National and Kapodistrean University of Athens and conducted a bachelor thesis in Physical Chemistry and an internship in the National Organization of Medicine. Before graduating in 2008, she spent a year in Sicily, Italy having received a Comenius Scholarship for Lifelong Learning Program. In 2008, she undertook a Masters in Pharmaceutical Analysis and Quality Control at department of Pharmacy at the National and Kapodistrean University of Athens, and worked part-time as a chemistry teacher in private schools. In 2011 she graduated with overall grade 8.5/10.00. Afterwards she pursued a PhD degree in the Group of Bionanotechnology, under the supervision of Prof. Dr Aldrik H. Velders, on the project Supramolecular Nanoparticle Interactions and Biomolecule Detection. During her PhD, she also participated as an Early Stage Researcher at the Marie Curie ITN network DYNAMOL (Dynamic Molecular Nanostructures).The results of her research are described in this thesis.

Scientific Publications

M.T.M. Rood, M. Oikonomou, T. Buckle, M. Raspe, Y. Urano, K. Jalink, A.H. Velders, F.W.B. van Leeuwen, An activatable, polarity dependent, dual-luminescent imaging agent with a long luminescence lifetime, Chemical Communications, 50 (2014) 9733-9736, 10.1039/C4CC04015E.

M. Oikonomou, J. Asencio-Hernández, A.H. Velders, M.-A. Delsuc, Accurate DOSY measure for out-of-equilibrium systems using permutated DOSY (p-DOSY), Journal of Magnetic Resonance, 258 (2015) 12-16, http://dx.doi.org/10.1016/j.jmr.2015.06.002.

S. Yapar, M. Oikonomou, A.H. Velders, S. Kubik, Dipeptide recognition in water mediated by mixed monolayer protected gold nanoparticles, Chemical Communications, 51 (2015) 14247-14250, 10.1039/C5CC05909G.

J. Wang, A. Groeneveld, M. Oikonomou, A. Prusova, H. Van As, J.W.M. van Lent, A.H. Velders, Revealing and tuning the core, structure, properties and function of polymer micelles with lanthanide-coordination complexes, Soft Matter, (2015), 10.1039/C5SM02166A.

M. Oikonomou, J. Wang, R. Rijo Carvalho and A. H. Velders, Ternary Supramolecular Quantum Dot Network Flocculation for Selective Lectin Detection, Accepted in Nano Research.

M. Oikonomou, G. Viilup, K. van der Ploeg, R. Steijsijger, N. Vos and A. H. Velders, Non-Dynamic Supramolecular Quantum Dot Functionalization for Improved Lectin Sensing, Manuscript in preparation.

Overview of completed training activities (VLAG)

Discipline specific

Dutch society for Biomaterials & Tissue Engineering^	Lunteren (NL)	2011
Dutch Polymer Days^	Lunteren (NL)	2012
Crystallography Workshop	Cambridge (UK)	2012
Analysis in SEDPHAT	Kaiserslautern (DE)	2012
PhD symposium*	Wageningen (NL)	2013
Molecules: Synthesis and Properties^	Lunteren (NL)	2013
Micronanoconference^	Ede (NL)	2013
Internship at Strasbourg University for DOSY NMR	Strasbourg (FR)	2013
CHAINS 2014^	Veldhoven (NL)	2014
CHAINS 2015^	Veldhoven (NL)	2015
MC DYNAMOL meetings (8-9/11/2011)*	Bordeaux (FR)	2011
MC DYNAMOL meetings (1-4/3/2012)*	Champery (CH)	2012
MC DYNAMOL meetings (15-17/7/2012)*	Rehovot (IL)	2012
MC DYNAMOL meetings (23-25/10/2012)*	Cambridge (UK)	2012
MC DYNAMOL meetings (17-20/4/2013)*,^	Barcelona (ES)	2013
MC DYNAMOL meetings (9-13/9/2013)*	Groningen (NL)	2013

MC DYNAMOL meetings (18-20/6/2014)*	Lyon (FR)	2014

General

Scientific writing and Presentation skills	Wageningen (NL)	2013
Project and Time Management	Wageningen (NL)	2013
Data Management	Wageningen (NL)	2013
Entrepneurship in and outside science	Wageningen (NL)	2014
Mock job interview, Feedback & Career Management	Lyon (FR)	2014
Research & Development in Industrial Setting Entrepreneurship / Commercialisation / Intellectual Property Rights	Lyon (FR)	2014
Writing grant proposals	Wageningen (NL)	2015

Optionals

Weekly group meetings	Wageningen (NL)	2011-2015
BiWeekly group meetings*	Wageningen (NL)	2011-2015
PhD excursion*	UK	2015
Preparation of project proposal	Wageningen (NL)	2011-2015

* Oral presentation, ^ Poster presentation

The research leading to these results has received funding from the People Programme (Marie Curie Actions) of the European Union's Seventh Framework Programme FP7/2007-2013/ under REA grant agreement no 264645.

Cover design by Thijs Appel

Printed & Lay Out by Proefschriftmaken.nl ||Digiforce Vianen

Published by Uitgeverij BOXPress, Vianen